Mercury Transformation and Release from Contaminated Soil Following Perturbations in Solution Chemistry and Application of Polysulfide

by

Matthew Corriveau

A thesis
Presented to the University of Waterloo
in fulfillment of the
thesis requirement for the degree of
Master of Science
in
Earth Sciences

Waterloo, Ontario, Canada, 2018

Author's Declaration

I hereby declare that I am the sole author of this thesis.

This is a true copy of this thesis, including any final required revisions, as accepted by my examiners.

I understand that this thesis may be made electronically available to the public.

Abstract

Mercury (Hg) is a contaminant of concern due to the very high toxicity and bioaccumulating nature of organic Hg and the persistent leaching of Hg to water bodies from contaminated soils and sediments. The deleterious properties of Hg pose challenges for remediation as point source contamination can expand over time to affect much wider areas.

Saturated, flow-through column experiments were conducted with riverbank sediment and floodplain soil collected from a contaminated reach of the South River near Waynesboro, VA. In one experiment, the composition of input solutions was varied to observe relationships among mobilized Hg, aqueous parameters and effluent constituents and identify dominant mechanisms and controls on Hg transport. Effluent Hg concentrations increased and remained elevated when a higher pH and alkalinity solution was input to the column. Effluent Hg and DOC concentrations were generally positively correlated. Increased effluent Hg concentrations broadly coincided with increased effluent iron (Fe) and manganese (Mn) concentrations and redox (Eh) minima. The lowest effluent Hg concentrations were observed upon decreasing the input solution pH from ~8.7 to ~6, whereas an increase in input pH from ~6 to ~12 coincided with the highest effluent Hg concentrations along with spikes in effluent Fe, Mn and DOC concentrations.

Saturated flow-through column experiments with floodplain soil were conducted under both aerobic and anaerobic environments. Greater concentrations of effluent Hg were observed from the column operated in an aerobic environment as opposed to in an anaerobic environment. Two distinct effluent Hg concentration maxima were observed from the aerobic column with increased Hg concentrations observed together with a relatively high Eh (490 mV compared to average Eh of 360 mV) and low Fe and Mn concentrations, whereas the latter and greater Hg maximum broadly coincided with a sharp decrease in Eh (85 mV) and increased effluent Fe and

Mn concentrations. The maximum effluent Hg concentration from the anaerobic column also broadly coincided with an increase in effluent Fe and Mn and a minimum Eh but the Hg release was of a much lower magnitude than from the aerobic column. Despite higher total effluent Hg concentrations from the aerobic column, methylmercury (MeHg) concentrations were consistently higher from the anaerobic column.

A potassium polysulfide (KPS) solution (1 mM S) was applied to a fully-saturated, flow-through column of floodplain soil for approximately 10 pore volumes (PVs) under anaerobic conditions to assess the potential for polysulfide to stabilize Hg. Effluent Hg concentrations were very high during the application of the KPS solution and remained elevated above the control for the remainder of the experiment after the KPS application ceased; most other parameters were similar in the KPS and control column effluents for the duration of the experiment. An increase in effluent Hg from the KPS column was observed post-KPS application that broadly coincided with a decrease in Eh and increased effluent Fe and Mn. The relationship between increased Hg, Mn and Fe and decreased Eh was also observed in the control column, but the magnitude of Hg release was lower than from the KPS column. XANES sulfur spectra collected from the KPS-treated soil and the control were similar indicating that there was not an apparent change in solid-phase sulfur in the KPS-treated soil compared to the control soil. Dissolution of HgS and formation of highly mobile HgS_x^{2-} was likely the dominant mechanism for the Hg release. *In situ* immobilization of Hg in the floodplain soil was not achieved with the flow-through application of a polysulfide solution; contrary to past studies where immobilization was achieved by *in situ* formation of HgS via polysulfide application to elemental Hg^0 in a glass bead medium.

Acknowledgements

I would like to thank my supervisor Dr. Carol Ptacek for giving me the opportunity to study at the graduate level and work on this project with her direction and support. I would also like to thank my committee members Dr. David Blowes and Dr. Doug Gould for imparting expert input and advice. Additionally, thank you to Rich Landis and Jim Dyer for supporting this project and providing essential guidance.

Nothing would have been possible without the patient and exceedingly generous support of Krista Elena for getting my project going and keeping it afloat by sharing her experiences and teaching invaluable laboratory skills. Similarly, thank you to Alana Wang and Peng Liu for being gracious resources of mercury knowledge and analytical expertise. A huge thank you as well to Jing Ma for endless laboratory support with a smile and who many times deftly rescued me from what I perceived to be sure a disaster operating one of many intimidating analytical apparatuses.

Thank you to my research companion Sara Fellin for motivating and helping me get through this! The same goes to everyone else I have met and befriended during my time in Waterloo. I wish you all well!

Most importantly, I would never have completed this project without the complete and unwavering encouragement, love and support of my family and loved ones. Mom, Dad, Catherine, Madeleine and Laura - thank you so very much and I am sorry for complaining all the time! All of you will be sure to get signed copies of my thesis.

Table of Contents

List of Figures

List of Tables

List of Abbreviations

CLS	Canadian Light Source
CVAFS	Cold vapour atomic fluorescence spectrometry
DIRB	Dissimilatory iron-reducing bacteria
DOC	Dissolved organic carbon
DOM	Dissolved organic matter
DSRB	Dissimilatory sulfate-reducing bacteria
HDPE	High-density polyethylene
ICP-MS	Inductively coupled plasma mass spectrometry
ICP-OES	Inductively coupled plasma optical emission spectrometry
KPS	Potassium polysulfide
LCF	Linear combination fitting
MeHg	Methylmercury
OM	Organic Matter
PFTE	Polytetrafluoroethylene
PV	Pore volume
SRW	South River Water
THg	Total mercury (unfiltered)
THg-0.45	0.45 μm filtered total mercury
SOM	Soil organic matter
SXRMB	Soft X-ray Microcharacterization Beamline
TOC	Total organic carbon
U.S.-EPA	Environmental Protection Agency

XANES	X-ray absorption near edge structure

Chapter 1: Introduction

Mercury (Hg) has been sought after and utilized by humans for thousands of years due to its unique properties - notably its use in amalgamation processes first discovered in the 1st century BCE (Parsons & Percival, 2005). Over the years Hg, mined primarily in the ore mineral cinnabar (HgS), has been used for many processes and products; as pigment, in industry (*e.g.* as a cathode in the chlor-alkali industry) and in scientific instrumentation (*e.g.* the Hg barometer, Hg thermometer and in the study of electricity and development of early electronics) (Parsons & Percival, 2005). It has since been discovered that Hg, particularly in the organic methylmercury (MeHg) form, is highly toxic to humans and animals, with adverse effects to the nervous system, kidneys, cardiovascular system and increasing evidence of damage to the immune and reproductive systems of animals (Gupta et al., 2005; Goyer et al., 2000). Inorganic Hg can be converted to MeHg in aquatic environments, which bioaccumulates (concentrates) in the food chain (Environment and Climate Change Canada, 2013). Thus, the most common human exposure to Hg is through the consumption of fish and other marine foods (United Nations Environment Programme, 2013). Elevated Hg concentrations have broad ecosystem health and socioeconomic implications for those who rely on aquatic food stocks for both sustenance and income. Such is the case in Northwestern Ontario, Canada where the Ojibwa communities of Grassy Narrows and White Dog, located downstream of a chlor-alkali plant that discharged Hg from 1962 to 1970, were found to be exposed to high levels of Hg through fish consumption. Aside from food, fish provide these communities with an economic source in the form of tourism and commercial fishing. Thus, advising the Ojibwa to not eat the fish in the effected watercourse has had a crippling effect on their livelihood (Gupta et al., 2005).

Having a comprehensive understanding of the physical and chemical conditions that influence the transport and transformation of Hg is of utmost importance to characterizing Hg, identifying factors or perturbations that could impact the stability of Hg and developing remediation approaches for Hg-contaminated sites.

1.1 Mercury in the Environment: Speciation and Transport

Mercury occurs in the environment in a variety of forms including elemental Hg (Hg^0), inorganic Hg (Hg^+, Hg^{2+}) and organic MeHg [monomethylmercury, CH_3Hg^+, dimethylmercury, $(CH_3)_2Hg$]. Mercuric sulfide (HgS), which occurs naturally as the mineral cinnabar, is the most common form of Hg in the environment and, due to its extremely low solubility when in crystalline form, is considered to be relatively low toxicity (Boening, 2000; Greenwood & Earnshaw, 1997).

Transport of Hg and Hg complexes through soil depends on many factors including the characteristics of the soil surfaces, composition and particle size of Hg complexes, electrostatic forces between Hg complexes and soil surfaces and water chemistry (Bengtsson and Picado 2008; Zheng et al., 2016). The presence of natural organic matter (NOM) is very important in controlling the mobility of Hg, and the affinity of Hg for reduced sulfur sites within NOM compounds has been well documented (Loux, 1998; Ravichandran, 2004; Dittman et al., 2010). The Hg transported from soils and sediments into water bodies often forms complexes with particulate or dissolved organic matter (DOM). In aerobic, fresh waters aqueous Hg complexes with DOM ligands are dominant (Hintelmann & Harris, 2004; Hammerschmidt et al., 2008), whereas in anaerobic waters, Hg complexation with reduced sulfur species is favoured and HgS is the dominant form of Hg (Krabbenhoft et al., 2005). However, DOM can both dissolve, and

inhibit the precipitation and aggregation of HgS, resulting in a greater portion of smaller particle-size HgS particles that are more bioavailable (Ravichandran et al., 1998; Ravichandran et al., 1999; Zhang et al., 2011). Hg also has an affinity for clay minerals (Farrah & Pickering, 1978; Sarkar et al., 2000) and the presence of clay particles has been shown to increase Hg mobility through porous media (Zhu et al., 2012).

1.2 Site Background

The South River is located in Virginia, USA, within the Shenandoah Valley and with the North River and Middle River forms the South Fork of the Shenandoah River (Landis et al., 2014). Between 1929 and 1950, Hg was used in the production of textile fibres at a manufacturing plant in Waynesboro, Virginia and was discharged to the South River (Virginia Department of Environmental Quality, 2016). Elevated concentrations of Hg in the South River have resulted in MeHg in fish tissue well over the guideline for safe consumption of wild fish (consumption advisories are currently in effect over a 169-km span of river)(Brent & Berberich, 2013; Foran et al., 2015). Due to erosional processes, inundation of the South River bank and surface and groundwater transport, Hg contamination has developed into complex, non-point Hg sources up to 40 km downstream of the historical discharge point that continue to release Hg and MeHg to the river at elevated concentrations despite the long period of time that has passed since Hg was initially discharged to the environment (Flanders et al., 2010; Eggleston, 2009; Bergeron et al., 2010; Rhoades et al., 2009). The contaminated reach of the South River is relatively high gradient (4.25 m^3/s mean flow measured at Waynesboro, VA) with a coarse-grained substrate and low organic carbon (OC) and dissolved sulfate in surface water (Eggleston, 2009; Flanders et al., 2010).

The study area included two sampling locations: a riverbank sediment and a floodplain soil. The South River in the area where the riverbank sediment was acquired - relative river mile (RRM) 2.4, approximately 4 kilometers downstream of Waynesboro, VA - has a bankfull width and depth of 2.6 m and 1.9 m, respectively (Pizzuto, 2012). The floodplain study soil was acquired at RRM 11.8 at the Augusta Forestry Center, Crimora, VA, where studies identify higher MeHg biomagnification in floodplain food webs relative to aquatic foodwebs in the adjacent South River (Newman et al., 2011; Wang et al., 2013).

1.3 Mercury Remediation

The remediation of mercury contaminated sites is often challenging due to the large volumes of contaminated material that are frequently involved (Randall & Chattopadhyay, 2013). Due to the ability of Hg to methylate into a highly toxic form and enter food webs, relatively low concentrations of Hg necessitate evaluation of the environmental impact of Hg in the environment and whether remediation is required. Anthropogenic Hg sources near aquatic environments are problematic because they can continually release Hg to the environment long after initial placement, due to the formation of mobile Hg complexes like Hg-DOM (Gai et al., 2016). For example, increasing Hg concentrations in fish in lower East Fork Poplar Creek in Oak Ridge, Tennessee have been observed into the 2000s despite the cessation of Hg discharge in the 1960s (Han et al., 2006; Brooks & Southworth, 2011). The distribution of Hg at contaminated sites pose issues for remediation as contamination can be highly variable and not evenly distributed within sediments (Horvat et al., 2003). At South River, Hg contamination is widely-dispersed and *ex situ* remediation via extensive excavation or dredging of contaminated soil or sediment or pumping and treating of groundwater is unfeasible due to the environmental disruption, potential for resuspension of contaminants, and high costs and labour associated with

remediating large volumes of material necessary to capture complex and variable Hg distributions (Wang et al., 2012; Ghosh et al., 2011). Thus, *in situ* remediation techniques involving the adsorption or precipitation of immobile Hg compounds may be required to address wide-spread, non-point-source Hg contamination.

The introduction of reactive materials or solutions into contaminated soil and sediments may represent a practical and effective approach to stabilization and immobilization of Hg (Ghosh et al., 2011; Devasena & Nambi, 2013; Patmont et al., 2014). Removal of mobile Hg(II) from aqueous solutions has been achieved by addition of several reactive solids including metallic iron filings and zerovalent iron (Vernon & Bonzongo, 2014; Weisener et al., 2005), clay treated with thiol-containing complexes and high-temperature biochars with Hg forming Hg-O bonds in oxic, SO_4^{2-}poor environments (P. Liu et al., 2016; P. Liu et al., 2017) or forming Hg-S in the presence of sulfur thiols (Gibson et al., 2011). Stabilization of Hg has also been achieved by applying solutions including sodium thiosulfate ($Na_2S_2O_3$) to promote enhanced coagulation of Hg and the *in situ* formation of Mn- and Fe- (hydr)oxides as complexation surfaces for Hg (Lu et al., 2014; Lu et al., 2014).

While immobilization of Hg through adsorption to Fe- and Mn-(oxyhydr)oxides is viable in controlled and/or short-term circumstances, these mineral surfaces are not stable in environments where fluctuating redox environments and exposure to reducing bacteria can result in reductive dissolution of Fe- and Mn-(oxyhydr)oxides and release and mobilization of sorbed Hg (Chadwick et al., 2006; Harris-Hellal et al., 2011). Such is the case in the contaminated reach of the South River where fluctuations in river stage and inundations of the river bank result in the establishment of anoxic conditions in river sediments and floodplain soils where Hg could be adsorbed to (oxyhydr)oxide mineral surfaces. In sites such as South River, the promotion of Hg-

S binding or formation of HgS would be more thermodynamically favourable in the environment and preferable to less stable oxide binding (Gibson et al., 2011).

1.4 Research Objectives

This thesis presents two main research components: 1) an examination of the changes in Hg mobilization and transport from contaminated sediment in response to perturbations in solution chemistry, and 2) an evaluation of a sulfur solution as a stabilizer of Hg and a remediation option for Hg-contaminated soil. As part of the second component, Hg transport from both an aerobic and anaerobic control is also examined.

In the first component, perturbations to the input solution composition were made sequentially and applied to Hg-contaminated riverbank sediments in a saturated, flow-through column simulating groundwater conditions. The objective of this experiment was to identify changes in Hg transport as solution composition was varied in ways that could occur naturally or as a result of human intervention.

In the second component, a dilute sulfur (as polysulfide) solution was applied to an Hg-contaminated floodplain soil and the mobility of Hg and other parameters was observed both during and after the polysulfide application. Successful stabilization of Hg using a polysulfide solution has been achieved previously in a flow-through experiment (Devasena & Nambi, 2013). However, the experiment by Devasena and Nambi (2013) was carried out using a glass-bead porous media and elemental Hg. Thus, the objective of the research presented in this component was to assess Hg stabilization with a polysulfide solution application in a soil acquired from a contaminated field site. The anaerobic and aerobic control column experiments allow for a comparison of Hg transport from the same floodplain soil but under different redox conditions;

of interest when dealing with Hg contamination on a floodplain that undergoes inundation and fluctuating aerobic and anaerobic conditions.

The operational goal for the experiments of both research components is to simulate actual conditions that would be encountered at a contaminated site and thus, soil and sediment derived from the South River (*i.e.,* a historic contaminated site with Hg that has aged with the soil/sediment for over 60 years) is examined and flow rates approximate groundwater flow rates. Additionally, considering the serious detrimental impact of MeHg on human and environmental health, MeHg was also monitored throughout this research to examine how perturbations in solution chemistry may affect the Hg bioavailability to methylating bacteria. The overall goal for this research is to better understand the controls on Hg mobility in the soil and sediment of South River with attention to implications related to potential remediation strategies at South River and similar Hg contaminated sites.

1.5 Thesis Organization

This thesis is composed of two main research components introduced in Section 1.4 presented as two independent journal articles. Chapter 2 discusses saturated, flow-through column experiments with South River sediment where the input solutions are varied and effluent Hg, MeHg and other parameters are observed over time. Perturbations to the solution composition – including pH, ionic strength and alkalinity adjustments - approximate those that could occur naturally in the environment or due to human activity - and effluent concentrations provide indications of Hg release mechanisms and the dominant controls of Hg mobility. In Chapter 3, the mobility of Hg from a contaminated floodplain soil in a saturated, flow-through column experiment with the application of a dilute sulfur (as polysulfide) solution is presented. The experiment is conducted in an anaerobic environment to simulate a flooded, anoxic floodplain.

The results and discussions presented in both chapters aim to better understand the mechanisms involved in Hg transport by identifying relationships between solution chemistry and mobilized Hg while observing any potential connections to MeHg production.

Figure 1.1 - Maps showing the historic discharge point in Waynesboro, VA and the two sample locations: riverbank sediment from RRM 2.4 and floodplain soil from RRM 11.8. Satellite images acquired from Google Earth.

Chapter 2: Input Solution Amendments on Mercury Transformation and Release from Contaminated Soil under Saturated Flow Conditions

2.1 Synopsis

Mercury is a highly neurotoxic element that bioaccumulates in aquatic ecosystems. Historic discharge of Hg to the environment often leads to pervasive and extensive contamination due to persistent mobilization and transport of Hg from the initial release point for long periods of time after the discharge has occurred. Saturated, flow-through column experiments were conducted at relatively low flow rates to simulate natural groundwater flow. The input solutions to the columns varied in pH, ionic strength and alkalinity; effluent Hg and other parameters were measured to better understand the controls on Hg mobility. Release of weakly-bound Hg was observed in the early stages of the control and experimental column experiments. More reducing conditions and higher concentrations of Hg were observed in the effluent after changing to an input solution with increased pH (pH 8.2 to pH 8.7) and alkalinity (130 to 700 mg L^{-1} as $CaCO_3$). The increase in effluent Hg coincided with Fe and Mn maximum concentrations, suggesting that reductive dissolution of Fe-/Mn- (oxyhydr)oxides may have occurred and resulted in the release of Hg bound to these Fe-/Mn- (oxyhydr)oxide phases. Higher Hg concentrations also coincided with increased DOC in the effluent (26 mg/L in effluent relative to ~3 mg/L in the influent) and is attributed to strong complexation between Hg and organic matter contained in the sediment. The increased pH of the input solution was within the pH range in which electrostatic repulsive forces between DOC and Fe oxide minerals is favoured which may be another potential mechanism for Hg release at elevated pH. Effluent Hg concentrations rapidly decreased to control concentrations when the input pH was decreased from pH 8.7 to pH~6, which is consistent with the pH at which maximum Hg^{2+} sorption to various soils (pH ~6) has been

reported. The decreased pH would also favour electrostatic attraction between Hg-DOM complexes and Fe oxide mineral surfaces. A pronounced increase in input solution pH (pH~12) (Stage 4, 132 PVs) coincided with a sharp increase in Hg release along with elevated concentrations of effluent Fe, Mn and DOC and a drop in Eh, indicative of reductive dissolution of Fe-/Mn-(oxyhydr)oxides and associated release of Hg. This study suggests that Hg is mobilized with increasing pH and alkalinity and with the onset of more reducing conditions due to the reductive dissolution of Fe-/Mn-(oxyhydr)oxides and DOC and modification of electrostatic forces between DOC and Fe oxide mineral surfaces. Implications of these findings are: 1) the use of calcareous aggregate or cement for construction or remediation activities in Hg contaminated soil could significantly increase groundwater pH and mobilize Hg; 2) increased saturation of normally oxic sediments and soils could induce reducing conditions and increase mobilization of Hg; and 3) generation of slightly acidic conditions in Hg contaminated sediments or soils could potentially decrease Hg mobilization.

2.2 Introduction

Mercury (Hg) is a neurotoxin that can bioaccumulate in foodwebs and cause extreme health effects to ecosystems and has been classified as a major pollutant by Environment Canada (Environment and Climate Change Canada, 2011). Due to its unique properties, Hg has been used for numerous purposes - in base metal smelting and in the chlor-alkali industry – and in consumer products such as lightbulbs, thermometers and batteries. Since the 1950s and 1960s, the detrimental environmental impacts have become better understood and the use of Hg in manufacturing and industry has been greatly reduced. Stringent regulations for the disposal of Hg and Hg-containing goods have been developed and enforced, especially in the developed world. However, prior to the 1950s, the toxic nature of Hg was not well understood and proper

handling practices were not established and enforced resulting in unregulated discharge of Hg to the environment from many industries and users (Environment and Climate Change Canada, 2011). In Canada, the two main types of Hg-contaminated sites are former gold mines that used Hg amalgamation and chlor-alkali plants (Environment Canada, 2000).

Methymercury (MeHg) is considered the most toxic form of Hg. Severe detrimental health effects, including damage to the central nervous system and reproductive and development effects, can occur from both acute and chronic exposure to MeHg at lower concentrations than elemental and inorganic Hg (United States Environmental Protection Agency, 2000). Inorganic Hg is transformed to MeHg by dissimilatory iron- and sulfate-reducing and methanogenic bacteria (Graham et al., 2012; Gilmour et al., 2013; Paulson et al., 2016). Thus, MeHg concentrations in the environment significantly depend on the bioavailability of the form of inorganic Hg to methylating bacteria (Hsu-kim et al., 2013). Once MeHg is produced, it can biomagnify in aquatic food webs and reach concentrations in piscivores that are 10^7 times greater than aqueous concentrations (Environment and Climate Change Canada, 2013).

Due to industry often being proximal to water sources, Hg released to the environment is also often found accumulated in riparian soils (Poulin et al., 2016). Mercury(II) in soil bonds readily with soil organic matter (SOM) to form Hg-SOM complexes within days or weeks of deposition (Skyllberg et al., 2006; Hintelmann et al., 2002; Biester et al., 2002). Over time, Hg can form mercury sulfide phases in anoxic conditions (Barnett et al., 1997) and has recently been discovered to also form through the breaking of Hg-sulfur bonds of thiol-bound Hg in oxic conditions (Manceau et al., 2015). Mercury sulfide can be a desirable form of Hg in the environment, as it is very insoluble, less mobile relative to other Hg species and aggregation and growth of crystalline HgS can make Hg less bioavailable to methylating bacteria (Patnaik, 2003;

Gai et al., 2016; Zhang et al., 2011. However, in the presence of SOM, growth and aggregation of HgS can be inhibited or limited to the formation of nanoparticulate HgS particles or Hg-SOM complexes that are more bioavailable and mobile in the environment than more ordered, crystalline HgS (Ravichandran et al., 1999; Aiken et al., 2011; Graham et al., 2013; Deonarine & Hsu-Kim 2009; Pham et al., 2014). The mobility of Hg-SOM complexes through soils is relatively higher than other common Hg species (Zhu et al., 2014; Gai et al., 2016). Organic matter can release Hg through the enhanced dissolution of mercuric sulfide (Ravichandran et al., 1998) and organic acids can desorb and mobilize particulate-associated Hg or release colloidal HgS by dissolving mineral cements (Slowey et al., 2005).

As riparian soils periodically become saturated by river inundations, fluctuating water tables, and precipitation, it is important to understand the chemical controls that influence Hg mobility, as well as the mobility and stability of Hg complexes in saturated conditions. Changes in chemical characteristics of water as a result of natural processes or anthropogenic activities, such as remediation efforts, construction, or road runoff, can affect pore water pH, alkalinity and ionic strength. For example, groundwater pH could be greatly elevated proximal to deposition of cement or basic oxygen furnace slag (Lundén & Andersson, 1991; Stimson et al., 2010). Perturbations in ionic strength, for example, can arise from high precipitation events that dilute porewater ion concentrations or from road salt runoff or soil treatments that may raise ionic strength.

The pH of water in contact with Hg-contaminated soil can influence Hg mobility by affecting the sorption of Hg and Hg complexes to soil surfaces. Desorption of Hg^{2+} from soils is pH-dependant and generally follows a U-shape pattern where Hg^{2+} sorption to soil is strongest between pH 5 and 7 and decreases at pH<5 and pH>7 (Jing et al., 2007; Barrow & Cox, 1992;

Meng et al., 1998). At high pH (high -OH^- concentrations), Hg(II) forms very stable $Hg(OH)_2$ complexes, weakening Hg^{2+} adsorption to soil surfaces and potentially mobilizing Hg (Gabriel & Williamson 2004). However, variations in this sorption pattern have also been observed. Xu et al. 2014, noted increased sorption of Hg to soil as pH increased from pH 7 to 9, attributing it to the greater concentration of negative charges in the soil that can attract Hg(II) ions (Xu et al., 2014).

It is important to consider how solution pH affects natural organic matter (NOM) mobility as Hg discharged from industrial uses would likely associate with NOM over time (Biester et al., 2002) and NOM stability would be the primary control on Hg mobility. NOM with strong acid functional groups can coat particles and dominate surface charges, establishing negative surface charges on NOM-complexes if the pH is greater than pH ~3 (Santschi et al., 2002; Thompson et al., 2006). Commonly occurring iron (oxy)hydroxides have points of zero charge ranging from pH 8.1 to 9.5 (goethite; Kosmulski, 2011) and at circumneutral or slightly acidic pH, ligand exchange of the carboxyl and hydroxyl functional groups of NOM to iron oxide surfaces strongly adsorb NOM and limit mobility of NOM complexes (Vermeer et al., 1998; Gu et al., 1994). At pH values that are at or above the point of zero charge of iron oxides, neutralization or reversal of the positive surface charges of iron oxides occurs, leading to the development of repulsive forces between NOM-associated particles and soil surfaces (Tipping, 1981; Avena & Koopal, 1998). This same interaction would also be expected with NOM on aluminum and manganese oxide surfaces (Zuyi et al., 2000; Tipping & Heaton, 1983). Additionally, at much higher pH (pH 11-13), dissolution of NOM would occur (Grybos et al., 2009), releasing complexed Hg into solution (Xu et al., 2014).

Ionic strength can impact the mobility of Hg by affecting Hg adsorption to soil (Semu et al., 1987) and result in the release of colloidal HgS particles (Lowry et al., 2004). With other chemical properties held constant (*i.e.*, constant pH), a decrease in ionic strength typically results in higher concentrations of mobilized colloids (Grolimund & Borkevec, 1999). Conversely, a change in solution chemistry to an ionic composition with higher concentrations of divalent than monovalent cations can decrease colloid mobilization if concentrations approach the critical coagulation concentration (CCC) for colloids and destabilization occurs (Bunn et al., 2002; Bouby et al., 2011). The stronger charges of divalent cations than monovalent cations more effectively neutralize repulsive negative surface charges of colloids and promote deposition of colloids (Sen & Khilar 2006). For example, at sufficiently high Ca^{2+} concentrations, aggregation of metacinnabar has been observed (Ravichandran et al., 1999). Additionally, in the presence of divalent cations, the adsorption capacity of Fe and Mn oxide surfaces for NOM increases as cations compete for the negatively charged humic acid groups causing settlement and sorption (Tipping, 1981; Tipping & Heaton, 1983). Chloride can interfere with Hg binding and an inverse relationship between increasing Cl^- concentrations and Hg bound to organic matter has been observed (Gabriel & Williamson 2004).

In this study, saturated, controlled-flow column experiments were conducted to observe the release of Hg as the chemical composition of the input solution was varied. The experiments were designed to observe how changes to groundwater chemistry (*i.e.*, ionic strength, pH, alkalinity) affect Hg mobilization and methylation. Other constituents of the column effluent were quantified to identify relationships with Hg mobility and to better understand Hg release mechanisms. River bank sediment from the contaminated reach of a river impacted by Hg derived from a former textile manufacturing plant was acquired and used in the experiment. Five

different solutions were used in sequence as the column input. The five input solutions were amended from river water acquired upstream of the contaminated site and are summarized as follows:

1. Increased ionic strength with the addition of a divalent cation salt.
2. Increased pH and carbonate alkalinity without changing the ionic strength from input 1 but using a monovalent cation amendment.
3. Decreasing the pH and alkalinity keeping the ionic strength similar to inputs 1 and 2 with the addition of a monovalent cation salt.
4. Increasing the pH (with hydroxide) without increasing carbonate alkalinity (as in input 2) and without changing the ionic strength from inputs 1, 2 and 3 but by using a monovalent cation amendment.
5. Decreasing the pH of input 4 through acid addition to a value similar to the unamended input.

Two additional experiments were conducted to observe Hg mobilization when the input solution was amended to have:

1. a very low ionic strength input solution; and
2. an ionic strength (via divalent cation addition) at the CCC for typical soil colloids.

The details of these latter two experiments can be found in the Supporting Information for Chapter 2.

2.3 Methods and Materials

Sediment was obtained from within the Hg contaminated reach of the South River, 2.4 miles (3.8 km) downstream from the historic site of the textile manufacturing plant in Waynesboro, VA.

The sediment was collected in 5 L buckets from the bank of the river and shipped to the University of Waterloo where it was stored at 4^{o}C for approximately two years before use. The sediment was mechanically homogenized in 1 L Nalgene bottles before use in column experiments.

THg content in the sediment was determined after aqua regia digestion by cold vapour atomic fluorescence spectroscopy (CVAFS, Tekran© 2600 Sample Analysis System) following the U.S. Environmental Protection Agency (U.S.-EPA) 1631 Revision E method (U.S. EPA, 2002). Sequential extraction analyses were conducted on the sediment according to the methodology of Bloom et al. (2003) to determine the solid-phase THg soluble in the following reagents: deionized water (F1 fraction), 0.1 M CH_3COOH and 0.01 M HCl at pH 2 (F2 fraction), 0.1 M KOH (F3 fraction), 12 M HNO_3 (F4 fraction), and aqua regia (F5 fraction). The THg fractions were measured using the CVAFS and method outlined above.

Water (SRW) was collected regularly from South River upstream from the point of historic Hg release and was shipped to the University of Waterloo. Acrylic columns of 14.6 cm length and 3.81 cm inner diameter were constructed by fastening circular end-plates to the hollow cylindrical column with rubber gaskets for a water-tight seal. The bottom plate was fastened to the bottom (influent) end of the column and a layer of approximately 1 cm of silica sand was placed at the bottom of the column. Sediment was packed on top of the silica sand layer to approximately 1 cm from the top of the column as water flowed into the influent of the column using a high-precision multi-channel peristaltic pump (Ismatec, Switzerland). A silica sand layer was then placed at the top (effluent) end of the column to be flush with the end of the column and the top plate was fastened to the top of the column. Packing was completed in a fume hood and the columns were kept in an aerobic atmospheric environment. The pore volume

(PV) of the columns was determined as the mass difference between the final packed column and the column filled completely with water (measured before packing). Calculations of PV were made using the dry weight of the sediment to account for moisture contained in the sediment prior to packing.

Input solutions stored in 1.5 L amber bottles were pumped to the influent (bottom) of the columns through Teflon tubing using a high-precision peristaltic pump. Effluent flowed from the top of the columns through Teflon tubing and was collected in N_2-purged 250 mL amber bottles (Figure 2.1). Sample collection bottles were connected via Teflon tubing to overflow bottles containing water traps to reduce O_2 ingress into the collected effluent.

Input solutions were prepared in 0.5 L reaction flasks. Reagent masses were weighed and added to the reaction flasks with 0.5 L of SRW. The solutions were agitated manually until reagents were fully dissolved. Input solutions were applied to the column sequentially over various durations. Descriptions of the input solutions and the durations they were applied (in PVs) are provided in Table 2.1.

Water samples were collected regularly from a three-way valve at the top of the sample collection cell using sterile, single-use polypropylene/polyethylene 24 mL luer-lock syringes (Norm-Ject™). The samples were passed through 0.45 µm Supor® membrane filters (Acrodisc®, Pall Corporation) except for when periodic unfiltered (THg-unf) and 0.1 µm-filtered THg (THg-0.1) or unfiltered organic carbon (TOC) samples were collected. Samples for analysis of total Hg (THg), MeHg, dissolved organic carbon (DOC) and nutrients (phosphate and ammonia) were stored in 15 mL amber borosilicate vials (Qorpak®) with PFTE-lined screw caps; cation and anion samples were stored in 15 mL HDPE narrow mouth bottles (Nalgene™). All samples except anions were acidified to pH <2 immediately after collection; samples for THg and cation

analyses were acidified with ACS grade 69-70% HNO_3 (JT Baker), samples for MeHg analysis were acidified with ACS grade 36.5-38% HCl (JT Baker), and samples for organic carbon and nutrient analyses were acidified with High Purity H_2SO_4 (OmniTrace Ultra™, EMD Millipore Corporation). Samples for THg, OC, nutrients and cation analyses were stored at 4°C and samples for MeHg and anion analysis were frozen at -20°C immediately after collection and until analysis.

Concentrations of THg were determined using CVAFS and the technique stated above for the aqua regia digested sediments. MeHg analysis was carried out with the distillation, aqueous ethylation and purge and trap CVAFS technique (Tekran® 2750 methylmercury distillation system and a Tekran® 2700 automated methyl mercury analyzer) according to the U.S.-EPA 1630 method (U.S. EPA, 2001). Cation analysis was completed using inductively coupled plasma optical emission spectrometry (ICP-OES, iCAP 6000, Thermo Scientific) for major cations and inductively coupled plasma mass spectroscopy (ICP-MS, X-Series 2, Thermo Scientific) for trace elements. Anions were analyzed using ion chromatography (Dionex DX 600, Thermo Scientific) using a carbonate eluent for major anions.

Measurements of pH were made on unfiltered samples with an ROSS™ combination pH electrode (Orion™ 815600, Thermo Scientific™) calibrated with pH 4, 7 and 10 buffer solutions (Orion™, Thermo Scientific™). Redox potential (Eh) was measured with a platinum redox combination electrode with a $Ag/AgCl_2$ reference electrode (Orion™) checked against Zobell's (Nordstrom 1977) and Light's (Light 1972) solutions. Alkalinity was measured on 0.45 µm-filtered samples at the time of collection with a digital titrator and standardized 0.16 M H_2SO_4 (HACH). Bromocresol-green methyl-red was used as an indicator to measure bicarbonate alkalinity (reported as mg L^{-1} $CaCO_3$).

Ionic strength and saturation index calculations were made using the PHREEQCi geochemical speciation program (United States Geological Survey, 2017) and the PHREEQC database (Parkhurst et al., 1990).

2.4 Results and Discussion

2.4.1 South River Water and Sediment

The composition of South River bank sediment used in the flow through column experiments is presented in Table 2.2. The sediment contained 7.8 μg g^{-} dry weight Hg. The results of Hg content obtained through sequential extraction analyses are presented in Table 2.3. The highest proportion (50.4%) of Hg was found in the F3 (organo-complexed compounds) fraction, with 30.5% and 18.7% of Hg in the F5 (Hg sulfide/residual) and F4 (elemental/strong complexes) fractions, respectively. The chemical composition of the South River water used for column influent solutions is presented in Table 2.4.

2.4.2 Control Column Effluent

Effluent THg-0.45 increased initially in the control column to a maximum concentration of 113 ng L^{-1} after 6.2 PVs then decreased sharply to 37 ng L^{-1} at 22 PVs. Aside from an increased effluent THg-0.45 concentration plateau of between 60 and 71 ng L^{-1} from 63 to 92 PVs, effluent THg-0.45 varied between 13 and 24 ng L^{-1}. Effluent pH generally decreased throughout the experiment from pH 7.5 in the first sample to a minimum of pH 6.76 at 131 PVs before rebounding slightly to a pH of 7 at 179 PVs. Effluent Eh decreased sharply from an initial measurement of 462 mV in the first sample to a minimum of -41 mV at 15 PVs, increased to a maximum of 482 at 81 PVs, then remained relatively stable for the remainder of the experiment between ~300 and 400 mV. Effluent concentrations of NO_3, Mn, Fe and SO_4^{2-} are consistent

with the typical terminal electron acceptor sequence commonly observed from the submersion of organic carbon-rich soils (Weber et al., 2009); effluent NO_3^- concentrations decreased rapidly, effluent Mn increased after, then effluent Fe concentrations increased while SO_4^{2-} concentrations remained very low. Alkalinity in the effluent increased sharply to a maximum concentration of 446 mg L^{-1} as $CaCO_3$ then decreased and was generally between 96 and 169 mg L^{-1} as $CaCO_3$ from 36 to 178 PVs. Effluent THg-0.45 and DOC concentrations were strongly correlated throughout the experiment ($r^2 = 0.78$), as shown in (Figure 2.5).

2.4.3 Stage 1 – $CaCl_2$ Input

Stage 1 consisted of applying an input solution of SRW with 3.5 mM Ca (as $CaCl_2$) over 0 to 29 pore volumes (PVs). The input solution had a pH of 8.0 (control pH 8.2), alkalinity of 65 mg L^{-1} as $CaCO_3$ (control 130 mg L^{-1}) and ionic strength of 15 mM (control 5.7 mM).

During Stage 1, effluent THg-0.45 concentrations were similar to the control, decreasing steadily from 132 ng L^{-1} after 0.6 PVs to 31 ng L at 29 PVs (Figure 2.2). Initially, Hg bound to weaker binding sites in the soil, such as carboxyl or phenol functional groups, was likely mobilized by the Hg-free input solution and was eluted from the column (Drexel et al., 2002). The pool of weakly bound Hg became depleted during Stage 1 and correspondingly, a decreasing trend in effluent Hg was observed. Concentrations of NO_3^- and SO_4^{2-} did not decrease during Stage 1 as rapidly as observed in the control column. Effluent Mn concentrations were elevated during Stage 1, likely due to Mn(IV) reduction to Mn(III) and the dissolution of Mn(IV)-(hydr)oxide minerals within the column (Poulin et al., 2016). The maximum Fe concentration in the effluent (14.8 mg L^{-1}) also occurred during Stage 1 (12.5 PVs) and coincided with the lowest Eh value (61.5 mV) during Stage 1. The spike of effluent Fe suggests that reductive dissolution of Fe(III)-(hydr)oxides and release of Fe(II) into solution could be occurring in the column

(Poulin et al., 2016). Effluent dissolved organic carbon (DOC) was relatively high in early pore volumes reaching a maximum concentration of 35.6 mg L^{-1} at 2.2 PVs and decreased steadily to 7.4 mg L^{-1} at 29 PVs (Figure 2.3). As shown in Figure 2.5, DOC and effluent THg-0.45 concentrations appear to be correlated, albeit less strongly so than in the control column effluent. The pattern of effluent DOC concentrations resembled that of effluent Hg concentrations over time, suggesting a similar release mechanism for Hg and DOC. Dissolved organic carbon has a strong sorption affinity to Fe(III)/Mn(IV)-(hydr)oxides and would be desorbed from the (hydr)oxide soil surfaces upon reductive dissolution of Fe(III)/Mn(IV)-(hyrd)oxides (Grybos et al., 2009). Thus, in the event of Fe(III)/Mn(IV) dissolution and DOC release, Hg complexed with DOC would also be released into solution. The Ca^{2+} concentration in the input (3.5 mM Ca^{2+}) was above the critical coagulation concentrations (CCC) for typical soil colloids (1.9 to 2.6 mM Ca^{2+}) (Séquaris, 2010) and thus colloidal mobilization should have been suppressed. Unfiltered THg (THg-unf) reached a greater maximum concentration (209 ng L^{-1} at 8.9 PVs) than the control and THg-0.45 concentrations did not vary significantly from the control during Stage 1 with a relatively higher ionic strength input solution. Effluent DOC concentrations, however, were often lower with the increased Ca^{2+} concentrations in Stage 1 than in the control. Binding of Ca^{2+} to negatively charged humic acid molecules reduce the negative repulsive forces between molecules and can cause aggregation and deposition of humic-associated particles (Kloster et al., 2013). Similar effluent DOC results were observed in an additional column experiment in which the same elevated Ca^{2+} input solution was used and it is possible aggregation of DOC complexes occurred resulted in reduced mobility of DOC (see Supporting Information for Chapter 2).

Effluent MeHg increased initially reaching a maximum of 3.8 ng L^{-1} at 6.0 PVs then decreased to 0.65 ng L^{-1} by the end of Stage 1. The higher MeHg concentrations coincide with

the development of more reducing conditions in the column as suggested by the decreasing Eh and NO_3^- and increased Mn and Fe potentially indicating Mn(IV) and Fe(III) reduction. It is possible that bioavailable Hg was transformed to MeHg during Stage 1 as conditions became more reducing by dissimilatory iron-reducing or sulfate-reducing bacteria (DIRB and DSRB, respectively) and was eluted from the column with the initial mobilization of Hg from the column (Kerin et al., 2006). Effluent MeHg concentrations decreased as redox rebounded to more oxidizing conditions in the later pore volumes of Stage 1. The concentration of effluent MeHg was similar to that of the control and, as a percent of THg-0.45, was less during Stage 1 than the control which reached 11.0% MeHg at 19 PVs (compared to 5.3% MeHg at 13 PVs). DOM has been found to limit particle growth and aggregation and thus, increase bioavailability of small HgS particles to methylating bacteria (Graham et al., 2013). DOC concentrations were often lower than the control during Stage 1, potentially due to the relatively elevated Ca^{2+} concentration and ionic strength of the input solution. It is possible that the amended input solution suppressed methylation or decreased transport of MeHg by aggregating and reducing the mobility of DOC-associated Hg complexes.

2.4.4 Stage 2 – $KHCO_3$ Input

During Stage 2, a solution of SRW with 11 mM K^+ as $KHCO_3$ was input to the column from 29 to 108 PVs. The input solution pH (pH 8.7) and alkalinity (706 mg L^{-1} as $CaCO_3$) were greater than the Stage 1 input solution pH and alkalinity of pH 8.0 and 65 mg L^{-1} as $CaCO_3$ alkalinity and the control input (pH 8.2 and 130 mg L^{-1} as $CaCO_3$). The ionic strength of the Stage 2 input solution of 13 mM was similar to that of the Stage 1 input (15 mM) and greater than the control (5.7 mM).

Significant Hg mobilization occurred when the input was changed to the higher alkalinity and pH input solution, as shown in Figure 2.2, with a marked increase in cumulative THg-0.45 released during Stage 2. Effluent THg-0.45 increased steadily from 29 PVs reaching a maximum of 226 ng L^{-1} at 52 PVs. Effluent THg-0.45 concentrations decreased slightly throughout Stage 2 but remained elevated well above the control. The last sample taken during Stage 2 at 108 PVs (after 79 PVs of the Stage 2 input solution) of 173 ng L^{-1} THg-0.45 was an order of magnitude greater than the control (17 ng L^{-1}). Effluent alkalinity increased sharply to input concentrations within 3 PVs. Effluent pH increased from pH 6.74 at the end of Stage 1 to pH 7.47 at 39 PVs, 9 PVs after changing to the Stage 2 input solution. Effluent pH continued to increase after 39 PVs but at a slower rate reaching pH 7.8 at 108 PVs.

The Eh of the effluent initially decreased after the input change to a minimum of 35 mV at 43 PVs – less than the Eh in the control of 115 mV at 43 PVs. Redox increased to 370 mV at 56 PVs and was fairly stable for the remainder of Stage 2. Effluent Fe concentrations were less than 1.4 mg L^{-1} apart from a very high Fe concentration of 13.5 mg L^{-1} measured at 43 PVs. Effluent Mn concentrations decreased after the change of input solution and throughout Stage 2 from 7.6 mg L^{-1} at 30 PVs to 0.46 mg L^{-1} at 98 PVs. Effluent sulfate decreased sharply after the Stage 2 input switch from 33 mg L^{-1} at the end of Stage 1 to 0.15 mg L^{-1} after 1 PV in Stage 2. Effluent sulfate remained low (between 0.75 and 2.2 mg L^{-1}) until 84 PVs then increased to near input concentrations at 98 PVs and was 32 mg L^{-1} at the end of Stage 2 (108 PVs).

Effluent MeHg increased following the change to the Stage 2 input, reaching a maximum of 3.86 ng L^{-1} at 43 PVs which comprised 2.3% of THg-0.45 in the effluent sample. Concentrations of MeHg remained fairly stable for the remainder of Stage 2 ranging between 1.1 and 2.2 ng L^{-1} from 49 to 98 PVs. Effluent MeHg concentrations were greater than or similar to

the control throughout the Stage 2 PVs. However, effluent MeHg as a percentage of THg-0.45 released was lower than the control, ranging from 0.7 to 2.3% of THg-0.45 compared to 1.0 to 3.5% of THg-0.45 in the control effluent.

Dissolved organic carbon concentrations increased in the effluent following the input solution change reaching a maximum concentration during Stage 2 of 26.3 mg L^{-1} at 43 PVs (Figure 2.3). DOC concentrations decreased after 43 PVs but remained elevated relative to DOC concentrations in the control, resulting in a higher rate of cumulative DOC release relative to the control (Figure 2.4).

There is evidence for the contribution of several mechanisms to the increased mobilization of Hg from the column during Stage 2 relative to during Stage 1 and the control. Iron (III)-reducing conditions likely developed in the column during Stage 2; the maximum effluent Fe concentration in Stage 2 was coincident with the lowest Eh measured during Stage 2. The maximum Fe concentration preceded the maximum Hg concentration in the effluent during Stage 2, suggesting reductive dissolution of Fe(III)-(hydr)oxides resulted in the release of Hg and/or Hg-associated particles previously bound to Fe(III)-(hydr)oxide mineral surfaces.

Effluent THg-0.45 remained elevated after the high effluent Fe concentration was observed at 43 PVs and effluent Mn concentrations decreased to below control levels. A potential explanation for the consistent, elevated release of Hg from the column is the association of Hg to DOM complexes and mobilization of DOM with increased solution pH. The affinity of Hg to DOM complexes has been well documented (Ravichandran et al., 1998; Drexel et al., 2002) and the mobility of Hg-DOM is greater relative to inorganic Hg species (Gai et al., 2016). Correlations between DOC and Hg release have been observed in the environment (Brigham et al., 2009; Johannesson & Neumann, 2013) and in laboratory leaching experiments where high

pH reagents were used (Biester & Zimmer 1998). A strong correlation between THg-0.45 and DOC concentrations was also evident in the effluent of the control column (Figure 2.5). Adsorption of DOC to Fe and Mn oxides decreases with increasing pH as the electrostatic attraction between the negatively and positively charged surfaces of humic matter and oxide minerals, respectively, weaken (Gu et al., 1994; Avena & Koopal, 1998; Tipping, 1981; Tipping & Heaton, 1983). Effluent pH increased steadily throughout Stage 2 to within the point of zero charge (PZC) range of goethite (pH_{PZC} 7.2 to 9.6; for synthetic goethite) and the input solution of pH 8.7 was within the PZC range for ferrihydrite (pH_{PZC} 8.2 to 8.7) (Kosmulski, 2011). As the pH of the pore water in the column increased the surface charge of ferric (oxyhydr)oxide would become neutral or negative and mobilize humic complexes with negative surface charges through electrostatic repulsion (Vermeer et al., 1998). Desorption of DOM can increase the saturation of DOM on soil surfaces and subsequently mobilize more DOM complexes through molecule-molecule repulsion (Avena & Koopal, 1998). The stability of DOM in solution would then be maintained due to electrostatic repulsion (Angelico et al., 2014). Thus, DOM molecule-molecule repulsion, as well as the migration of higher pH pore water through the column developing electrostatic repulsion between DOM molecules and soil surfaces, could explain the continual, enhanced release of DOM and Hg occurring throughout Stage 2. Effluent Al concentrations during Stage 2 followed a similar trend to THg-0.45 and DOC. This correlation between Al and DOC is expected as dissolved organic matter controls the mobility of aluminum through soil (Hughes et al., 1990).

Another potential factor for the elevated Hg release is the increase of DOM solubility with increased pH as Hg bound to DOM would be released into solution upon DOM dissolution

(Grybos et al., 2009). Additionally, at higher pH and increased concentrations of –OH ligands, Hg could form Hg(OH) complexes which adsorb less strongly (Kim et al., 2004).

The maximum MeHg in the effluent during Stage 2 coincided with the most reducing Eh value of 34.8 mV, the maximum value effluent Fe concentration during input 2 and relatively very low sulfate concentrations at 43 PVs. Thus, transformation of Hg to MeHg is likely occurring in the column via DSRB and/or DIRB respiration (Kerin et al., 2006). However, after redox conditions increased, MeHg concentrations decreased to control levels and were stable for the remainder of Stage 2. As a percentage of THg-0.45, MeHg was consistently lower than the control after the maximum concentration at 43 PVs and could suggest that the MeHg concentrations in the effluent in Stage 2 could also be a factor of higher effluent THg concentrations overall and not necessarily greater MeHg production during Stage 2 relative the control.

2.4.5 Stage 3 – KCl Input

Stage 3 consisted of a solution of SRW with 11 mM K as KCl with pH adjusted to pH ~6 with HCl input to the column from 108 to 132 PVs. The input solution of Stage 3 was lower than in Stage 2 (pH 8.7) and the control (pH 8.2). The alkalinity of the Stage 3 input solution (38 mg L^{-1} as $CaCO_3$) was lower than alkalinity of the Stage 2 input (706 mg L^{-1} as $CaCO_3$) and the control (130 mg L^{-1} as $CaCO_3$). The ionic strength of the KCl input solution was 22 mM – greater than the ionic strengths of the Stage 1 (15 mM) and Stage 2 (13 mM) inputs.

Effluent THg-0.45 concentrations decreased sharply after the input was switched at Stage 3 from 173 ng L^{-1} at the end of Stage 2 (108 PVs) to 13 ng L^{-1} at 131 PVs after 23 PVs of the Stage 3 input solution (Figure 2.2). Effluent pH also decreased after the input was changed and

was pH 6.6 at 131 PVs, compared to pH 6.8 in the control column effluent. Effluent alkalinity decreased sharply from the Stage 2 input concentration to 102 mg L^{-1} at 114 PVs and decreased more gradually to 53 mg L^{-1} at 131 PVs. Effluent DOC concentrations also decreased throughout Stage 3 and reached 1.3 mg L^{-1} at 131 PVs, similar to the control effluent DOC concentration of 1.0 mg L^{-1} (Figure 2.3).

A strong correlation between effluent pH and THg-0.45 concentrations was evident throughout Stage 3. The decrease in THg during Stage 3 was expected as the pH of the input was within the pH 6-6.5 range where maximum Hg sorption has been reported in the literature (Jing et al., 2007; Barrow & Cox, 1992; Meng et al., 1998).

The decrease of both THg and DOC supports the hypothesis that a significant portion of mobilized THg is controlled by or associated with DOC. The pore water pH rapidly decreased to below the PZC of ferric (oxyhydr)oxides and thus, positive surface charges would form on ferric (oxyhydr)oxide minerals. Desorption of humic matter resulting from a pH increase is reversible (Avena & Koopal 1998). Therefore, DOC mobilized during Stage 2 that was not yet eluted from the column would be electrostatically attracted to soil surfaces and settlement and immobilization would become more favourable. Mercury associated with the mobilized DOC would also be immobilized in this scenario.

2.4.6 Stage 4 – KOH Input

During Stage 4, an input solution of SRW with 11 mM K^+ as KOH was applied to the column from 132 to 143 PVs. The Stage 4 input solution was pH 12.2, much greater than the control input and other experimental stages. The input alkalinity of 569 mg L^{-1} as $CaCO_3$ was greater

than Stage 3 but less than Stage 4. The ionic strength of the Stage 4 input solution was 6.4 mM, lower than Stage 3 (22 mM) and slightly higher than the control (5.7 mM).

When the input was changed to the highly basic pH, effluent THg-0.45 concentrations increased sharply and dramatically (Figure 2.2). Effluent THg-0.45 increased by two orders of magnitude from Stage 3 at 134 PVs (after 2.3 PVs) and reached a maximum of 6420 ng L^{-1} at 138 PVs. Effluent pH increased throughout Stage 4 reaching pH 8.27. Redox decreased sharply to a minimum Eh of 69 mV. Effluent NO_3^- increased throughout Stage 4 to 23 mg L^{-1} at the end of Stage 4. Effluent Mn and Fe also increased during Stage 4 reaching maximums of 2.3 and 7.0 mg L^{-1}, respectively, at 138 PVs. However, both Mn and Fe decreased in the next sample at 143 PVs. Effluent SO_4^{2+} also increased throughout Stage 4 reaching a maximum of 125 mg L^{-1}. Effluent MeHg increased to 25.3 ng L^{-1} at 138 PVs and was 0.4% of THg-0.45 in the effluent. At the end of Stage 4, MeHg in the effluent was 16.6 ng L^{-1} and comprised 0.3% of THg-0.45. Effluent DOC also increased sharply during Stage 4 to 32.9 mg L^{-1} at 138 PVs.

The sharp increase of the Stage 4 input solution pH would have resulted in significant dissolution of Hg complexes, minerals and adsorption surfaces as evidenced by the increase in effluent DOC, Fe and Mn during Stage 4. Dissolution of OM would occur at the very alkaline pH of the input and release in complexed Hg into solution (Xu et al., 2014). Effluent Mn and Fe concentrations increased during Stage 4 as solubility of solid-phase $Fe(OH)_3$ and MnO_2 would greatly increase at the pH of the input. Dissolution of mineral phases at high pH likely was the predominant factor in the high effluent concentrations during Stage 4 as a portion of the soil matrix would have been solubilized. At pH 12, the concentration of OH^- ligands present is high enough to dissolve HgS (Ravichandran et al., 1998). Once in solution, pore water conditions within the column would favour the formation of higher mobility, uncharged Hg-OH species like

$Hg(OH)_2$ (Kim et al., 2004). Uncharged Hg species adsorb much less strongly to mineral surfaces and would eluted from the column more readily (Xu et al., 2014).

The high concentrations of THg-0.45 in the effluent during Stage 4 was likely a significant factor in the relatively elevated effluent MeHg concentrations. The MeHg in the effluent comprised a very small fraction of THg-0.45 (0.3-0.4%).

2.4.7 Stage 5 – KOH with Decreased pH Input

During Stage 5, the input solution pH was lowered to pH 8.5 with HCl while maintaining the same concentration of K^+ (as 11 mM K^+). This solution was input to the column from 143 PVs until 171 PVs when the column was terminated. The alkalinity of the input of 38 mg L^{-1} as $CaCO_3$ was similar to the Stage 3 input solution. The ionic strength of the Stage 3 input solution was 11 mM, similar to the Stage 1 and 2 input solutions.

Effluent THg-0.45 concentrations decreased rapidly upon switching to the Stage 5 input solution (Figure 2.2). Concentrations of effluent THg-0.45 decreased from 1790 ng L^{-1} at 146 PVs to 20 ng L^{-1} at 158 PVs, similar to the concentrations in the control at this PV (15 ng L^{-1}). Effluent pH decreased rapidly from pH 8.3 at the end of Stage 4 to pH 7.4 at 158 PVs. Redox rebounded from the Stage 4 Eh of 69 mV to more oxidized conditions in Stage 5 ranging from Eh of 299 to 328 mV from 149 to 171 PVs. Effluent NO_3^- decreased following the input change and was <1 mg L^{-1} at 171 PVs. Effluent Mn and Fe concentrations continued to decrease from Stage 4 into Stage 5 and were 0.04 and 0.14 mg L^{-1}, respectively, at 158 PVs. Effluent SO_4^{2-} continued to increase from Stage 4 to a maximum of 450 mg L^{-1} at 146 PVs. Effluent DOC decreased from Stage 4 and was 4.9 mg L^{-1} at 158 PVs (Figure 2.3). Effluent MeHg concentrations in Stage 5 decreased from Stage 4 and ranged from 0.9 to 1.5 ng L^{-1}. However, MeHg concentrations at 158 and 171 PVs comprised 7.5 and 9.1% of effluent THg-0.45.

The decrease of both DOC and THg-0.45 with the input change further suggests a relationship between Hg and DOC association and transport mechanisms. Although, the decrease in DOC could also be due to the gradual depletion of mobile DOC from the column soil over the course of the experiment. The percentage of MeHg in the effluent as a fraction of THg-0.45 during Stage 5 was much higher than the control during these PVs and the highest of all experimental stages. A possible explanation for these relatively high MeHg fractions in the effluent during Stage 5 is that dissolution of Hg complexes, minerals and sorption surfaces that occurred during Stage 4 produced a larger pool of inorganic Hg(II) that was readily bioavailable to methylating bacteria (Hsu-kim et al., 2013).

2.5 Conclusions

This research demonstrates that Hg in contaminated riparian soils can be mobilized by increasing pH from pH~8.2 to pH~8.7 through bicarbonate addition and that the elevated release rate can be maintained for the duration of the increased pH input application (79 PVs) at 4 to 10 times the concentration of the control column (pH~8.2). Lowering input pH to pH ~6.1 resulted in decreased effluent Hg and DOC concentrations – in agreement with maximum Hg adsorption pH values reported in the literature (pH 6-6.5). The greatest flux of Hg occurred with hydroxide addition when the pH increased to pH~12, likely due to the dissolution of Hg organic complexes and Hg-bearing minerals and formation of highly mobile Hg-OH complexes. DOC and Hg concentrations were shown to be correlated, particularly in the control column. This correlation supports the hypothesis that Hg complexation with organic matter in the study sediment are significant and that controls on Hg and DOC mobility are similar.

It was also evident in this research that Hg mobility was sensitive to changes in redox variations. Increased Hg concentrations coincided with relatively low Eh and relatively high concentrations of aqueous Fe and/or Mn. Reductive dissolution of Mn(IV) and Fe(III)-(hydr)oxide minerals and consequent release of previously adsorbed Hg and associated complexes provides an explanation for the seemingly redox-dependent Hg mobilization.

Table 2.1 - Description of input solutions used in the varied input column experiment.

Input Solution	Description	Duration
Control	SRW	-
1	SRW + 3.5 Ca as $CaCl_2$	0 to 29 PVs
2	SRW + 11 mM K as $KHCO_3$	29 to 108 PVs
3	SRW + 11 mM K as KCl (adjusted to pH ~6 with HCl)	108 to 132 PVs
4	SRW + 11 mM K as KOH	132 to 143 PVs
5	SRW + 11 mM K as KOH (adjusted to pH ~8.5 with HCl)	143 to 171 PVs
CA[a]	SRW + 3.5 Ca as $CaCl_2$	0 to 116 PVs
NP[a]	Ultra-pure water (Milli-Q®)	0 to 65 PVs

[a] *Input solutions for columns in Supporting Information for Chapter 2.*

Table 2.2 - Chemical composition of South River bank sediment used in column experiments.

(μg g^{-1}) dry weight						
Hg	Fe	Mn	TOC	TIC	Total C	Total S
7.6	25 000	560	34 600	19 560	54 000	0.5

Table 2.3 – Hg (by dry weight and percent of total) obtained through sequential extraction in the South River bank sediment before used in the column experiments. (Ma & Paulson, 2014).

Fraction	Description	Targeted Compounds	Hg (ng g^{-1}, dry weight)	%
F1	Water Soluble	$HgCl_2$, $HgSO_4$	16	0.3
F2	Stomach Acid	HgO, $HgSO_4$	5	0.1
F3	Organo-complexed	Hg_2Cl_2, CH_3Hg	3270	50.4
F4	Elemental/Strong complexes	Hg_2Cl_2, Hg^0	1210	18.7
F5	Hg Sulfide/Residual	HgS, HgSe, HgAu	1980	30.5

Table 2.4 - Chemical composition of South River water (SRW) from upstream of historic mercury contamination source.

Influent Solution	
Parameter	**SRW**
pH	8.21
Eh (mV)	362
Alkalinity (mg L^{-1} as $CaCO_3$)	130
Cl^- (mg L^{-1})	60.2
NO_3^- (mg L^{-1})	14.6
SO_4^{2-} (mg L^{-1})	39.4
Ca (mg L^{-1})	29.0
K (mg L^{-1})	2.15
Mg (mg L^{-1})	10.8
Na (mg L^{-1})	5.16
Si (mg L^{-1})	3.14
Mn (µg L^{-1})	1.78
Fe (µg L^{-1})	14.3
DOC (mg L^{-1})	2.8
Ionic Strength (mM)	5.7

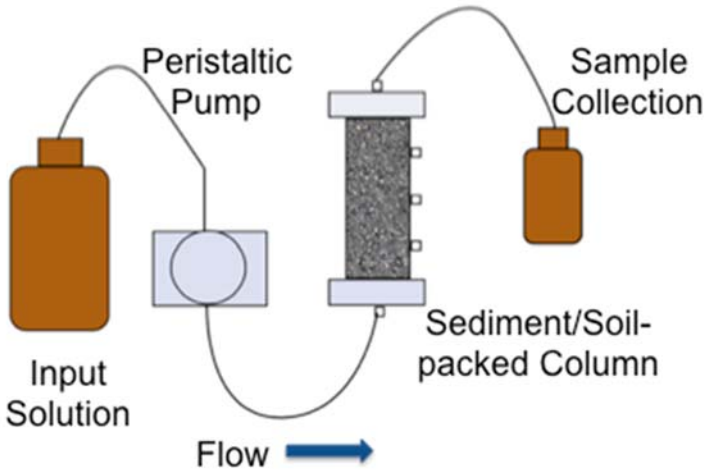

Figure 2.1 - Schematic diagram showing the experimental set-up.

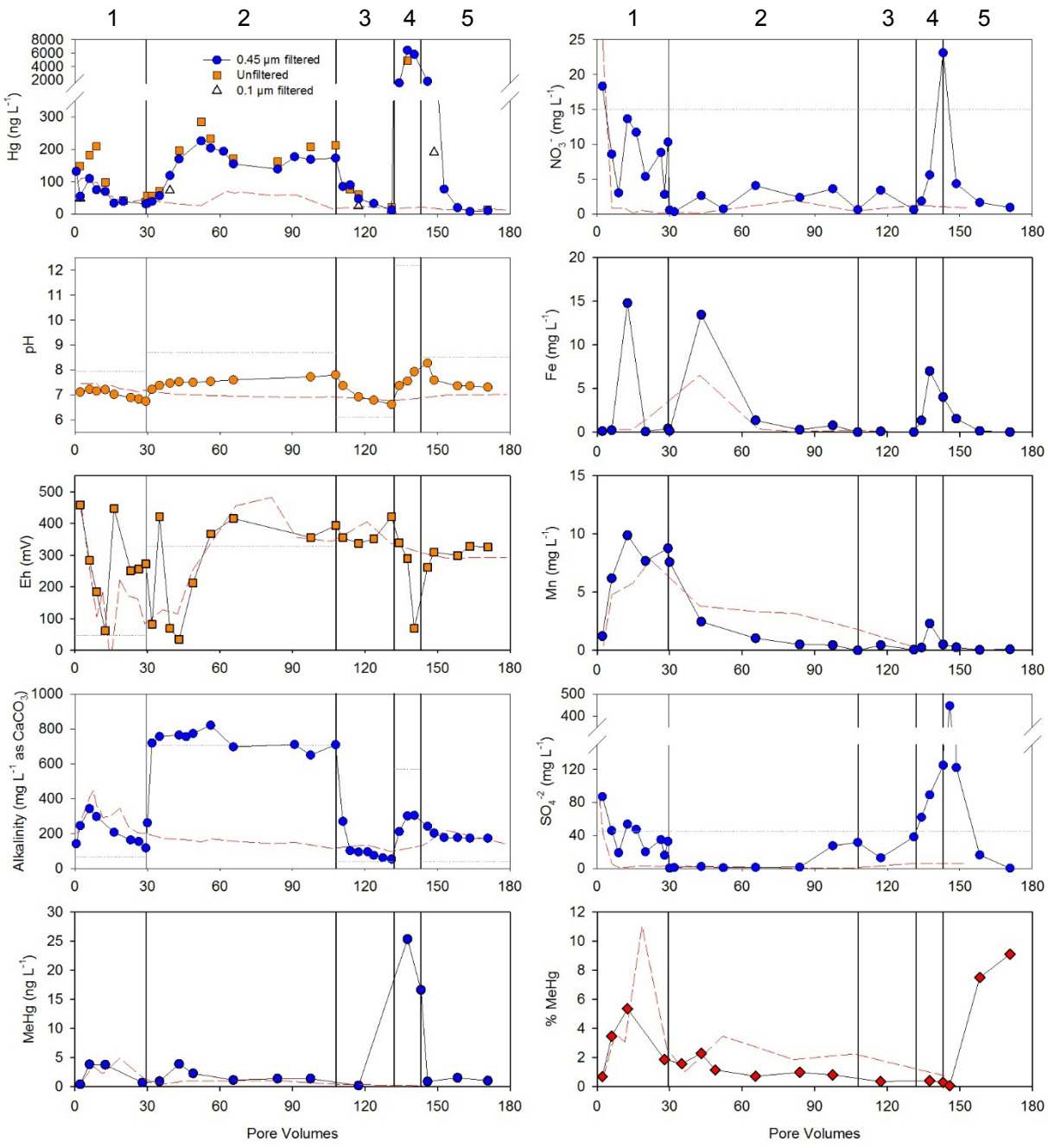

Figure 2.2 - Aqueous concentrations monitored over time in the varied input column effluent. Note vertical lines indicate a change of input solution, dashed lines represent control column effluent concentrations over time and dotted lines represent the input concentrations of the experimental column. Numbers 1 through 5 at the top of the page represent the five input solutions: 1) $CaCl_2$; 2) $KHCO_3$; 3) KCl; 4) KOH; and 5) KOH with decreased pH.

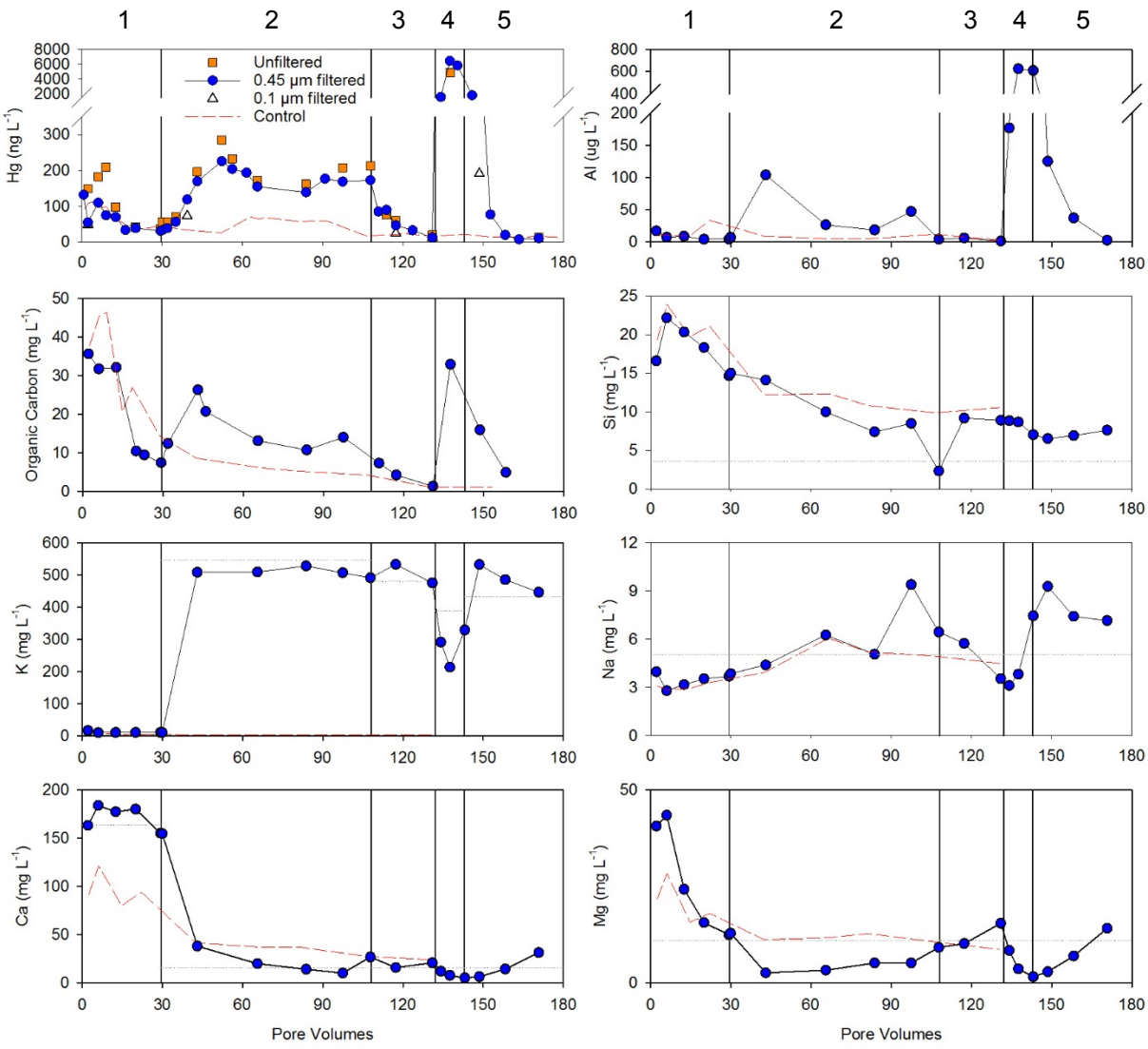

Figure 2.3 – Additional aqueous concentrations monitored over time in the varied input column effluent. Note vertical lines indicate a change of input solution, dashed lines represent control column effluent concentrations over time and dotted lines represent the input concentrations of the experimental column. Numbers 1 through 5 at the top of the page represent the five input solutions: 1) $CaCl_2$; 2) $KHCO_3$; 3) KCl; 4) KOH; and 5) KOH with decreased pH.

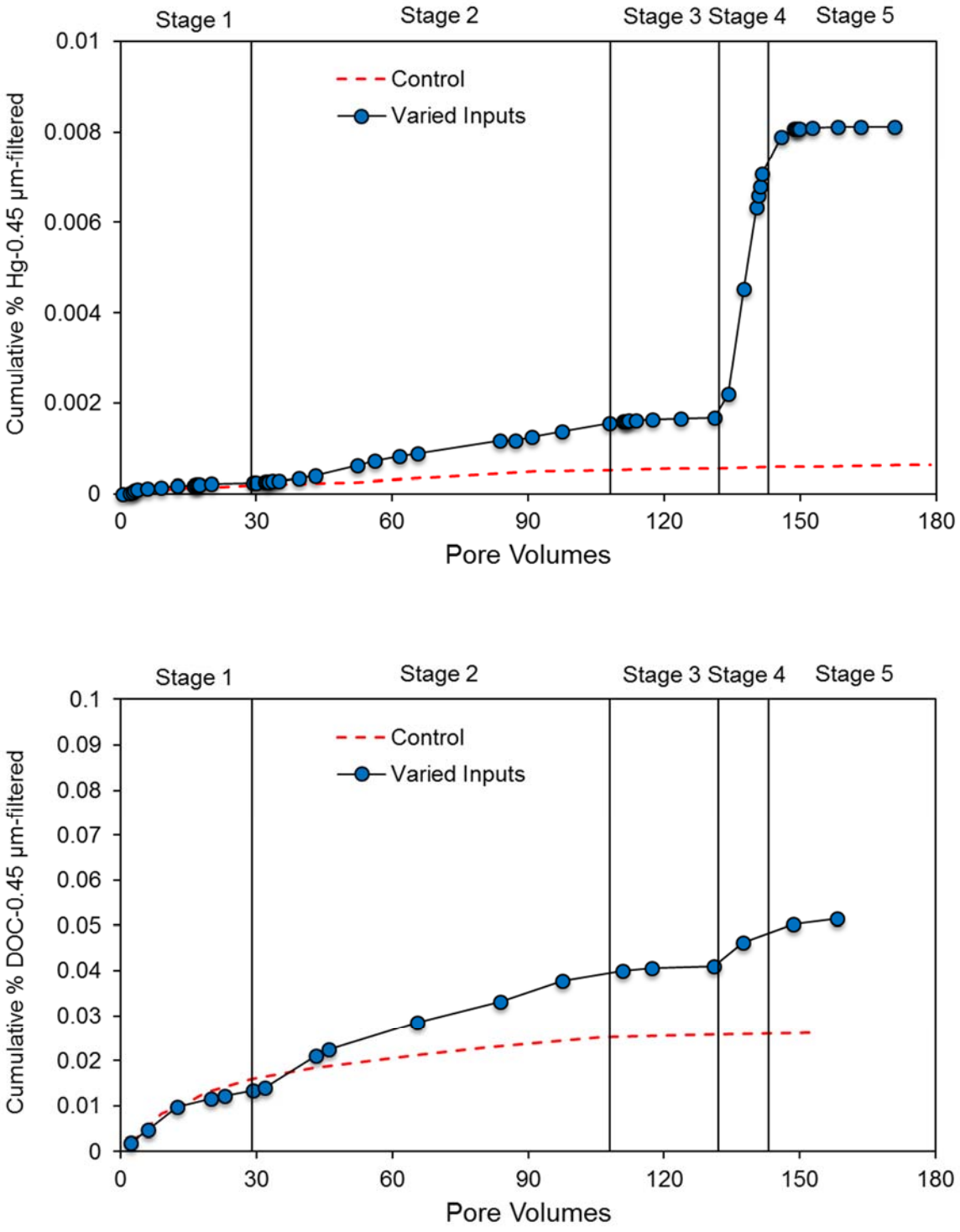

Figure 2.4 – Cumulative mass of 0.45 µm-filtered Hg (top) and DOC (bottom) measured in the control column and varied input column effluents over time. Note vertical lines indicate a change of input solution.

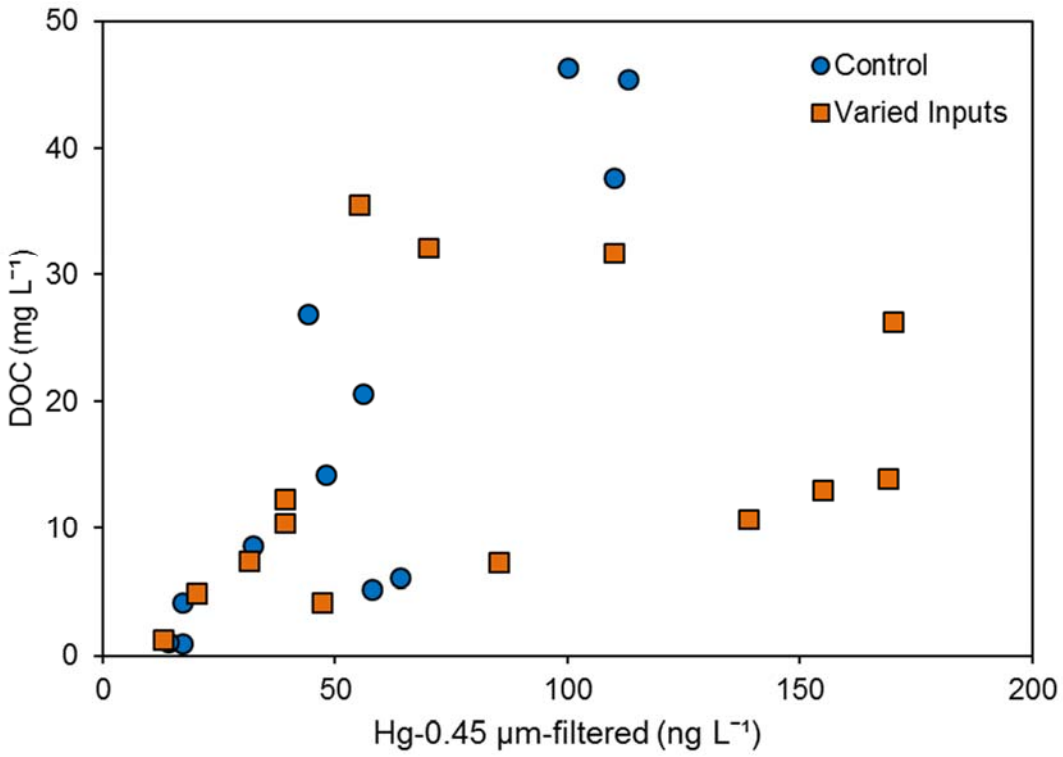

Figure 2.5 – Correlation between 0.45 µm-filtered Hg and DOC concentrations in control and varied input column effluents. Note: Hg-0.45 concentrations of 6,420 and 572 ng L^{-1} from the varied input column effluent are not shown on the plot.

Chapter 3: Addition of Polysulfide on Mercury Release from Contaminated Soil under Saturated Flow Conditions

3.1 Synopsis

Mercury is a persistent pollutant that is highly neurotoxic in its organic MeHg form. Historic Hg contaminated sites can leach Hg long after initial deposition, resulting in widespread contamination that presents many remediation challenges. Hg has a high affinity for sulfur species and HgS is less soluble and generally bioavailable to methylating bacteria and thus, *in situ* promotion of HgS precipitation is attractive as a remediation approach. Flow-through, saturated column experiments were conducted to investigate the effects of a dilute potassium polysulfide (KPS) solution on Hg mobility in contaminated floodplain soil. Additionally, the effects of aerobic and anaerobic conditions on Hg transport were investigated. Higher Hg concentrations were observed from sediment in aerobic conditions than sediment in an anaerobic environment receiving an anoxic input solution. Under aerobic conditions, two distinct effluent Hg maxima were observed and two separate release mechanisms were hypothesized: 1) oxidative dissolution of disordered HgS releasing Hg at earlier pore volumes of flow and 2) reductive dissolution of Fe-/Mn-(oxyhydr)oxides releasing sorbed Hg compounds at later pore volumes with the onset of more reducing conditions. A similar early pore volume Hg maximum was not observed in the anaerobic column effluent and the later Hg maximum was much less pronounced suggesting that oxidative processes in the aerobic column were significant in increasing the pool of mobile Hg in the column. Effluent Hg concentrations increased by three orders of magnitude relative to the control when a dilute KPS solution (1 mM S) while no significant changes in other effluent concentrations were observed. The increase effluent Hg is consistent with the increase in HgS solubility in the presence of polysulfide as reported in the literature and Hg likely was

released from the column in the mobile $Hg(S_x)_2^{2-}$ form. In addition to the dissolution of HgS, Hg could also be stripped from NOM thiol groups which would be outcompeted by polysulfide Hg complexation. An additional Hg increase observed after the cessation of KPS solution application coincided with the onset of reducing conditions in the column. The magnitude of the second effluent Hg increase was greater than the increase observed in the control column when more reducing conditions were identified, suggesting that the KPS application increased the overall mobility of the Hg pool by increasing the amount of Hg compounds sorbed to Fe-/Mn-(oxyhydr)oxides. XANES analysis of the column soil after the KPS application indicated that S species in the soil did not vary from the control column suggesting the addition of KPS did not substantially alter the soil S speciation. This research demonstrated that remediation of Hg-contaminated soil with addition of polysulfide is problematic due to the formation of mobile Hg-S species.

3.2 Introduction

Mercury (Hg) is a metal with unique properties and detrimental environmental impacts; particularly when present as the highly neurotoxic, organic methylmercury (MeHg) (Hsu-kim et al., 2013). Despite stricter regulations regarding the use and disposal of Hg, past anthropogenic activities such as mining, metal refining, manufacturing and chemicals production have discharged large quantities of Hg and caused contaminated sites worldwide (Pacyna & Pacyna, 2005). Mercury in the environment can be methylated in reducing, anoxic environments by sulfur-reducing bacteria (SRB) or iron-reducing bacteria (FeRB) (Gilmour et al., 1992; Fleming et al., 2006). MeHg can be taken up in vegetation or biomagnify in aquatic food chains with a very high bioaccumulation factor and can be found in fish at concentrations 3 million times

greater than in the water (Wang et al., 2012; Zillioux et al., 1993), presenting the need for the development of remediation methods for sites with very low concentrations of Hg (<100 ng L^{-1}).

For sites with Hg contamination above 260 mg kg^{-1}, excavation is generally used for removal and the contaminated material is either stored or treated *ex situ* (Wang et al., 2012). In the case of a more disseminated contaminant distributed both laterally and at depth in low concentrations, extensive excavation and treatment or storage of large quantities of material may not be a practical or feasible remediation option. Immobilization through the addition of sulfur-containing solutions has shown promise as a method of *in situ* treatment of Hg due to the high affinity of Hg, a soft Lewis acid, for soft bases; particularly sulfide (S(-II)) and organic thiolate (RS-) (Behra et al., 2001; Haitzer et al., 2003). In the presence of sulfide minerals, Hg is removed from solution through adsorption to sulfide mineral surfaces or is coprecipitated as Hg sulfide (HgS) (Wolfenden et al., 2005). Formation of HgS (or cinnabar) is desirable due to its water insolubility (Patnaik, 2003) and the decreased bioavailability of Hg to methylating bacteria as crystalline HgS as opposed to dissolved and nanoparticulate species (Zhang et al., 2011). *In situ* mercuric sulfide formation in the subsurface of a contaminated site has been identified (Barnett et al., 1997).

Successful stabilization of aqueous Hg with iron sulfide has been demonstrated in several experiments (Liu et al., 2008; Piao & Bishop, 2006). Bower, et al. decreased Hg mobility in a flow-through column experiment with a reactive barrier containing pyrite (Bower et al., 2008); which could be implemented as an *in situ* treatment option. However, where subsurface Hg contamination is wide-spread and flow paths through groundwater cannot be predicted or sufficiently contained, application of a reactive solution may be more feasible than a reactive barrier that requires the contaminant to pass through. Xiong, et al. demonstrated a 67% reduction

of water-leachable Hg in flow-through column experiments with a solution containing stabilized iron sulfide nanoparticles (Xiong et al., 2009). Treatment of Hg-spiked, natural soil with colloidal sulfur significantly reduced Hg transport in laboratory pot experiments (Kot et al., 2007). In a flow-through, glass bead-porous media micromodel experiment, a sodium polysulfide solution was used to *in situ* stabilize elemental Hg by conversion to HgS (Devasena & Nambi 2013). In the experiment by Devasena and Nambi, ~10% of entrapped elemental Hg was stabilized as HgS and the remainder of Hg was immobilized through encapsulation within the precipitated HgS.

In this study, the application of polysulfide to a soil from a site with historic Hg contamination was investigated. Polysulfide (S_x^{2-}, where x = 3 – 6) is formed through sulfur and sulfide reaction or as an intermediate in sulfur cycling (Jay et al., 2000). While stabilization of Hg with the addition of sodium polysulfide via HgS formation and entrapment has been successful with inorganic Hg, this approach has not been investigated with Hg contaminated soil where the Hg has been present in soil for a long time (~50 years) and at relatively low concentrations. Increasing the sulfur concentration can have adverse environmental effects on Hg form and stability. Mercury solubility can increase in the presence of excess sulfur by forming soluble Hg disulfide (HgS_2^{2-}), especially under alkaline conditions (Svensson et al., 2006). Additionally, concentrations of elemental sulfur contained in polysulfides can redissolve stable HgS that had formed (Paquette & Helz, 1995; Paquette & Helz, 1997). It was found that calcium polysulfide needed to react with air and breakdown to thiosulfate and sulfide species in order to be effective and otherwise increased the leachability of elemental Hg and HgS (Osborne-Lee et al., 1999). Forming sulfate species would not be desirable however, due to an increased potential for Hg methylation by sulfate-reducing bacteria.

The objective of this study is to observe Hg release from soil obtained from within the Hg-contaminated reach of the South River, downstream from the historic site of a textile manufacturing plant in Waynesboro, VA. The experiments were conducted in fully-saturated, flow-through columns in an anaerobic environment with and without the addition of a potassium polysulfide (KPS) solution. For comparison, an additional control column was conducted in an aerobic environment. Effluent Hg concentration and other parameters were measured temporally and spatially along the length of the column.

3.3 Methods and Materials

Soil containing approximately 47.6 μg g^{-1} dry weight Hg was obtained from within the Hg-contaminated reach of the South River, 11.8 miles (19 km) downstream from the historic site of the textile manufacturing plant in Waynesboro, VA. The soil was collected from the floodplain and stored in 5 L buckets. The soil was shipped to the University of Waterloo, stored at 4°C and used in the columns after approximately 20 months of storage.

The soil was digested in aqua regia and analyzed for THg using cold vapour atomic fluorescence spectroscopy (CVAFS, Tekran© 2600 Sample Analysis System) according to the U.S. Environmental Protection Agency (U.S.-EPA) 1631 Revision E method (U.S. EPA, 2002). Fractionation of inorganic Hg in the soil was determined via sequential extraction with the following leaching media (Bloom, et al. 2003): deionized water (F1 fraction), 0.01 M HCL and 0.1 M CH_3COOH (F2 fraction), 1 M KOH (F3 fraction), 12 M HNO_3 (F4 fraction), and aqua regia (F5 fraction). THg in the leachate was measured using the CVAFS method stated above.

Water not impacted by the historic Hg contamination (SRW) was acquired from the South River upstream of the historic contamination source. The columns were constructed by

fastening two circular acrylic plates to a hollow cylindrical acrylic column of 14.6 cm length and 3.81 cm i.d.. Before packing, perforated Teflon tubing was adhered to a threaded fitting (Suagelock©) and inserted into the port openings. Rubber tubing with two-way valves at one end was connected to the fittings along the lengths of the columns for sampling of pore water during the experiment. To pack the column, the bottom plate was fastened to the column and SRW allowed to flow into the influent (bottom) end of the column using a high-precision, multi-channel peristaltic pump (Ismatec, Switzerland). A 1 cm layer of silica sand was first placed at the bottom of the column, followed by soil up to approximately 1 cm below the top of the column. A top layer of silica sand was placed to be flush with the top of the column and then the top plate was fastened to the effluent end of the column. The anaerobic columns were packed in an oxygen-free glovebox and were housed there for the duration of the experiment. The pore volume (PV) of each column was calculated using the difference between the weight of the final packed column and the column packed fully with water (measured before packing) taking in consideration the starting water content of the soil.

Input solutions were stored in 1.5 L amber bottles. Influent was pumped to the columns through Teflon tubing using a peristaltic pump. Flow occurred upwards from the bottom to the top of the columns against gravity. Effluent was collected in 250 mL amber bottles via Teflon tubing as shown in Figure 3.1. For the anaerobic columns, input solutions were purged with Ar gas inside the glovebox before use.

A 1 mM sulfur as KPS solution was prepared by mixing 59.2 mg of K_2S_x (Sigma-Aldrich) with 1 L of Ar-purged SRW inside the glovebox. The solution was manually agitated until the K_2S_x was dissolved. For the first 3 PVs, Ar-purged SRW was inputted to the experimental column. The input solution was changed to the KPS solution from ~3 to ~11 PVs in

order for 1 mmol to enter the column. The input was then returned to purged SRW for the duration of the experiment (61 ± 2.1 PVs). The aerobic and anaerobic control columns received unamended SRW for the duration of the experiment.

Effluent samples were collected regularly from a 3-way valve at the top of the sample collection bottle with a sterile, single-use polypropylene/polyethylene 24 mL luer-lock syringe (Norm-Ject™). Port samples were collected at 7.0 (± 0.1) and 47.5 (± 1.2). Samples were collected from these ports by attaching a 30 mL glass syringe to the two-way valve of one port and opening the valve while closing off all other effluent openings. Sample collection occurred at the flow rate held constant by the peristaltic pump over the duration of the experiment and was completed sequentially from the top to the bottom port.

Samples were passed through 0.45 μm Supor® membrane filters (Acrodisc®, Pall Corporation) at the time of sampling except for periodic unfiltered THg (THg-unf) and organic carbon (TOC) samples or 0.1 μm filtered THg (THg-0.1). Total Hg (THg), MeHg, dissolved organic carbon (DOC) and nutrients (phosphate and ammonia) were stored in 15 mL amber borosilicate vials (Qorpak®) with PFTE-lined screw caps. Cation and anion samples were stored in 15 mL HDPE narrow mouth bottles (Nalgene©). Samples for THg and cation analyses were acidified with ACS grade 69-70% HNO_3 (JT Baker), samples for organic carbon and nutrient analyses were acidified with High Purity H_2SO_4 (OmniTrace Ultra™, EMD Millipore Corporation) and samples for MeHg analysis were acidified with ACS grade 36.5-38% HCl (JT Baker) to pH <2 immediately after collection. Samples for T-Hg, TOC, DOC, nutrients (phosphate and ammonia) and cation analysis were stored at 4°C and samples for MeHg and anion analysis were frozen and stored at -20°C immediately.

Mercury was analyzed using CVAFS (Tekran© 2600 Sample Analysis System) and the EPA 1631 Revision E method (U.S. EPA, 2002). MeHg analysis was carried out with the distillation, aqueous ethylation and purge and trap CVAFS technique (Tekran® 2750 methylmercury distillation system and a Tekran® 2700 automated methyl mercury analyzer) according to the EPA 1630 method (U.S. EPA, 2001). Cation analysis was completed using inductively coupled plasma optical emission spectrometry (ICP-OES, iCAP 6000, Thermo Scientific) for major cations and inductively coupled plasma mass spectroscopy (ICP-MS, X-Series 2, Thermo Scientific) for minor cations. Anions were analyzed using ion chromatography (Dionex DX 600, Thermo Scientific) using a hydroxide eluent for organic acids (lactate, acetate, propionate and formate) and a carbonate eluent for major anions.

Measurements of pH were made on unfiltered sample with a ROSS™ combination pH electrode (Orion™ 815600, Thermo Scientific™) calibrated with pH 4, 7 and 10 buffer solutions (Orion™, Thermo Scientific™). Redox potential (Eh) was measured using a platinum redox combination electrode with a $Ag/AgCl_2$ reference electrode (Orion™, Thermo Scientific™) checked against Zobell's (Nordstrom, 1977) and Light's (Light, 1972) solutions. Bromocresol-green methyl-red indicator was used to measure bicarbonate alkalinity (reported as mg L^{-1} $CaCO_3$). Alkalinity was measured on 0.45 μm-filtered samples at the time of collection with a digital titrator and standardized 0.16 M H_2SO_4 (HACH).

K-edge X-ray absorption near edge structure (XANES) spectra were collected for sulfur on samples and reference materials at the Soft X-ray Microcharacterization Beamline (SXRMB) at the Canadian Light Source (CLS, University of Saskatchewan, Saskatoon, SK, Canada). Inorganic S reference materials analyzed were gypsum, pyrite and K_2S_x. The spectra of ferrous sulfate ($FeSO_4$), pyrrhotite ($Fe_{1-x}S$), dimercaptan (an organosulfide compound), tetramethylene

sulfoxide (C_4H_8OS), butyl sulfone ($[CH_3(CH_2)_3]_2SO_2$) and sodium methanesulfonate (CH_3SO_3Na) were obtained from a previous beamtime and thianthrene was obtained from an online database (European Synchrotron Radiation Facility 2017). The solid K_2S_x used for the KPS input solution was also analyzed. Solid samples were acquired from the bottom and top ports of each column after ~30 PVs by stopping flow, removing the port tubing and scraping a small (<0.5 g) amount of material out of the top and bottom port openings with a sterilized, single-use needle. Samples were freeze-dried for a minimum of 24 hours and transported in an anaerobic container to CLS. Samples were homogenized and ground with pestle and mortar then spread evenly on double-sided tape adhered to a copper plate. The sample plate was placed in a chamber under vacuum for synchrotron analysis. Total electron yield spectra were collected for each sample and reference materials.

Three scans were collected for the samples, K_2S_x and reference materials. The ATHENA program was used to aggregate data and compare sample and reference material spectra (Ravel & Newville, 2005). Linear combination fitting (LCF) was performed with Athena to estimate relative percentages of S species in each sample and K_2S_x using reference material spectra with peaks at the same energy as sample spectra peaks in the Athena LCF computations.

3.4 Results and Discussion

3.4.1 Input Solution Aqueous Chemistry

The SRW was pH 8.5 and alkalinity of 170 mg L^{-1} as $CaCO_3$. Calcium (33 mg L^{-1}), Mg (12.3 mg L^{-1}) and Na (6.6 mg L^{-1}) were the dominant cations and Cl (4.5 mg L^{-1}), SO_4^{2-} (4.1 mg L^{-1}) and NO_3^- (1.8 mg L^{-1}) were the dominant anions. The SRW aqueous chemistry is summarized in Table 3.1.

The input solution to apply KPS to the experimental column had a S concentration of 34.2 mg L^{-1} and K concentration of 29.7 mg L^{-1}, compared to 4.2 mg L^{-1} S and 3.4 mg L^{-1} K in SRW. The SO_4^{2-} concentration in the KPS solution was 18.3 mg L^{-1} compared to 4.1 mg L^{-1} in SRW.

3.4.2 S XANES Characterization of KPS

The S XANES spectra collected from the K_2S_x used for the KPS input solution showed peak positions that indicated the presence of reduced sulfur species (2471.9 eV) and oxidized sulfur species represented by sulfoxide-like (2476.2 eV), sulfone-like (2479 eV) and sulfonate-like (2481.4 ev) peak positions (Figure 3.2).

The relative proportions of S species in K_2S_x estimated using LCF are shown in Table 3.4. The best fit was achieved with the reference material S spectra for pyrite, tetramethylene sulfoxide, butyl sulfone and sodium methanesulfonate. Sulfide-like sulfur was estimated to comprise the greatest proportion of sulfur in the K_2S_x (39%), followed by sulfone-like (30%) and sulfoxide-like sulfur (28%).

3.4.4 Floodplain Soil Solid Phase

The solid phase concentrations of the floodplain soil used in the saturated flow-through column experiment are summarized in Table 3.2. The mass of solid-phase Hg of the soil was determined through sequential extractions and the results are tabulated by dry weight and percent of total Hg content in Table 3.3. The majority of Hg (89% of total) was found in the F5 fraction with a reagent that targets Hg sulfides, while the F4 fraction targeting strongly-complexed and elemental Hg and the F3 fraction targeting organo-complexed Hg comprised 6.0% and 4.4% of solid-phase Hg in the soil, respectively.

3.4.5 Aerobic and Anaerobic Control Column Effluent

The aqueous concentrations in the effluent of the aerobic and anaerobic control columns over time are shown in Figure 3.3. As shown in Figure 3.5, a greater mass of THg was released from the aerobic column relative to the anaerobic column over the course of the experiment. Two distinct THg concentrations maxima were observed in the aerobic column effluent: a lesser maximum of 5.93×10^3 ng L^{-1} at 14 PVs and a maximum THg concentration of 7.11×10^3 ng L^{-1} at 33 PVs. The anaerobic control had a maximum THg concentration of 1.47×10^3 ng L^{-1} at 27 PVs.

The effluent pH in both columns increased from pH~6.3 to maximum values then decreased at a more gradual rate for the remainder of the experiment. The maximum pH was observed in the anaerobic column effluent at 16 PVs (pH 7.7) and in the aerobic column effluent at 33 PVs (pH 7.4). Effluent pH in the anaerobic column was consistently higher than the aerobic column effluent. Similar to pH, effluent alkalinity increased at a higher rate in the anaerobic column than the aerobic column. The maximum alkalinity concentrations were 274 mg L^{-1} as

$CaCO_3$ in the anaerobic effluent at 16 PVs and 307 mg L^{-1} as $CaCO_3$ in the aerobic column at 33 PVs. Alkalinity decreased gradually in both control effluents after the maxima were observed.

Redox determinations (Eh) were lower in the anaerobic column for the entirety of the experiment with the exception of between 33 and 38 PVs when Eh increased to a maximum value of 260 mV at 34 PVs in the anaerobic effluent while Eh decreased to a minimum of 82 mV in the aerobic column effluent. The anaerobic column Eh was a minimum of -110 mV at 16 PVs. Effluent NO_3^- concentrations in the anaerobic column decreased from 2.4 mg L^{-1} at 2.4 PVs and were <1.1 mg L^{-1} for the duration of the experiment. The aerobic column effluent had a very high NO_3^- concentration at 1.4 PVs but decreased and was <1.2 mg L^{-1} for the duration of the experiment. The maximum Mn concentration in the anaerobic column effluent was 25.8 mg L^{-1} at 21 PVs and the maximum Mn concentration in the aerobic column effluent 29.0 mg L^{-1} at 33 PVs. Concentrations of Fe were generally greater in the anaerobic column effluent than the aerobic column effluent. The maximum Fe concentration in the anaerobic effluent was 10.2 mg L^{-1} at 45 PVs compared to a maximum Fe concentration of 8.0 mg L^{-1} at 46 PVs from the aerobic column. Effluent SO_4^{2-} concentrations were generally higher in the anaerobic column than the aerobic column. The maximum SO_4^{2-} concentration in the anaerobic effluent of 38 mg L^{-1} was observed at 6.3 PVs and was much greater than the maximum SO_4^{2-} concentration in the aerobic effluent of 22 mg L^{-1} at 60 PVs.

The maximum DOC concentration of 50.8 mg L^{-1} observed in the anaerobic column effluent at 21 PVs was much greater than DOC concentrations in the aerobic column effluent which did not exceed 18 mg L^{-1} during the 60 PVs.

Effluent MeHg concentrations were much higher in the anaerobic column effluent than the aerobic column reaching a maximum concentration of 31.7 ng L^{-1} at 46 PVs before

decreasing to <0.02 ng L^{-1} at 61 PVs. The maximum MeHg concentration in the anaerobic column comprised 3.4% of THg-0.45, and was the highest MeHg fraction measured in the aerobic or anaerobic control column effluent. The maximum MeHg concentration in the aerobic column effluent was 10.2 ng L^{-1} at 33 PVs and comprised 0.14% of THg-0.45 in the effluent at the corresponding PV. At 60 PVs, the MeHg concentration in the aerobic effluent was 5.6 ng L^{-1}, but was a higher fraction of THg-0.45 (1.7%) than at the maximum observed MeHg concentration.

The two distinct THg maxima in the aerobic column effluent could indicate two potential release processes or mechanisms. The first THg maximum could be the release of Hg following oxidative dissolution of HgS. It has been found that elemental Hg discharged to a floodplain in the 1950s and 1960s at a similar contaminated site had since formed authigenic HgS through sulfate reduction (Barnett et al., 1997). Manceau et al., found that HgS could also form in soil organic matter through Hg(II)-thiol sulfur complexes (Manceau et al., 2015). Synchrotron analysis of several riverbank sediments and floodplain soils from the South River site indicate Hg in the form of HgS (Gibson, 2013). Therefore, it is likely that a significant fraction of Hg in the experiment soil had undergone transformation from elemental Hg to crystalline HgS during annual inundations of the South River that could result in anoxic, sulfate-reducing conditions. Due to the reduced sulfur component, HgS is thermodynamically unstable, as evident by the equilibrium constant for oxidative dissolution by aqueous O_2 (Barnett et al., 2001; Desrochers, 2013):

$$HgS_{(s)} + 2O_{2(aq)} + 2H_2O \leftrightarrow Hg(OH)_2^0 + SO_4^{2-} + 2H^+ \qquad K = 10^{93}\ (I = 0\ M, 25^oC) \qquad \text{Eq. 1}$$

The elevated dissolved O_2 in the aerobic column influent relative to the anaerobic column influent thus makes oxidative dissolution of HgS and/or other sulfides relatively more

favourable, as shown in Equation 1. Barnett et al., observed very low Hg release rates from flow-through column experiments and found the weathering rate of HgS to be very slow relative to other minerals considered to be stable in soil (Barnett et al., 2001). Holley et al. found oxidative dissolution rates of HgS by O_2 were 10-100 times higher than Barnett et al. when 10 times less initial solid-phase HgS was used in the experiment (Holley et al., 2007). As the initial THg concentration in this experiment was much lower than that in Holley et al., it is possible that the oxidative dissolution rate of HgS is perhaps exponentially higher still.

Oxidative dissolution would be catalyzed by the presence of dissolved organic matter (DOM) present in the soil and, at lesser concentrations, in the input solution. The facilitation of HgS dissolution by DOM has been observed extensively (Ravichandran et al., 1998; Waples et al., 2005; Slowey, 2010). Sulfur-Hg bonds could be weakened through sulfide oxidation by oxidized DOC, resulting in surface complexation and release of Hg according to the following (Ravichandran et al., 1998):

$$>HgS + DOM_{oxidized} \rightarrow > \text{new site} + Hg^{2+} + S^0 + DOM_{reduced} \qquad \text{Eq. 2}$$

Ravichandran et al. did not detect sulfide oxidation by DOM in a deoxygenated experiment indicating that the effect of DOM on HgS-sulfide oxidative dissolution is of a catalytic nature as opposed to the driving factor (Ravichandran et al., 1998). Under anaerobic conditions, the impact of DOM on HgS dissolution would likely be reduced, and could be a factor in the lower Hg release from the anaerobic column.

Additionally, HgS formed in the presence of DOM is more disordered and is much more soluble and more readily dissolved than HgS (Slowey, 2010). It is reasonable to assume that any HgS that formed in the study soil *in situ* occurred with significant DOM concentrations that would increase the solubility of HgS to higher values than observed by Barnet et al. (2001) and

Holley et al (2007). The likelihood of a more unstable form of HgS form would be greater at the relatively low Hg concentration in this soil compared to at higher Hg concentrations where larger aggregates of HgS particles would likely form (Slowey, 2010).

The early Hg release could also be in part due to a release of relatively poorly sorbed Hg from the soil upon the onset of pumping. Mercury can be initially sorbed to strong organic thiol functional group binding sites or weak carboxyl or phenol functional group binding sites (Drexel et al., 2002). When the Hg-free input solution flowed through the column, poorly sorbed Hg could desorb from the soil and be eluted from the column. This early PV release of Hg has been observed in other flow-through experiments (Xiong et al., 2009; Desrochers, 2013; Paulson et al., 2016).

The second Hg maximum in the aerobic column effluent at 33 PVs could be the result of Hg sorbed to the surface of Fe- and/or Mn-(hydr)oxides minerals that are reductively dissolved following a decrease in Eh. Following dissolution of HgS, an amount of THg(II) and Hg-DOM complexes would likely sorb to Mn(IV)/ Fe(III)-(hydr)oxide mineral surfaces in the soil (Kim et al., 2004) (Grybos et al., 2009). At 33 PVs, the Eh of the aerobic column effluent decreased from 349 mV to 85 mV and then to a minimum of 82 mV at 38 PVs. Effluent NO_3^- concentrations were <1 mg L^{-1}. Effluent Mn increased to a maximum concentration of 29.0 mg L^{-1} at 33 PVs and effluent Fe increased sharply to 5.9 mg L^{-1} at 33 PVs. Decreasing NO_3^-, followed by increases in Mn and Fe concentrations agrees with the expected sequence of electron acceptor reduction (Stumm & Morgan, 1981) and provides evidence for the reductive dissolution of Mn(IV)- and Fe(III)-(hydr)oxides minerals. The THg release following the observation of electron receptor reduction in this experiment has been observed in other soil flooding experiments conducted both with and without the presence of atmospheric oxygen (Hofacker et

al., 2013; Poulin et al., 2016) as well as in field measurements of a deep confined aquifer where increased Hg concentrations coincided with a region of dissimilatory Fe reduction and increased dissolved Fe(II) concentrations (Johannesson & Neumann, 2013).

The relatively lower release of THg from the anaerobic column could be a result of the lack of dissolved oxygen in the input solution and the aerobic conditions in which oxidative dissolution of HgS is favoured. The maximum THg-0.45 concentration of 1470 ng L^{-1} (1710 ng L^{-1}) in the anaerobic control effluent was measured at 27 PVs, later than the aerobic control THg-0.45 maximum (27 PVs). At 21 PVs, effluent NO_3^- concentrations were <1 mg L^{-1}, effluent Mn concentrations increased from <0.5 mg L^{-1} to a maximum concentration of 25.8 mg L^{-1} and effluent Fe increased from <1 mg L^{-1} to 8.6 mg L^{-1}. As the maximum effluent THg concentration was observed at 27 PVs and followed the maximum effluent Mn and a sharp increase in effluent Fe concentrations, it is possible that reductive dissolution of Mn(IV)- and Fe(III)-(hydr)oxide minerals occurred releasing sorbed THg species. In the aerobic column, Hg could have been released following HgS oxidative dissolution and either be eluted from the column or sorb onto Mn(IV)- and Fe(III)-(hydr)oxide minerals to later be released as Mn(IV) and Fe(III) reduction occurred. However, in the anaerobic column where dissolution of HgS may be limited due to relatively low O_2 concentrations, Hg mobilization was dominated by the reductive dissolution of sorption surfaces in the form of Mn(IV)/Fe(III)-(hydr)oxide minerals. Thus, the pool of Hg sorbed to Mn(IV)/Fe(III)-(hydr)oxide mineral surfaces was likely smaller relative to the aerobic column where HgS dissolution occurred and less Hg is released following Mn and Fe reduction. Additionally, DOC, which can enhance the dissolution of HgS and was hypothesized to be a catalyst for Hg release in the aerobic column, does not oxidize sulfide in the absence of oxygen (Ravichandran et al., 1998).

Methylmercury production was higher in the anaerobic column than the aerobic column which is in agreement with the requirement for reducing conditions in an anoxic environment for Hg methylation to occur (Gilmour et al., 1992). Effluent MeHg from the anaerobic column increased throughout the experiment and reached a maximum of 31.7 ng L^{-1} at 46 PVs (3.4% of THg-0.45) before dropping to below detection level (<0.02 ng L^{-1}) by 61 PVs. In the aerobic column, MeHg reached a maximum effluent concentration of 10.2 ng L^{-1} (0.14% of THg-0.45) at 33 PVs. The MeHg maximum concentration coincided with the maximum effluent Hg concentration from the aerobic column. This correlation could suggest a shared release mechanism for inorganic and MeHg or a potential analytical artifact that can occur with the analysis of samples with relatively high inorganic Hg content (Perez et al., 2017). Effluent Eh was lowest at around this PV, and Mn and Fe increased in the effluent indicating Mn(IV)/Fe(III)-(hydr)oxide reductive dissolution could be occurring. A significant fraction of MeHg adsorbed to these (hydr)oxide minerals, along with inorganic Hg, could therefore be released at their highest concentrations at the onset of the dissolution of the sorbing surfaces.

While MeHg decreased to below detection level in the anaerobic column at 61 PVs, MeHg continued to be eluted from the aerobic column at significant concentrations (<3.7 ng L^{-1}) until 86 PVs (not pictured in Figure 3.3). This difference could be due to the less efficient methylation of Hg in the aerobic column. More reducing conditions were established earlier and generally maintained in the anaerobic column which would likely stimulate Hg-methylating bacteria populations at an earlier PV than in the aerobic column. The aerobic column had higher Eh and increased effluent Fe - an indicator of Fe(III) reduction - at a later pore volume than the anaerobic column. The establishment of Fe-reducing conditions is particularly important as

dissimilatory FeRB have been found to be significant methylators of Hg (Fleming et al., 2006; Kerin et al., 2006).

3.4.6 Polysulfide Application

For the first 3.3 PVs of the experiment, Ar-purged SRW without KPS was input to condition the column. A 1 mM KPS solution was applied from 3.3 to 15 PVs. During the KPS application, THg was eluted from the column at much greater concentrations than from the anaerobic control (as shown in Figure 3.4, and as cumulative mass in Figure 3.5) and aerobic control column. The effluent THg-0.45 concentration reached a maximum of 129×10^3 ng L^{-1} (244×10^3 ng L^{-1} THg-unf) at 6.2 PVs, three orders of magnitude greater than the anaerobic control. Effluent pH, alkalinity and Eh in the KPS column were similar to the anaerobic control for the duration of the experiment. The similarity of the measured effluent parameters in the KPS and control columns during the KPS application suggests that the interaction between Hg and polysulfide is the dominant factor in the large flux of effluent THg-0.45.

Solubility of HgS increases in the presence of excess sulfur as polysulfide (Paquette & Helz, 1997) and thiols will be outcompeted by polysulfide at S(-II) concentrations greater than 0.01 μM (Skyllberg, 2008). In the presence of polysulfide and in the pH range encountered in this experiment, HgS solubility was found to be 200 times greater than without polysulfide due to the form of the dominant aqueous complex $Hg(S_x)_2^{2-}$ (Jay et al., 2000). This increase in solubility is approximately equal to the difference between the maximum effluent THg concentration in the control and the KPS column and it is reasonable to assume that the initial maximum of Hg eluted during KPS application was caused by the dissolution of HgS and the formation of aqueous $Hg(S_x)_2^{2-}$.

Another process potentially contributing to the observed Hg release is the displacement of Hg sorbed to Fe(III)-hydr(oxides) by polysulfide. This could occur via exchange of bisulfide for a hydroxyl group (Slowey & Brown Jr., 2007):

$$=FeOHHgOH + HS^- \rightarrow =FeSH^- + Hg(OH)_2 \qquad \text{Eq. 3}$$

or by complexing to Hg and weakening the surface bonds (Slowey & Brown Jr., 2007):

$$=FeOHHgOH + HS^- \rightarrow =FeOHHgSH + OH^- \rightarrow =FeOH + Hg(SH)(OH)_{aq} \qquad \text{Eq. 4}$$

With the KPS application occurring for ~12 PVs, it is likely that the process of HgS dissolution, adsorption of a fraction of aqueous Hg not eluted from the column to (hydr)oxide minerals and subsequent displacement by polysulfide was an ongoing process during the KPS application.

Effluent THg concentrations remained elevated relative to the control after the KPS application ceased and the input was returned to unamended SRW, as demonstrated by the higher slope of cumulative THg released after 13 PVs (Figure 3.5). These elevated concentrations were likely due to an increased pool of aqueous Hg species formed through HgS dissolution sorbed to the soil matter. An increase in effluent Hg concentrations occurred after the KPS application at 21 PVs to 12.7×10^3 ng L^{-1} THg-0.45 (17.6×10^3 ng L^{-1} unfiltered). This spike in Hg concentration followed an increase in effluent Mn at 18 PVs suggesting reductive dissolution of Mn(IV)-(hydr)oxides. Another slight increase in effluent Hg at 45 PVs coincided with an increase in Fe eluted from the column. This suggests, as was observed with the control, that Hg complexes are sorbed to Mn(IV) and Fe(III) (hydr)oxides and are released upon Mn(IV) and Fe(III) reduction and dissolution of (hydr)oxide minerals (Kim et al., 2004; Poulin et al., 2016). It is reasonable to assume that during the KPS application when pore water Hg concentrations were very high, Hg complexes sorbed to weak binding sites like carboxyl or phenol functional groups (Drexel et al., 2002). When the KPS application was ceased and pore

water Hg concentrations decreased, weakly sorbed Hg would be gradually mobilized from the column resulting in a gradual decrease in effluent Hg concentration as opposed to a sharp decrease.

3.4.7 Pore Water Aqueous Concentrations

Sampling of the ports along the length of the column was conducted at 7 PVs during the KPS input application and at 49 PVs – 38 PVs after the KPS input application was changed to the SRW. Aqueous concentrations of the sampled pore water at 7 and 49 PVs are shown in Figure 3.6 and Figure 3.7, respectively.

3.4.7.1 Early Pore Water Sampling (7 PVs)

At 7 PVs, THg-0.45 concentrations in water extracted from the KPS column ports increased along the length of the column in the direction of flow and were roughly two orders of magnitude greater than the control. The maximum THg-0.45 concentration of 1.86×10^6 ng L^{-1} - in the top port of the KPS column – was approximately 200-fold greater than the maximum THg-0.45 concentration sampled from the control column ports (1.47×10^4 ng L^{-1}). This discrepancy in aqueous THg-0.45 concentrations in the KPS and control column ports was similar to the discrepancy in THg-0.45 concentrations in the KPS and control column effluent. The relatively higher aqueous THg-0.45 concentration in the KPS column was also in agreement with the 200-fold increase of HgS solubility in the presence of polysulfide as opposed to without polysulfide reported in the literature (Jay et al., 2000).

Concentrations of Mn and Fe were greater in the water from the bottom port of the KPS column relative to the control column and could indicate reductive dissolution of Mn(IV)/

Fe(III)-(hydr)oxides facilitated by polysulfide (Chrysochoou & Johnston, 2015; Zhong et al., 2009). Increases in aqueous Fe and Mn concentrations were observed in other experiments where polysulfide was applied to soils (Chrysochoou et al., 2012; Ridley, 2007). Pore water Fe and Mn concentrations were not elevated relative to the control in the middle and top ports indicating that mobilized Fe and Mn could have adsorbed to the soil as it flowed upward. The reducing effect of the polysulfide is supported by the more reducing Eh in the lower and middle ports of the KPS column compared to the control.

Concentrations of MeHg were elevated well above the control in the water extracted from the bottom and top ports of the KPS column at 7 PVs. The maximum MeHg concentration was 119 ng L^{-1} in the bottom port pore water and was <0.03 ng L^{-1} in the middle port of the KPS column. The maximum MeHg concentration in the control column was 2.9 ng L^{-1} in the bottom port and was also <0.03 ng L^{-1} in the middle port. As a fraction of THg-0.45, however, MeHg concentrations were similar in the KPS and control columns and comprised a very low percentage of THg-0.45 – evidence of potential analytical bias of MeHg in samples with relatively higher inorganic Hg. In the bottom port pore water, MeHg concentrations were 0.028% and 0.039% of THg-0.45 in the KPS and control columns, respectively.

3.4.7.2 Late Pore Water Sampling (49 PVs)

At 49 PVs, the pore water chemistry of the KPS column was very similar to that of the control. The bottom and middle ports of the KPS column had lower pore water THg-0.45 concentrations (38 and 66 ng L^{-1}, respectively) compared to the control (151 and 462 ng L^{-1}, respectively). During the KPS input application, the soil at the bottom of the column would be exposed to KPS first, mobilizing THg as dissolved Hg-S_x^{2-} complexes upwards in the direction of flow. Polysulfide would also react with other constituents (*e.g.* DOM, surface minerals), decreasing the

pool of reactive S_x^{2-} along the flow path. Thus, the impact on THg by polysulfide would be greatest at the bottom of the column and decrease along the flow path. Lower concentrations of reactive S_x^{2-} at the top of the column would have resulted in less THg mobilized from the soil at the top of the column relative to the bottom. Thus, at later PVs, concentrations of THg-0.45 would be greater in the water extracted from the port at the top of the column than the bottom of the column, where a large fraction of the THg pool had already been mobilized and eluted from the column by the KPS input.

Pore water MeHg concentrations were greatest in the top ports relative to the middle and bottom ports in both the KPS and control columns. The maximum MeHg concentration was higher in the top port of the control column at 341 ng L^{-1} than the KPS column at 86.3 ng L^{-1}. As a fraction of THg-0.45, MeHg was highest in the bottom ports of the KPS and control columns (12.6 ± 0.2% MeHg).

3.4.8 S XANES Characterization of Column Soil

The S XANES spectra collected for the soil samples extracted from the bottom and top ports of the anaerobic control and KPS-treated columns after approximately 30 PVs along with the reference materials used in analyses are displayed in Figure 3.8. The XANES reference spectra represent reduced sulfur species (pyrrhotite through thiophene) to oxidized sulfur species (SO_4^{2-}) (P. Liu et al., 2016). The spectra for all four samples display peaks that are consistent with thianthrene- and thiophene-like (2474.3 eV), sulfoxide-like (2476.2 eV) and sulfate-like (2482.5 eV) S species. A peak corresponding to sulfide-like S species (pyrrhotite, 2470.4 eV), however, only appeared to be present in the spectra from the samples extracted from the bottom ports of the control and KPS columns and not from the top port samples. The peaks corresponding to

sulfate-like S species in both the top ports are more pronounced in the top port sample spectra than the bottom port sample spectra.

Analysis by LCF was conducted to determine the relative concentration of S species in the four columns, as shown in Table 3.4.

The reference material S spectra for the HgS, dibenzo-thiophene, butyl-sulfone and ferrous sulfate were used to provide the best fit for the spectra of top port samples, whereas pyrrhotite, dibenzo-thiophene, butyl-sulfone and ferrous/potassium sulfate were used to provide the best fit for the bottom port spectra. The best fits as determined by LCF for the top ports of each column are essentially identical, confirming the visual inspection. The best fits for the bottom ports are also quite similar with the exception of the sulfate-like peak coinciding more closely to $FeSO_4$ for the bottom port sample from the KPS-column and to K_2SO_4 for the bottom port sample from the control column. From visual inspection and LCF analysis it did not appear that the KPS-application had a significant impact on sulfur species that remained in the column soil.

3.5 **Conclusions**

Mercury release from contaminated flood plain soil in a series of fully-saturated, flow-through column experiments was observed to compare Hg transport in aerobic and anaerobic environments and to observe and quantify the impact of a 1 mM polysulfide application on Hg transport under anaerobic conditions. Higher concentrations of THg were mobilized from the soil receiving an oxygenated input than the column receiving an input purged of oxygen, both in the early stages of the experiment and continually for the duration of the experiment. The proposed hypothesis is that poorly crystalline and more soluble HgS undergoes oxidative dissolution with the aerobic input and Hg is converted to a more mobile form. A fraction of THg from the

dissolved HgS is eluted from the column earlier in the experiment and a fraction adsorbs to soil mineral surfaces like and Mn(IV)/ Fe(III)-(hydr)oxides. As reducing conditions develop in the columns during the experiment, reductive dissolution of Mn(IV)/ Fe(III)-(hydr)oxides release adsorbed Hg species into solution. Increased effluent Hg concentrations in both the anaerobic and aerobic column are preceded by or coincide with minimum Eh, and maximum Fe and Mn concentrations. However, due to the initial oxidative dissolution of HgS in the aerobic column, a higher fraction of Hg is weakly adsorbed to Fe/Mn-(hydr)oxide surfaces and released upon development of reducing conditions resulting in a greater flux of Hg from the aerobic column.

Very high concentrations of Hg were released from the soil during when a 1 mM potassium polysulfide (KPS) solution was applied over ~12 PVs. The maximum concentration of effluent Hg from the treated column was approximately 200 times that of the control and reflected the solubility of HgS in the presence of polysulfides as the aqueous $Hg(S_x)_2^{2-}$ would be the dominant Hg species. The rate of Hg release remained elevated above the control after the application of the KPS solution was ceased. The prolonged relatively elevated Hg release was likely due to some dissolved Hg species adsorbing to Fe(III)- and Mn(IV)-(hydr)oxide surfaces after dissolution of HgS by KPS occurred, as hypothesized in the aerobic control column. When reducing conditions develop and Fe(III)/Mn(IV)-(hydr)oxide minerals undergo reductive dissolution, the adsorbed Hg is released into solution and eluted from the column. Analysis of sulfur species by XANES did not indicate that the KPS application altered sulfur speciation in the soil suggesting that KPS significantly increased Hg mobility but stripped Hg from the soil without transforming sulfur species in the column soil. The results from this experiment indicate that applying polysulfide as a source of sulfur to promote in situ HgS formation would be difficult in practice in the field as it would be difficult to apply the correct dosage of polysulfide

to a low Hg concentration disseminated over a wide area. It would be expected that S_x^{2-} at too great of concentrations would be expected to dissolve HgS and transport Hg in full saturated soil systems.

Table 3.1- Aqueous chemistry of South River water.

Influent Solution	
Parameter	**SRW**
pH	8.5
Eh (mV)	145
Alkalinity (mg L^{-1} as $CaCO_3$)	170
Cl^- (mg L^{-1})	4.5
NO_3^- (mg L^{-1})	1.8
SO_4^{2-} (mg L^{-1})	4.1
Ca (mg L^{-1})	33.0
K (mg L^{-1})	2.5
Mg (mg L^{-1})	12.3
Na (mg L^{-1})	6.6
Si (mg L^{-1})	3.1
Mn (µg L^{-1})	7.5
Fe (µg L^{-1})	15.0
DOC (mg L^{-1})	<0.01

Table 3.2 - Solid phase concentrations of floodplain soil from RRM 11.8 on the South River.

	Hg	**Fe**	**Mn**	**Total C**	**Total S**
(µg g^{-1}) dry weight	47.6	25 000	2 400	26 400	430

Table 3.3 – Hg (by dry weight and percent of total) obtained through sequential extraction in the South River floodplain soil before used in the column experiments. (Ma & Paulson, 2014).

Fraction	Description	Targeted Compounds	Hg (ng g^{-1}, dry weight)	%
F1	Water Soluble	$HgCl_2$, $HgSO_4$	0.11	0.23
F2	Stomach Acid	HgO, $HgSO_4$	0.09	0.19
F3	Organo-complexed	Hg_2Cl_2, CH_3Hg	2.06	4.4
F4	Elemental/Strong complexes	Hg_2Cl_2, Hg^0	2.82	6.0
F5	Hg Sulfide/Residual	HgS, HgSe, HgAu	42.0	89.2

Table 3.4 - Percentage (%) of different S forms calculated by LCF.

Standards	KPS	Control Column Soil		KPS-treated Column Soil	
		Bottom Port	Top Port	Bottom Port	Top Port
Pyrite	0.39	-	-	-	-
Pyrrhotite	-	0.31	-	0.34	-
Metacinnabar	-	-	0.21	-	0.2
Dibenzo thiophene	-	0.25	0.24	0.27	0.23
Tetramethylene Sulfoxide	0.28	-	-	-	-
Butyl-sulfone	0.30	0.24	0.36	0.23	0.37
Sodium Metanesulfonate	0.03	-	-	-	-
$FeSO_4$	-	-	0.19	0.17	0.2
K_2SO_4	-	0.21	-	-	-
Reduced Chi squared	0.034	0.022	0.019	0.022	0.019

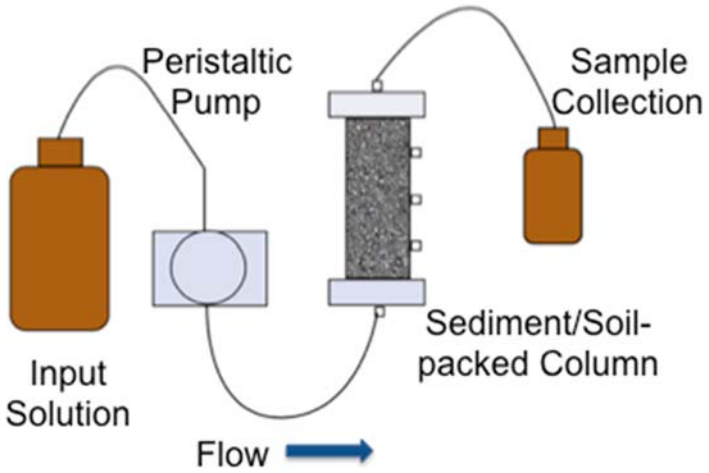

Figure 3.1 - Schematic diagram of the experimental set-up.

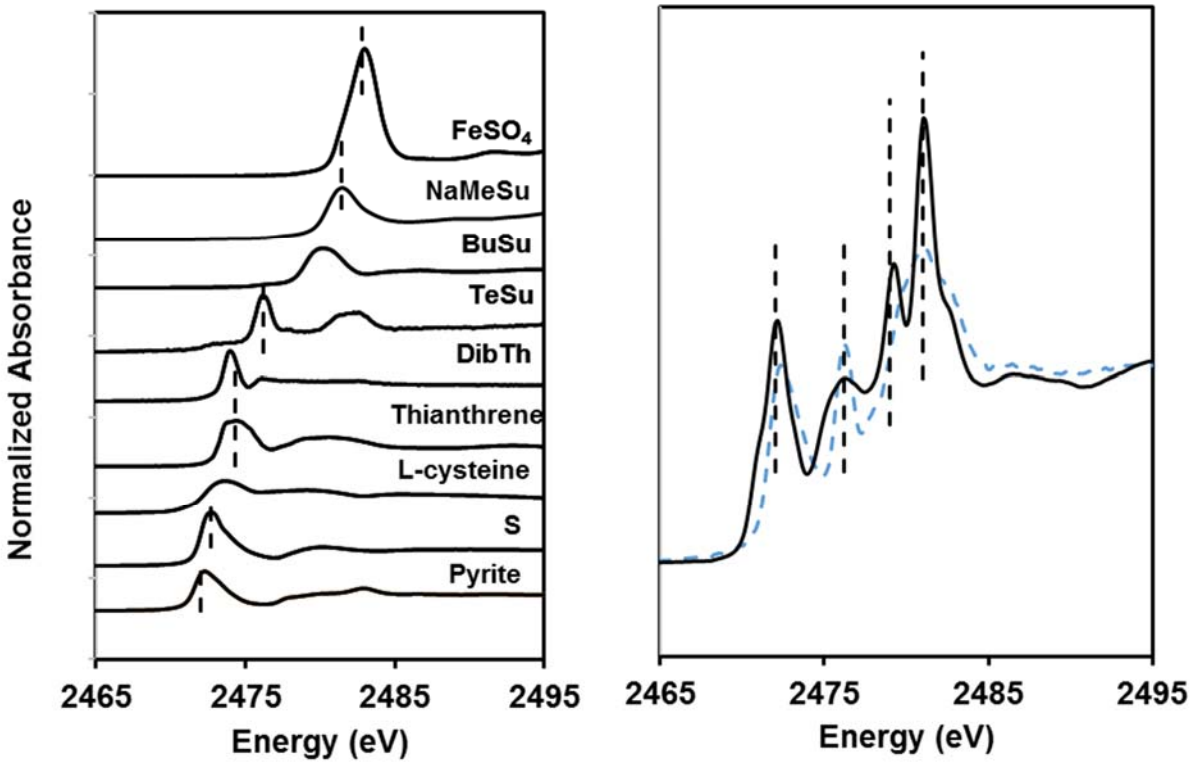

Figure 3.2 - S K-edge XANES spectra for ten S reference materials (left; DibTh = dibenzo thiophene; TeSu = tetramthylene sulfoxide; BuSu = butyl sulfone; NaMeSu = sodium methansulfonate). S K-edge XANES spectra for K_2S_x used for KPS input solution (right). The LCF fitted curve for the K_2S_x spectra is depicted with a blue, dashed line and the peak energy for (from left to right) sulfide-, sulfoxide-, sulfone-, and sulfonate-like spectra are represented by black, dashed vertical lines.

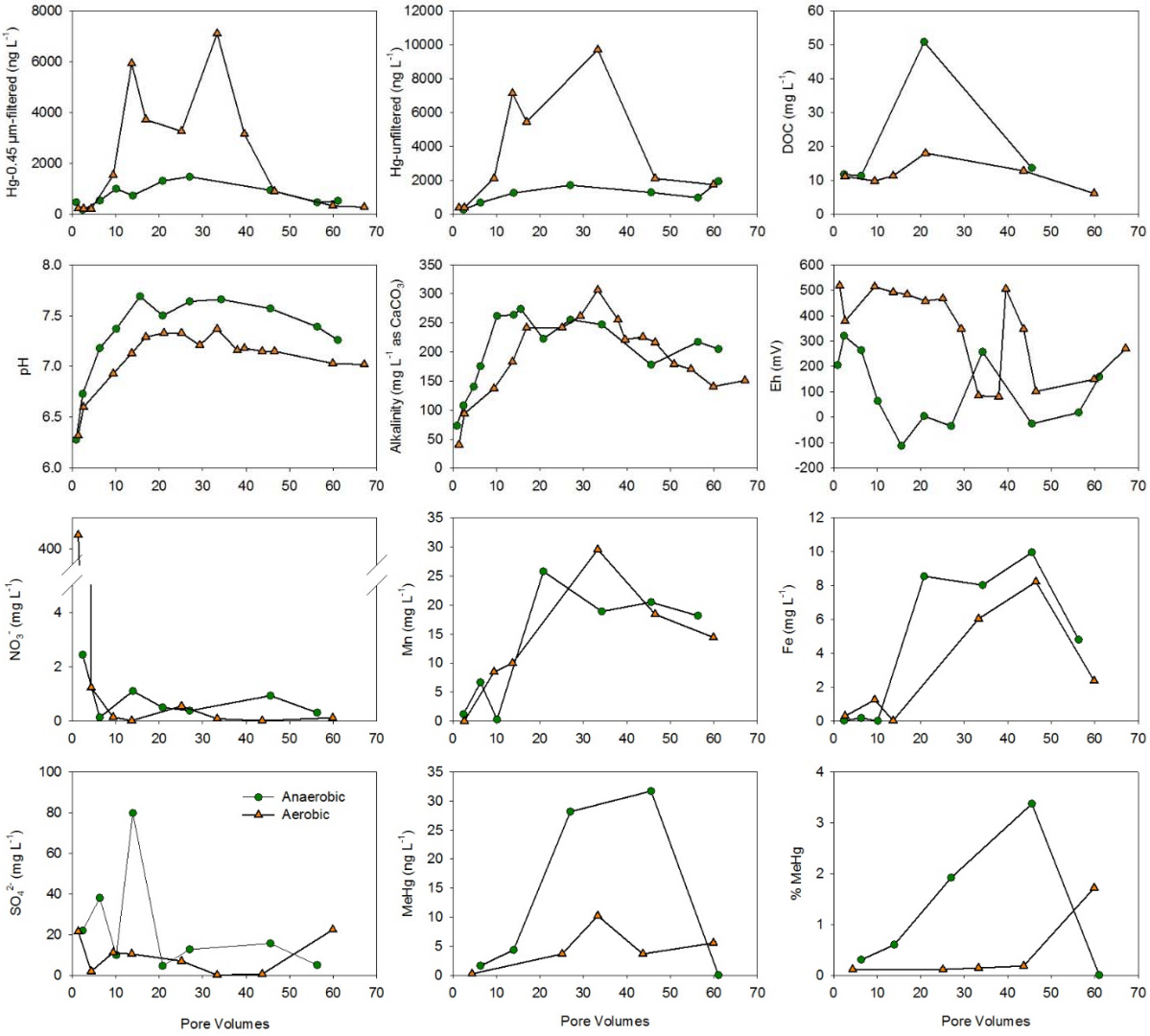

Figure 3.3 - Aqueous concentrations monitored over time in the aerobic (orange triangles) and anaerobic (green circles) control columns.

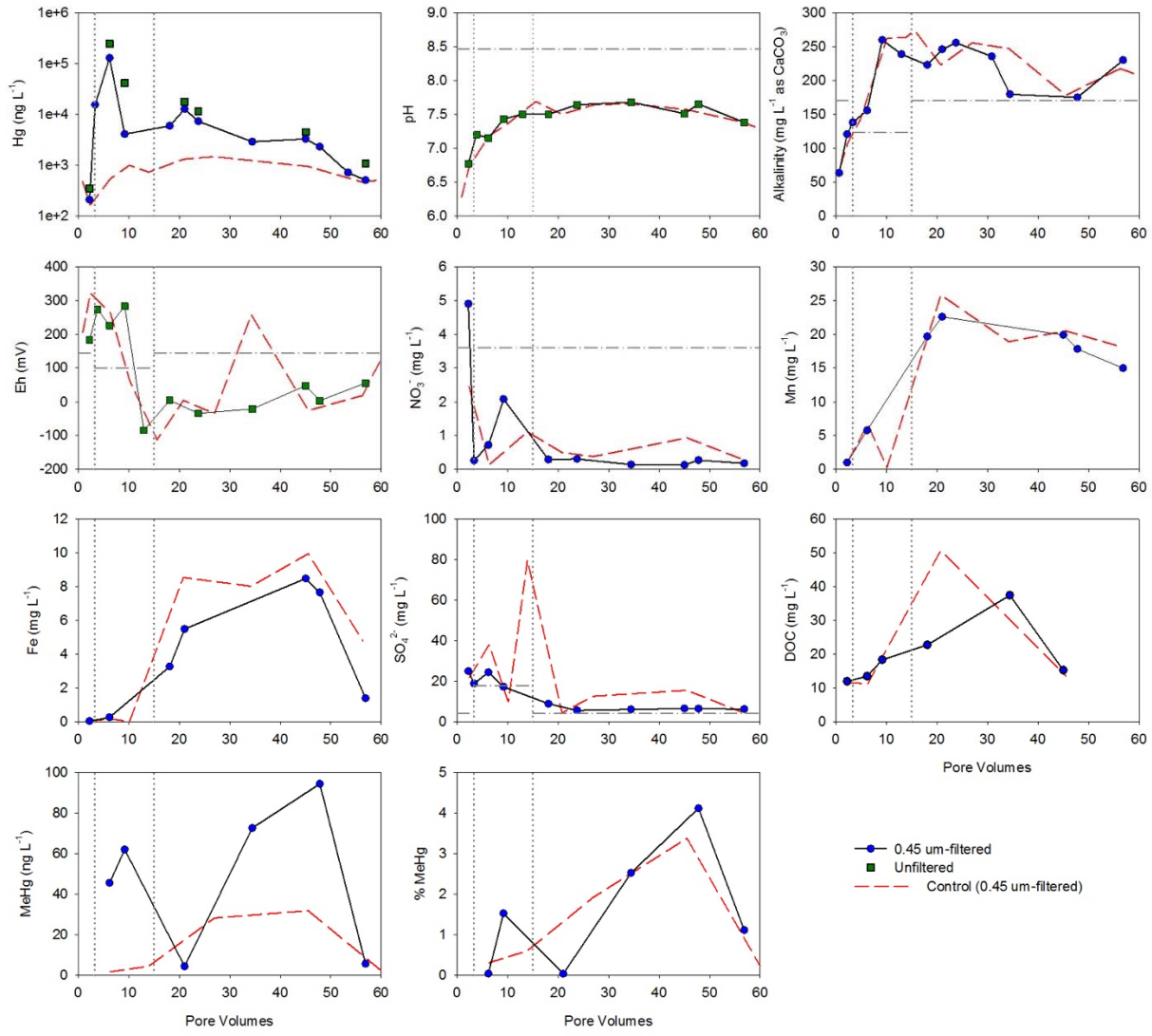

Figure 3.4 - Aqueous concentrations in the effluent of the KPS-application column over time. The concentrations of the 0.45 µm passing fractions are represented by blue circles and the unfiltered concentrations are shown by green squares. The dashed red line represents 0.45 µm filter-passing aqueous concentrations in the anaerobic control column effluent. The two vertical lines indicate the start of the KPS solution application at 3.3 PVs and the return to the SRW input at 15 PVs. The dashed, grey line represents the average input solution (SRW) concentration.

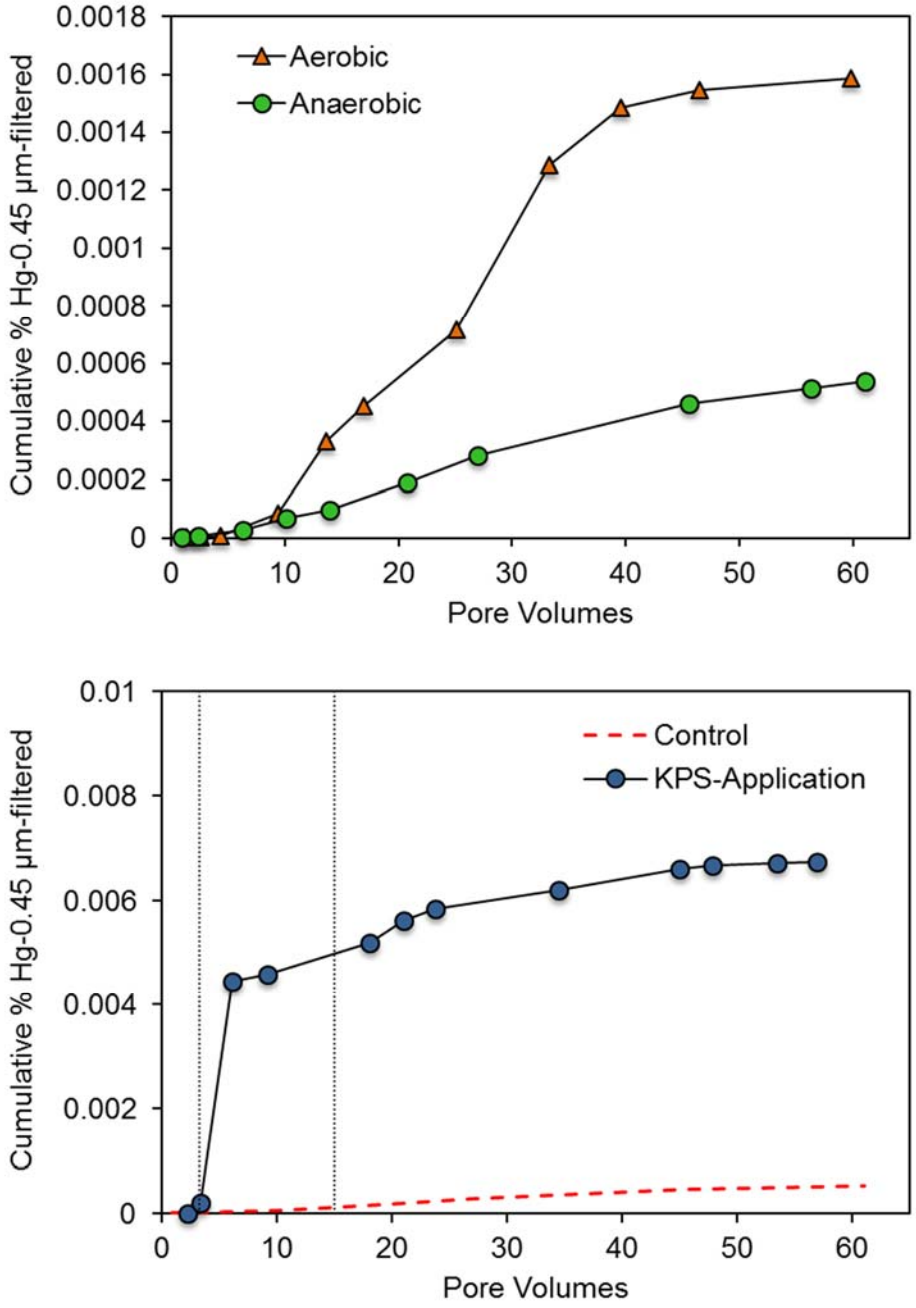

Figure 3.5 – Cumulative mass of 0.45 µm-filtered Hg measured in the aerobic and anaerobic control column effluents (top) and anaerobic control and KPS-application column effluents (bottom) over time. Note two vertical lines on bottom plot indicate a change of input solution.

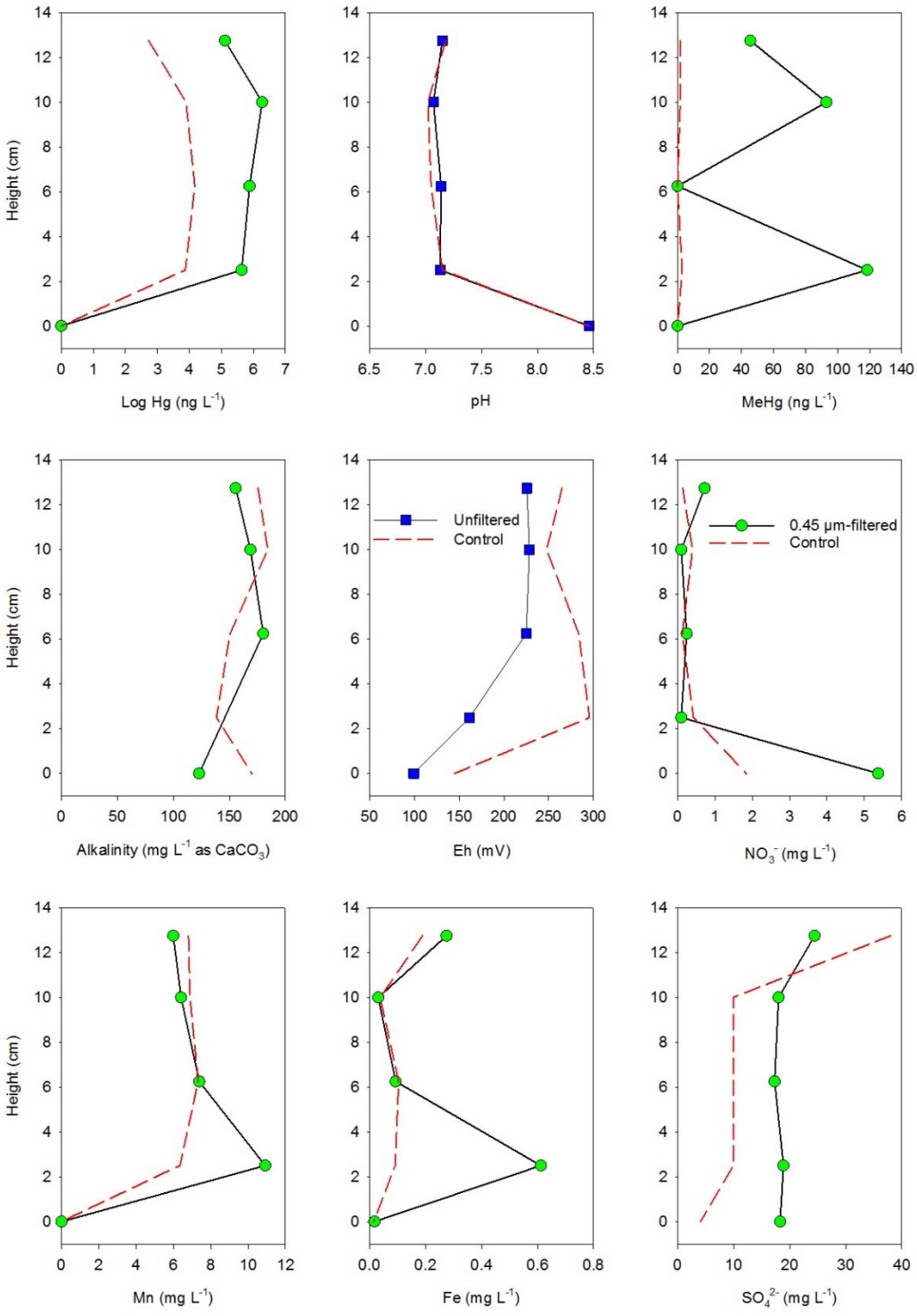

Figure 3.6 - Aqueous concentrations of THg-0.45, MeHg, pH, alkalinity (as $CaCO_3$), redox (Eh), NO_3^-, Mn, Fe and SO_4^{2-} along the column length at 7 PVs. The dashed, red line represents the control. Note that flow was from the bottom to the top of the column.

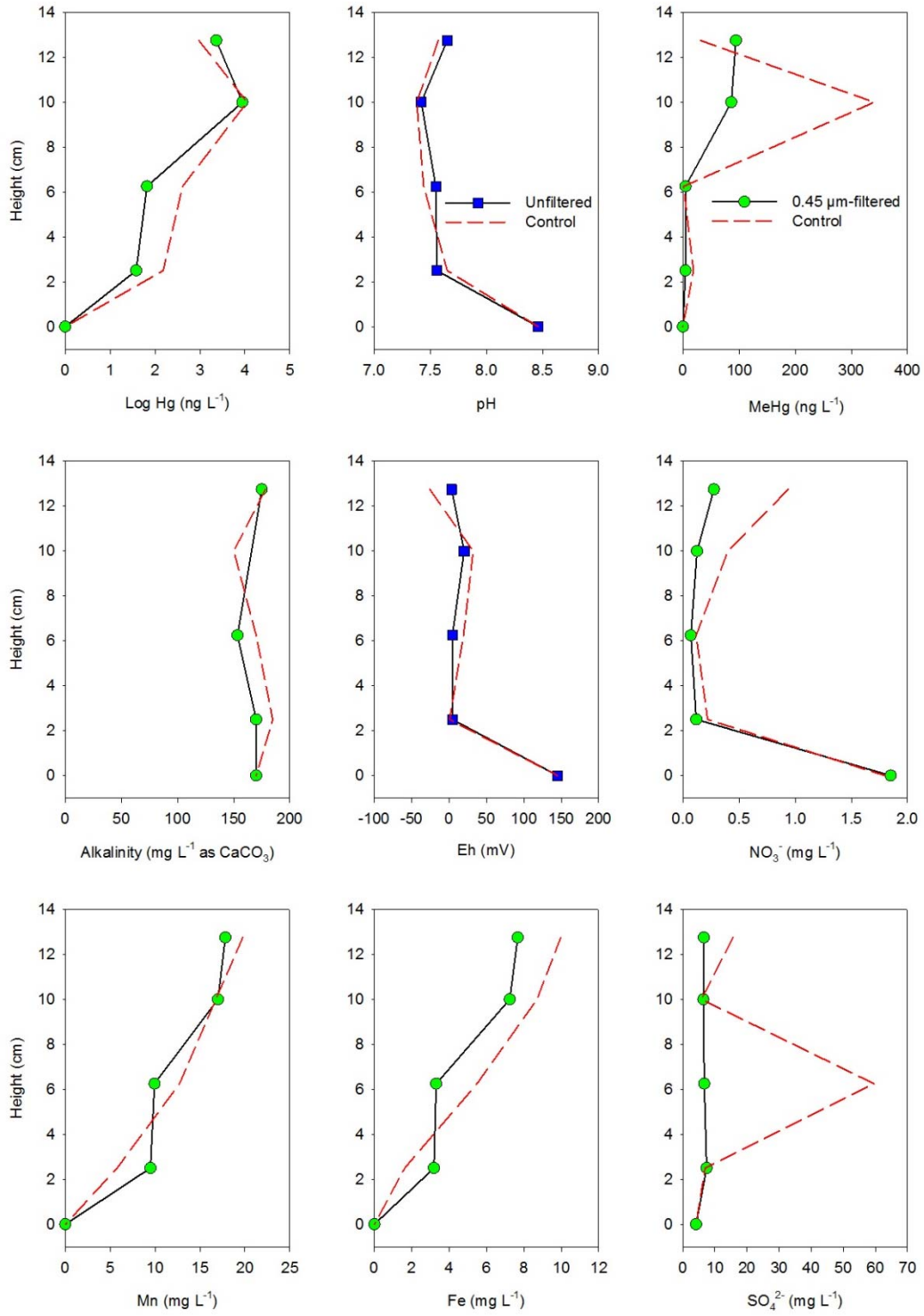

Figure 3.7 - Aqueous concentrations of THg-0.45, MeHg, pH, alkalinity (as $CaCO_3$), redox (Eh), NO_3^-, Mn, Fe and SO_4^{2-} along the column length at 49 PVs. The dashed, red line represents the control. Note that flow was from the bottom to the top of the column.

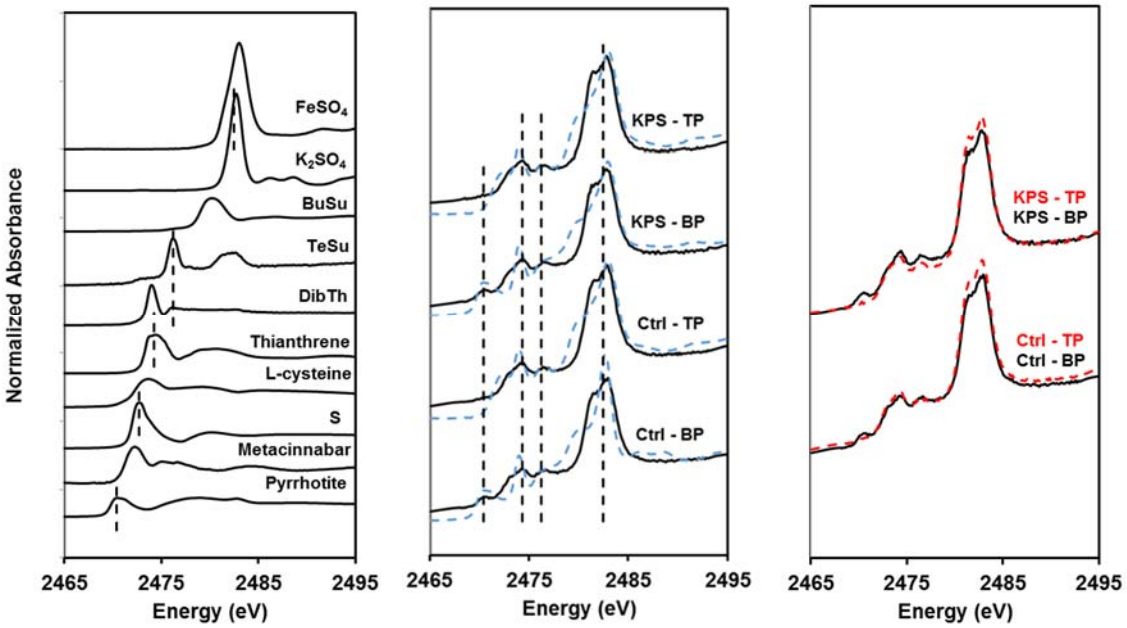

Figure 3.8 – S K-edge XANES spectra for ten S reference materials (left). S K-edge XANES spectra for soil extracted from the top and bottom ports of the control column and the KPS-application column extracted at ~30 PVs (middle). The LCF fitted curves for each spectra are represented by blue, dashed lines and the peak energy for (from left to right) sulfide-, thianthrene-/thiophene-, sulfone- and sulfate-like spectra represented by black, dashed vertical lines. The top port sample S spectra (dashed red) overlying the corresponding bottom port sample S spectra (solid black) (right).

Chapter 4: Conclusions and Recommendations

Mercury-containing soils and sediments in riparian environments can be persistent sources of Hg contamination due to complex factors controlling Hg mobility and prolonged release of Hg from an initial discharge point to extend to widespread areas. Additionally, the sensitivity of aquatic ecosystems to the highly neurotoxic and bioavailable MeHg warrants concern for relatively low concentrations of Hg-contaminated material. Understanding the controls on Hg mobility is essential for the management and remediation of extensive Hg-contaminated areas as removal of large swaths of soil and sediment is unfeasible due to high costs, invasiveness and potential to spread contamination further. Saturated, flow-through column experiments were conducted to investigate the impact of solution chemistry and redox conditions on Hg transport as well as the feasibility of polysulfide as a method of *in situ* stabilization of Hg, the results of which are presented in Chapter 2 and Chapter 3 of this thesis.

Mercury mobility increased when the solution pH and alkalinity increased and appeared to be closely tied to DOC mobility. Due to the affinity of Hg for organic matter, it is likely that a significant portion of Hg in the column was complexed with DOC, a relatively highly mobile Hg compound (Gai et al., 2016). The increase in pH to around the PZC of iron oxide minerals typically found in soil likely reversed the attractive electrostatic forces between NOM and soil surfaces and mobilized Hg-NOM complexes. Increases in effluent Hg concentrations coincided with the onset of more reducing conditions in the column indicated by increases in effluent Fe and Mn concentrations and decreased redox Eh. The increased Fe and Mn suggest that reductive dissolution of Fe-/Mn-(oxyhydr)oxides was occurring and releasing Hg complexes that were previously adsorbed to the Fe-/Mn-(oxyhydr)oxide surfaces. Decreasing the solution to pH~6 supported the pH reported in the literature at which Hg adsorption is greatest (Jing et al., 2007).

The findings of this research have implications for use of construction materials in the vicinity of Hg contamination that could contribute alkalinity, raise groundwater pH and mobilize Hg and Hg complexes (*e.g.* limestone-rich aggregate, cement, etc.). The observed relationship between reducing conditions, the dissolution of Fe-/Mn-(oxyhydr)oxides and Hg transport identifies Fe-/Mn-(oxyhydr)oxide mineral stability as a significant control on Hg mobility and suggests that significant Hg transport could occur if reducing conditions develop in normally well-oxidized soils (*e.g,.* in a flooding event).

Higher Hg mobilization was observed from a control column in aerobic conditions than in anaerobic conditions. Two separate Hg maxima concentrations were observed in the aerobic column effluent. It was hypothesized that HgS formed *in situ* since the initial discharge of Hg that is more disordered and less stable than more crystalline HgS formed in reducing conditions goes through oxidative dissolution when submitted to a solution in equilibrium with atmospheric oxygen (Holley et al., 2007). A fraction of the Hg released into solution following HgS dissolution was eluded from the column (*i.e.,* the first effluent Hg maximum) while some Hg adsorbed to Fe-/Mn-(oxyhydr)oxides. Upon the onset of more reducing conditions, indicated by increased effluent Fe and Mn and decreasing Eh, Fe-/Mn-(oxyhydr)oxide dissolution took place releasing adsorbed Hg complexes (*i.e.,* the second effluent Hg maximum). Increased effluent Hg concentrations were observed from the anaerobic control column that coincided with indicators of reducing conditions. However, the magnitude of the Hg release from the anaerobic column was smaller relative to the aerobic column suggesting that the initial aerobic phase of the experiment played a significant role in increasing the pool of Hg adsorbed to Fe-/Mn-(oxyhydr)oxide surfaces. The results of this experiment demonstrate the discrepancy in Hg mobility from the same floodplain soil given either an oxic or anoxic flow-through solution

which has important implications for Hg-contaminated soils that frequently fluctuate between aerobic and anaerobic conditions (*e.g.* within a frequently inundated floodplain). Future research on this subject should further investigate the effects of several sequences of alternating oxic and anoxic flow-through solutions to identify consistent indicators of Hg mobilization and the longevity of Hg release with cycling aerobic/anaerobic solutions over time.

Much higher concentrations of Hg were mobilized from the column when KPS was applied over approximately ~12 PVs. The maximum effluent Hg concentration observed during the KPS application was approximately 200 times greater than from the control – in line with the increase in solubility of HgS in the presence of polysulfides and the formation of highly mobile aqueous $Hg(S_x)_2^{2-}$ (Jay et al., 2000; Slowey & Brown Jr., 2007). At a later PV, after the cessation of KPS application, a second increase in effluent Hg concentration coincident with indicators of Mn-/Fe-(oxyhydr)oxide reductive dissolution and while a similar phenomenon was observed in the control column, the magnitude of Hg release was much less than from the KPS column. This relatively greater mobilization from the experimental column alongside dissolution of Mn-/Fe-(oxyhydr)oxides suggest that solubilisation of HgS and displacement of Hg by KPS increased the pool of Hg adsorbed to Mn-/Fe-(oxyhydr)oxide surfaces that was then mobilized upon reductive dissolution of those surfaces (Poulin et al., 2016). S XANES analysis of soil from the top and bottom ports at approximately 30 PVs did not show a discernable difference in S species between the control and KPS application column. The results of this flow-through experiment with application of a KPS solution do not support the use of KPS as a method of *in situ* immobilization of Hg via HgS formation, as the opposite effect – solubilisation of existing HgS – was likely achieved.

References

Aiken, G. R., Hsu-Kim, H., & Ryan, J. N. (2011). Influence of Dissolved Organic Matter on the Environmental Fate of Metals, Nanoparticles, and Colloids. *Environmental Science and Technology, 45*, 3196-3201.

Angelico, R., Ceglie, A., Ji-Zheng, H., Yu-Rong, L., Palumbo, G., & Colombo, C. (2014). Particle size, charge and colloidal stability of humic acids coprecipitated with Ferrihydrite. *Chemosphere, 99*, 239-247.

Avena, M. J., & Koopal, L. K. (1998). Desorption of Humic Acids from an Iron Oxide Surface. *Environmental Science and Technology, 32*(17), 2572-2577.

Barnett, M. O., Harris, L. A., Turner, R. R., Henson, T. J., Melton, R. C., & Hoffman, D. P. (1997). Formation of mercuric sulfide in Soil. *Environmental Science and Technology, 31*(11), 3037-3043.

Barnett, M. O., Harris, L. A., Turner, R. R., Stevenson, R. J., Henson, T. J., Melton, R. C., & Hoffman, D. P. (1997). Formation of Mercuric Sulfide in Soil. *Environmental Science and Technology, 31*(11), 3037-3043.

Barnett, M. O., Turner, R. R., & Singer, P. C. (2001). Oxidative dissolution of metacinnabar (b-HgS) by dissolved oxygen. (J. Herman, Ed.) *Applied Geochemistry, 16*, 1499-1512.

Barrow, N., & Cox, V. (1992). The effects of pH and chloride concentration on mercury sorption. II. By a soil . *Journal of Soil Science, 43*, 305-312.

Behra, P., Bonnissel-Gissinger, P., Alnot, M., Revel, R., & Ehrhardt, J. J. (2001). XPS and XAS Study of the Sorption of Hg(II) onto Pyrite. *Langmuir, 17*, 3970-3979.

Bengtsson, G., & Picado, F. (2008). Mercury sorption to sediments: Dependence on grain size, dissolved organic carbon, and suspended bacteria. *Chemosphere, 73*, 523-531.

Bergeron, C. M., Bodinof, C. M., Unrine, J. M., & Hopkins, W. A. (2010). Mercury accumulation along a contamination gradient and nondestructive indices of bioaccumulation in amphibians. *Environmental Toxicology and Chemistry, 29*(4), 980-988.

Biester, H., & Zimmer, H. (1998). Solubility and Changes of Mercury Binding Forms in Contaminated Soils after Immobilization Treatment. *Environmental Science and Technology, 32*(18), 2755-2762.

Biester, H., Müller, G., & Schöler, H. (2002). Binding and mobility of mercury in soils contaminated by emissions from chlor-alkali plants. *The Science of the Total Environment, 284*, 191-203.

Bloom, N. S., Preus, E., Katon, J., & Hiltner, M. (2003, March 10). Selective extractions to assess the biogeochemically relevant fractionation of inorganic mercury in sediments and soils. *Analytica Chimica Acta, 479*(2), 233-248.

Boening, D. W. (2000). Ecological effects, transport, and fate of mercury: a general review. *Chemosphere, 40*, 1335-1351.

Bouby, M., Geckeis, H., Lützenkirchen, J., Mihai, S., & Schäfer, T. (2011). Interaction of bentonite colloids with Cs, Eu, Th and U in the presence of humic acid: A flow-field fractionation study. *Geochimica et Cosmochimica Acta, 75*, 3866-3880.

Bower, J., Savage, K. S., Weinman, B., Barnett, M. O., Hamilton, W. P., & Harper, W. F. (2008). Immobilization of mercury by pyrite (FeS2). *Environmental Pollution*(156), 504-514.

Brent, R. N., & Berberich, D. A. (2013). Use of Artificial Stream Mesocosms to Investigate Mercury Uptake in the South River, Virginia, USA. *Archives of Environmental Contamination and Toxicology*(66), 201-212.

Brigham, M. E., Wentz, D. A., Aiken, G. R., & Krabbenhoft, D. P. (2009). Mercury Cycling in Stream Ecosystems. 1. Water Column Chemistry and Transport. *Environmental Science and Technology, 43*(8), 2720-2725.

Brooks, S. C., & Southworth, G. R. (2011). History of mercury use and environmental contamination at the Oak Ridge Y-12 Plant. *Environmental Pollution, 159*, 219-228.

Bunn, R. A., Magelky, R. D., Ryan, J. N., & Elimelech, M. (2002). Mobilization of Natural Colloids from an Iron Oxid-Coated Sand Aquifer: Effect of pH and Ionic Strength. *Environmental Science and Technology, 36*(3), 314-322.

Chadwick, S. P., Babiarz, C. L., Hurley, J. P., & Armstrong, D. E. (2006). Influences of iron, manganese, and dissolved organic carbon on the hypolimnetic cycling of amended mercury. *Science of the Total Environment, 368*, 177-188.

Chrysochoou, M., & Johnston, C. P. (2015). Polysulfide speciation and reactivity in chromate-contaminated soil. *Journal of Hazardous Materials*(281), 87-94.

Chrysochoou, M., Johnston, C. P., & Dahal, G. (2012). A comparative evaluation of hexavalent chromium treatment in contaminated soil by calcium polysulfide and green-tea nanoscale zero-valent iron. *Journal of Hazardous Materials*(201-202), 33-42.

Deonarine, A., & Hsu-Kim, H. (2009). Precipitation of Mercuric Sulfide Nanoparticles in NOM-Containing Water: Implications for the Natural Environment. *Environmental Science and Technology, 43*(7), 2368-2373.

Desrochers, K. (2013). *Geochemical Characterization and Assessment of Stabilization Mechanisms for Mercury-Contaminated Riverbank Sediments from the South River, Virginia (USA).* Master's Thesis, University of Waterloo, Waterloo.

Devasena, M., & Nambi, I. M. (2013). In situ stabilization of entrapped elemental mercury. *Journal of Environmental Management*(130), 185-191.

Dittman, J. A., Shanley, J. B., Driscoll, C. T., Aiken, G. R., Chalmers, A. T., Towse, J. E., & Selvendiran, P. (2010). Mercury dynamics in relation to dissolved organic carbon concentration and quality during high flow events in three northeastern U.S. streams. *Water Resources Research, 46*, 1-15.

Drexel, R. T., Haitzer, M., Ryan, J. N., Aiken, G. R., & Nagy, K. L. (2002). Mercury(II) Sorption to Two Everglades Peats: Evidence for Strong and Weak Binding and Competition by Dissolved Organic Matter Released by Peat. *Environmental Science and Technology, 36*(19), 4058-4064.

Eggleston, J. (2009). *Mercury loads in the South River and simulation of mercury total maximum daily loads (TMDLs) for the South River, South Fork Shenandoah River, and Shenandoah River-Shenandoah Valley, Virginia.* U.S. Geological Survey Scientific Investigations Report 2009-5076.

Environment and Climate Change Canada. (2011, 07 18). *Mercury Environment and Health Concerns*. Retrieved 05 29, 2016, from www.ec.gc.ca/mercure-mercury

Environment and Climate Change Canada. (2013, July 9). *Mercury in the Food Chain*. Retrieved from Environment and Health Concerns: https://www.ec.gc.ca/mercure-mercury

Environment Canada . (2000). *The Status of Mercury in Canada Report #2.* Environment Canada North American Task Force on Mercury, Transboundary Air Issues Branch . Environment Canada.

European Synchrotron Radiation Facility. (2017, September 29). *ID21 SULFUR XANES SPECTRA DATABASE HOME*. Retrieved September 29, 2017, from European Synchrotron Radiation Facility: http://www.esrf.eu/home/UsersAndScience/Experiments/XNP/ID21/php.html

Farrah, H., & Pickering, W. F. (1978). The Sorption of Mercury Species by Clay Minerals. *Water, Air and Soil Pollution , 9*, 23-31.

Flanders, J., Turner, R., Morrison, T., Jensen, R., Pizzuto, J., Skalak, K., & Stahl, R. (2010). Distribution, behavior, and transport of inorganic and methylmercury in a high gradient stream. *Applied Geochemistry*(25), 1756-1769.

Fleming, E. J., Mack, E. E., Green, P. G., & Nelson, D. C. (2006). Mercury Methylation from Unexpected Sources: Molybdate-Inhibited Freshwater Sediments and an Iron-Reducing Bacterium. *Applied and Environmental Microbiology, 72*(1), 457-464.

Foran, C. M., Baker, K. M., Grosso, N. R., & Linkov, I. (2015). An Enhanced Adaptive Management Approach for Remediation of Legacy Mercury in the South River. *PLoS One*, 1-15.

Gabriel, M. C., & Williamson, D. G. (2004). Principal biogeochemical factors affecting the speciation and transport of mercury through the terrestrial environment. *Environmental Geochemistry and Health, 26*, 421-434.

Gai, K., Hoelen, T. P., Hsu-Kim, H., & Lowry, G. V. (2016). Mobility of Four Common Mercury Species in Model and Natural Unsaturated Soils. *Environmental Science and Technology*.

Ghosh, U., Luthy, R. G., Cornelissen, G., Werner, D., & Menzie, C. A. (2011). In-situ Sorbent Amendments: A New Direction in Contaminated Sediment Management. *Environmental Science and Technology, 45*, 1163-1168.

Gibson, B. (2013, May 23). Application of synchrotron radiation-based X-ray absorption spectroscopy (XAS) techniques to characterize metal speciation in South River sediments. *[Unpublished]*.

Gibson, B. D., Ptacek, C. J., Lindsay, M. B., & Blowes, D. W. (2011). Examining Mechanisms of Groundwater Hg(II) Treatment by Reactive Materials: An EXAFS Study. *Environmental Science and Technology, 45*, 10415-10421.

Gilmour, C. C., Henry, E. A., & Mitchell, R. (1992). Sulfate Stimulation of Mercury Methylation in Freshwater Sediments. *Environmental Science and Technology, 26*, 2281-2287.

Gilmour, C. C., Podar, M., Bullock, A. L., Graham, A. M., Bron, S. D., Somenahally, A. C., . . . Elias, D. A. (2013). Mercury Methylation by Novel Microorganisms from New Environments. *Environmental Science and Technology, 47*, 11810-11820.

Goyer, R. A., Aposhian, H. V., Arab, L., Bellinger, D. C., Burbacher, T. M., Burke, T. A., . . . Stern, A. H. (2000). *Toxicological Effects of Methylmercury.* Washington, DC: National Academy Press.

Graham, A. M., Aiken, G. R., & Gilmour, C. C. (2012). Dissolved Organic Matter Enhances Microbial Mercury Methylation. *Environmental Science and Technology*, 2715-2723.

Graham, A. M., Aiken, G. R., & Gilmour, C. C. (2013). Effect of Dissolved Organic Matter Source and Character on Microbial Hg Methylation in Hg−S−DOM Solutions. *Environmental Science and Technology, 47*, 5746-5754.

Greenwood, N., & Earnshaw, A. (1997). *Chemistry of the Elements* (2nd Edition ed.). Elsevier.

Grolimund, D., & Borkevec, M. (1999). Long-Term Release Kinetics of Colloidal Particles from Natural Porous Media. *Environmental Science and Technology, 33*, 4054-4060.

Grybos, M., Davranche, M., Gruau, G., Petitjean, P., & Pédrot, M. (2009). Increasing pH drives organic matter solubilization from wetland soils under reducing conditions . *Geoderma, 154*, 13-19.

Gu, B., Schmitt, J., Chen, Z., Liang, L., & McCarthy, J. F. (1994). Adsorption and Desorption of Natural Organic Matter on Iron Oxide: Mechanisms and Models. *Environmental Science and Technology, 28*(1), 38-46.

Gupta, S., Barlow, M., & Donaldson, S. (2005). Chapter 13: Mercury Exposure and Human Health Effects: A Canadian Perspective. In M. P. Parsons, & J. B. Percival (Eds.), *Mercury Sources, Measurements, Cycles, and Effects* (Vol. 34, pp. 259-286). Halifax, NS: Mineralogical Association of Canada.

Haitzer, M., Aiken, G. R., & Ryan, J. N. (2003). Binding of Mercury(II) to Aquatic Humic Substances: Influence of pH and Source of Humic Substances. *Environmental Science and Technology, 37*, 2436-2441.

Hammerschmidt, C. R., Fitzgerald, W. F., Balcom, P. H., & Visscher, P. T. (2008). Organic matter and sulfide inhibit methylmercury production in sediments of New York/New Jersey Harbor. *Marine Chemistry, 109*, 165-182.

Han, F. X., Su, Y., Monts, D. L., Waggoner, C. A., & Plondinec, M. J. (2006). Binding, distribution, and plant uptake of mercury in a soil from Oak Ridge, Tennessee, USA. *Science of the Total Environment, 368*, 753-768.

Harris-Hellal, J., Grimaldi, M., Garnier-Zarli, E., & Bousserrhine, N. (2011). Mercury mobilization by chemical and microbial iron oxide reduction in soils of French Guyana. *Biogeochemistry, 103*, 223-234.

Hintelmann, H., & Harris, R. (2004). Application of multiple stable mercury isotopes to determine the adsorption and desorption dynamics of Hg(II) and MeHg to sediments. *Marine Chemistry, 90*, 164-173.

Hintelmann, H., Harris, R., Heyes, A., Hurley, J. P., Kelly, C. A., Krabbenhoft, D. P., . . . St. Louis, V. L. (2002). Reactivity and Mobility of New and Old Mercury Deposition in a Boreal Forest Ecosystem during the First Year of the METAALICUS Study. *Environmental Science and Technology, 36*(23), 5034-5040.

Hofacker, A. F., Voegelin, A., Kaegi, R., & Kretzschmar, R. (2013). Mercury Mobilization in a Flooded Soil by Incorporation into Metallic Copper and Metal Sulfide Nanoparticles. *Environmental Science and Technology, 47*, 7739-7746.

Holley, E. A., Craw, D., Kim, J. P., & Sander, S. G. (2007). Mercury mobilization by oxidative dissolution of cinnabar (-HgS) and metacinnabar (-HgS) . (D. Rickard, Ed.) *Chemical Geology, 240*, 313-325.

Horvat, M., Nolde, N., Fajon, V., Jereb, V., Logar, M., Lojen, S., . . . Drobne, D. (2003). Total mercury, methylmercury and selenium in mercury polluted areas in the province of Guizhou, China. *the Science of the Total Environment*, 231-256.

Hsu-kim, H., Kucharzyk, K. H., Zhang, T., & Deshusses, M. A. (2013). Mechanisms Regulating Mercury Bioavailability for Methylating Microorganisms in the Aquatic Environment: A Critical Review. *Environmental Science and Technology, 47*, 2441-2456.

Hughes, S., Reynolds, B., & Roberts, J. (1990). The influence of land management on concentrations of dissolved organic carbon and its effects on the mobilization of aluminum and iron in podzol soils in Mid-Wales. *Soil Use and Management, 6*(3), 137-145.

James, C. N., Copeland, R. C., & Lytle, D. A. (2004). Relationship between Oxidation-Reduction Potential, Oxidant, and pH in Drinking Water. *WQTC Conference* (pp. 1-13). San Antonio, TX: American Water Works Association.

Jay, J. A., Morel, F. M., & Hemond, H. F. (2000). Mercury Speciation in the Presence of Polysulphides . *Environmental Science and Technology, 34*(11), 2196-2200.

Jing, Y., He, Z., & Yang, X. (2007). Effects of pH, organic acids, and competitive cations on mercury desorption in soils . *Chemosphere, 69*, 1662-1669.

Johannesson, K. H., & Neumann, K. (2013). Geochemical cycling of mercury in a deep, confined aquifer: Insight from biogeochemical reactive transport modeling. *Geochimca et Cosmochimica Acta, 106*, 25-43.

Kaiser, K., & Zech, W. (1999). Release of Natural Organic Matter Sorbed to Oxides and a Subsoil. *Soil Science Society of America Journal, 63*(5), 1157-1166.

Kerin, E. J., Gilmour, C. C., Roden, E., Suzuki, M. T., Coates, J. D., & Mason, R. P. (2006, December). Mercury Methylation by Dissimilatory Iron-Reducing Bacteria. *Applied and Environmental Microbiology, 72*(12), 7919-7921.

Kim, C. S., Rytuba, J. J., & Brown Jr., G. E. (2004). EXAFS study of mercury(II) sorption to Fe- and Al-(hydr)oxides I. Effects of pH. *Colloid and Interface Science, 271*, 1-15.

Kloster, N., Brigante, M., Zanini, G., & Avena, M. (2013). Aggregation kinetics of humic acids in the presence of calcium ions. *Colloids and Surfaces A: Physiochemical and Engineering Aspects, 427*, 76-82.

Kosmulski, M. (2011). The pH-dependent surface charging and points of zero charge V. update. *Journal of Colloid and Interface Science, 353*, 1-15.

Kot, F. S., Rapoport, V. L., & Kharitonova, G. V. (2007). Immobilization of soil mercury by colloidal sulphur in the laboratory experiment. *Central European Journal of Chemistry, 5*(3), 846-857.

Krabbenhoft, D. P., Branfireun, B. A., & Heyes, A. (2005). Chapter 8: Biogeochemical Cycles Affecting the Speciation, Fate and Transport of Mercury in the Environment. In M. B. Parsons, & J. B. Percival, *Mercury: Sources, Measurements, Cycles, and Effects* (Vol. 34, pp. 139-156). Halifax, NS, Canada: Mineralogical Association of Canada.

Landis, W. G., Ayre, K. K., Harris, M., Herring, C. E., Johns, A. F., Stinson, J., . . . Markiewicz, A. J. (2014). *Results for the Integrated Regional Risk Assessment for the South River and Upper Shenandoah River, Virginia.* Western Washington University, Institute of Environmental Toxicology, Huxley College of the Environment, Bellingham, WA.

Light, T. (1972). Standard solution for redox potential measurements. *Analytical Chemistry, 44*, 1038-1039.

Liu, J., Valsaraj, K. T., Devai, I., & DeLaune, R. (2008). Immobilization of aqueous Hg(II) by mackinawite (FeS). *Journal of Hazardous Materials, 157*, 432-440.

Liu, P., Ptacek, C. J., Blowes, D. W., & Landis, R. C. (2016). Mechanisms of mercury removal by biochars produced from difference feedstocks determined using X-ray absorption spectroscopy. *Journal of Hazardous Materials*, 233-242.

Liu, P., Ptacek, C., Blowes, D., & Finfrock, Y. G. (2017). Stabilization of mercury in sediment by using biochars under reducing conditions. *Journal of Hazardous Materials, 325*, 120-128.

Loux, N. T. (1998). An assessment of mercury-species-dependent binding with natural organic carbon. *Chemical Speciation and Bioavailability, 10*(4), 127-136.

Lowry, G. V., Shaw, S., Kim, C. S., Rytuba, J. J., & Brown Jr., G. E. (2004). Macroscopic and Microscopic Observations of Particle-Facilitated Mercury Transport from New Idria and Sulphur Bank Mercury Mine Tailings. *Environmental Science and Technology, 38*, 5101-5111.

Lu, X., Huangfu, X., & Ma, J. (2014). Removal of trace mercury(II) from aqueous solution by in situ formed Mn–Fe (hydr)oxides. *Journal of Hazardous Materials, 280*, 71-78.

Lu, X., Huangfu, X., Zhang, X., Wang, Y., & Ma, J. (2014). Strong enhancement of trace mercury removal from aqueous solution with sodium thiosulfate by in situ formed Mn-(hydr)oxides. *Water Research, 65*, 22-31.

Lundén, I., & Andersson, K. (1991). Interaction of Concrete and Synthetic Granitic Groundwater in Air and Nitrogen Atmosphere. *Radiochimica Acta , 52/53*, 17-21.

Manceau, A., Lemouchi, C., Enescu, M., Gaillot, A.-C., Lanson, M., Magnin, V., . . . Nagy, K. L. (2015). Formation of Mercury Sulfide from Hg(II)-Thiolate Complexes in Natural Organic Matter . *Environmental Science and Technology*.

Meng, X., Hua, Z., Dermatas, D., Wang, W., & Kuo, H. Y. (1998). Immobilization of mercury(II) in contaminated soil with used tire rubber. *Journal of Hazardous Materials, 57*, 231-241.

Newman, M. C., Xu, X., Condon, A., & Liang, L. (2011). Floodplain methylmercury biomagnification factor higher than that of the contiguous river (South River, Virginia USA). *Environmental Pollution, 159*, 2840-2844.

Nordstrom, D. K. (1977). Thermochemical redox equilibria of ZoBell's solution. *Geochimica et Cosmochimica Acta, 41*(12), 1835-1841.

Osborne-Lee, I., Conley, T., Huley, G., & Morris, M. (1999). *Demonstration Results on the Effects of Mercury Speciation on the Stabilization of Wastes.* Oak Ridge National Laboratory. Oak Ridge, TN: Oak Ridge national Laboratory.

Pacyna, J. M., & Pacyna, E. G. (2005). Chapter 3: Anthropogenic Sources and Global Inventory of Mercury Emissions. In M. B. Parsons, & J. B. Percival (Eds.), *Mercury: Sources Measurements, Cycles and Effects* (pp. 43-56). Halifax, NS, Canada: Mineralogical Association of Canada.

Paquette, K. E., & Helz, G. R. (1997). Inorganic Speciation of Mercury in Sulfidic Waters: The Importance of Zero-Valent Sulfur. *Environmental Science and Technology, 31*, 2148-2153.

Paquette, K., & Helz, G. (1995). Solubility of Cinnabar (Red HgS) and Implications for Mercury Speciation in Sulfidic Waters. *Water, Air and Soil Pollution, 80*, 1053-1056.

Parkhurst, D., Thorstenson, D., & Plummer, L. (1990). *PHREEQE - A computer program for geochemical calculations: U.S. Geological Survey Water-Resources Investigations Report.* U.S. Geological Survey.

Parsons, M. B., & Percival, J. B. (2005). Chapter 1: A Brief History of Mercury and its Environmental Impact. In *Mercury Sources, Measurements, Cycles, and Effects* (pp. 1-20). Halifax, NS: Mineralogical Association of Canada.

Patmont, C. R., Ghosh, U., LaRosa, P., Menzie, C. A., Luthy, R. G., Greenberg, M. S., . . . Quadrini, J. (2014). In Situ Sediment Treatment Using Activated Carbon: A Demonstrated Sediment Cleanup Technology. *Integrated Environmental Assessment and Management, 11*(2), 195-207.

Patnaik, P. (2003). *Handbook of Inorganic Chemicals.* New York, NY, USA: McGraw-Hill Companies, Inc.

Paulson, K. M., Ptacek, C. J., Blowes, D. W., Gould, W. D., Ma, J., Landis, R. C., & Dyer, J. A. (2016). Role of Organic Carbon Sources and Sulfate in Controlling Net Methylmercury Production in Riverbank Sediments of the South River, VA (USA). *Geomicrobiology Journal*, 1-14.

Perez, P. A., Hintelman, H., Quiroz, W., & Bravo, M. A. (2017). Critical evaluation of distillation procedure for the determination of. *Chemosphere, 186*, 570-575.

Pham, A. L.-T., Morris, A., Zhang, T., Ticknor, J., Levard, C., & Hsu-Kim, H. (2014). Precipitation of nanoscale mercuric sulfides in the presence of natural organic matter: Structural properties, aggregation, and biotransformation. *Geochimica et Cosmochimica Acta, 133*, 204-215.

Piao, H., & Bishop, P. L. (2006). Stabilization of mercury-containing wastes using sulfides. *Environmental Pollution*(139), 498-506.

Pizzuto, J. (2012). Predicting the accumulation of mercury-contaminated sedimenton riverbanks—An analytical approach. *Water Resources Research, 48*, 1-13.

Poulin, B. A., Aiken, G. R., Nagy, K. L., Manceau, A., Krabbenhoft, D. P., & Ryan, J. N. (2016). Mercury transformation and release differs with depth and time in a contaminated riparian soil during simulated flooding . *Geochimica et Cosmochimica Acta, 176*, 118-138.

Randall, P. M., & Chattopadhyay, S. (2013). Mercury contaminated sediment sites—An evaluation of remedial options. *Environmental Research, 125*, 131-149.

Ravel, B., & Newville, M. (2005). ATHENA, ARTEMIS, HEPHAESTUS: data analysis for X-ray absorption spectroscopy using IFEFFIT. *Journal of Synchrotron Radiation, 12*, 537-541.

Ravichandran, M. (2004). Interactions between mercury and dissolved organic matter-a review. *Chemosphere, 55*, 319-331.

Ravichandran, M., Aiken, G. R., Reddy, M. M., & Ryan, J. N. (1998). Enhanced dissolution of cinnabar (mercuric sulfide) by dissolved organic matter isolated from the florida everglades. *Environmental Science and Technology*(32), 3305-3311.

Ravichandran, M., Aiken, G. R., Reddy, M. M., & Ryan, J. N. (1998). Enhanced Dissolution of Cinnabar (Mercuric Sulfide) by Dissolved Organic Matter Isolated from the Florida Everglades. *Environmental Science and Technology, 32*, 3305-3311.

Ravichandran, M., Aiken, G. R., Reddy, M. M., & Ryan, J. N. (1998). Enhanced Dissolution of Cinnabar (Mercuric Sulfide) by Dissolved Organic Matter Isolated from the Florida Everglades. *Environmental Science and Technology, 32*, 3305-3311.

Ravichandran, M., Aiken, G. R., Ryan, J. N., & Reddy, M. M. (1999). Inhibition of Precipitation and Aggregation of Metacinnabar (Mercuric Sulfide) by Dissolved Organic Matter Isolated from the Florida Everglades. *Environmental Science and Technology, 33*, 1418-1423.

Rhoades, E. L., O'Neil, M. A., & Pizzuto, J. E. (2009). Quantifying bank erosion on the South River from 1937 to 2005, and its importance in assessing Hg contamination. *Applied Geography, 29*, 125-134.

Ridley, M. (2007). *Summary Report on the Subsurface Chromium Reduction Treatment Test at Riverbank Army Ammunitions Plant.* Lawrence Livermore National Laboratory, University of California. Livermore: U.S. Department of Energy.

Rytuba, J. J. (2005). Chapter 2: Geogenic and Mining Sources of Mercury to the Environment. In M. B. Parsons, & J. B. Percival, *Mercury Sources, Measurements, Cycles, and Effects* (Vol. 34, pp. 21-41). Halifax, NS: Mineralogical Association of Canada.

Santschi, P. H., Roberts, K. A., & Guo, L. (2002). Organic Nature of Colloidal Actinides Transported in Surface Water Environments. *Environmental Science and Technology, 36*(17), 3711-3719.

Sarkar, D., Essington, M. E., & Misra, K. C. (2000). Adsorption of Mercury(II) by Kaolinte. *Soil Science Society of America Journal, 64*, 1968-1975.

Semu, E., Singh, B., & Selmer-Olsen, A. (1987). Adsorption of Mercury Compounds on Tropical Soils. *Water, Air and Soil Pollution*, 1-10.

Sen, T. K., & Khilar, K. C. (2006). Review on subsurface colloids and colloid-associated contaminant transport in saturated porous-media. *Advances in Colloid and Interface Science, 119*, 71-96.

Séquaris, J.-M. (2010). Modeling the effects of Ca2+ and clay-associated organic carbon on the stability of colloids from topsoils. *Journal of Colloid and Interface Science, 343*, 408-414.

Skyllberg, U. (2008). Competition among thiols and inorganic sulfides and polysulfides for Hg and MeHg in wetland soils and sediments under suboxic conditions: Illumination of controversies and implications for MeHg net production. *Journal of Physical Research, 113*.

Skyllberg, U., Bloom, P. R., Qian, J., Lin, C.-M., & Bleam, W. F. (2006). Complexation of Mercury(II) in Soil Organic Matter: EXAFS Evidence for Linear Two-Coordination with Reduced Sulfur Groups. *Environmental Science and Technology, 40*(13), 4174-4180.

Slowey, A. J. (2010). Rate of formation and dissolution of mercury sulfide nanoparticles: The dual role of natural organic matter. *Geochimica et Cosmochimica Acta, 74*, 4693-4708.

Slowey, A. J., & Brown Jr., G. E. (2007). Transformations of mercury, iron, and sulfur during the reductive dissolution of iron oxyhydroxide by sulfide. *Geochimica et Cosmochimica Acta, 71*, 877-894.

Slowey, A. J., Johnson, S. B., Rytuba, J. J., & Brown Jr, G. E. (2005). Role of Organic Acids in Promoting Colloidal Transport of Mercury from Mine Tailings. *Environmental Science and Technology, 39*(20), 7869-7874.

Stimson, J., Chae, G.-T., Ptacek, C. J., Emelko, M. B., Mesquita, M. M., Hirata, R. A., & Blowes, D. W. (2010). Basic oxygen furnace slag as a treatment material for pathogens: Contribution of inactivation and attachment in virus attenuation. *Water Research, 44*, 1150-1157.

Stumm, W., & Morgan, J. J. (1981). *Aquatic Chemistry: Chemical Equilibria and Rates in Natural Waters [2nd ed.]*. New York: Wiley.

Svensson, M., Duker, A., & Allard, B. (2006). Formation of cinnabar-estimation of favourable conditions in a proposed Swedish repository . *Journal of Hazardous Materials*(B136), 830-836.

Thompson, A., Chadwick, O. A., Boman, S., & Chorover, J. (2006). Colloid Mobilization During Soil Iron Redox Oscillations. *Environmental Science and Technology, 40*, 5743-5749.

Tipping, E. (1981). The adsoption of aquatic humic substances by iron oxides. *Geochimica et Cosmochimica Acta, 45*, 191-199.

Tipping, E., & Heaton, M. (1983). The adsorption of aquatic humic substances by two oxides of manganese . *Geochimica et Cosmochimca Acta, 47*, 1393-1397.

United Nations Environment Programme. (2013). *Global Mercury Assessment 2013: Sources, Emissions, Releases and Environmental Transport.* Geneva, Switzerland.

United States Environmental Protection Agency. (2000, January). *Mercury Compounds Hazard Summary*. Retrieved from Technology Transfer Network - Air Toxics Web Site: https://www3.epa.gov/airtoxics/hlthef/mercury

United States Geological Survey. (2017, November 12). *PREEQC (Version 3)--A Computer Program for Speciation, Batch-Reaction, One-Dimensional Transport, and Inverse*

Geochemical Calculations. Retrieved November 20, 2017, from https://wwwbrr.cr.usgs.gov/projects/GWC_coupled/phreeqc/

Vermeer, A., van Riemsdijk, W., & Koopal, L. (1998). Adsorption of Humic Acid to Mineral Particles. 1. Specific and Electrostatic Interactions. *Langmuir, 14*(10), 2810-2819.

Vernon, J. D., & Bonzongo, J.-C. J. (2014). Volatilization and sorption of dissolved mercury by metallic iron of different particle sizes: Implications for treatment of mercury contaminated water effluents. *Journal of Hazardous Materials, 276*, 408-414.

Virginia Department of Environmental Quality. (2016). *South River/South Fork Shenandoah River Mercury Information*. Retrieved February 6, 2017, from http://www.deq.virginia.gov/Programs/Water/WaterQualityInformationTMDLs/WaterQualityMonitoring/FishTissueMonitoring/ShenandoahMercury.aspx

Wang, J., Feng, X., Anderson, C. W., Xing, Y., & Shang, L. (2012). Remediation of mercury contaminated sites - A review. *Journal of Hazardous Materials*(221-222), 1-18.

Wang, J., Newman, M. C., Xu, X., & Liang, L. (2013). Higher and more variable methylmercury biomagnification factors for floodplain than the contiguous river (South River, Virginia USA). *Ecotoxicology and Environmental Safety, 92*, 191-198.

Waples, J. S., Nagy, K. L., Aiken, G. R., & Ryan, J. N. (2005). Dissolution of cinnabar (HgS) in the presence of natural organic matter. *Geochimica et Cosmochimica Acta, 69*(6), 1575-1588.

Weber, F.-A., Voegelin, A., & Kretzschmar, R. (2009). Multi-metal contaminant dynamics in temporarily flooded soil under sulphate limitation. *Geochimica et Cosmochimica Acta, 73*, 5513-5527.

Weisener, C. G., Sale, K. S., Smyth, D. J., & Blowes, D. W. (2005). Field Column Study Using Zerovalent Iron for Mercury Removal from Contaminated Groundwater. *Environmental Science and Technology, 39*(16), 6306-6312.

Wolfenden, S., Charnock, J. M., Hilton, J., Livens, F. R., & Vaughan, D. J. (2005). Sulfide Species as a Sink for Mercury in Lake Sediments. *Environmental Science and Technology*(39), 6644-6648.

Xiong, Z., He, F., Zhao, D., & Barnett, M. O. (2009). Immobilization of mercury in sediment using stabilized iron sulfide nanoparticles. *Water Research*(43), 5171-5179.

Xu, J., Kleja, D. B., Biester, H., Lagerkvist, A., & Kumpiene, J. (2014). Influence of particle size distribution, organic carbon, pH and chlorides on washing of mercury contaminated soil. *Chemosphere, 109*, 99-105.

Zhang, T., Kim, B., Levard, C., Reinsch, B. C., Lowry, G. V., Deshusses, M. A., & Hsu-Kim, H. (2011). Methylation of Mercury by Bacteria Exposed to Dissolved, Nanoparticulate, and Microparticulate Mercuri Sulfides. *Environmental Science and Technology, 46*, 6950-6958.

Zhang, T., Kim, B., Levard, C., Reinsch, B. C., Lowry, G. V., Deshusses, M. A., & Hsu-Kim, H. (2011). Methylation of Mercury by Bacteria Exposed to Dissolved, Nanoparticulate, and Microparticulate Mercuric Sulfides. *Environmental Science and Technology, 46*, 6950-6958.

Zheng, Y., Luo, X., Zhang, W., Wu, X., Zhang, J., & Han, F. (2016). Transport mechanisms of soil-bound mercury in the erosion process during rainfall-runoff events. *Environmental Pollution, 215*, 10-17.

Zhong, L., Qafoku, N. P., Szecsody, J. E., Dresel, P. E., & Zhang, Z. F. (2009, November). Foam Delivery of Calcium Polysulfide to the Vadose Zone for Chromium (VI) Immobilization: A Laboratory Evaluation. *Vadose Zone Journal, 8*(4), 976-985.

Zhu, Y., Ma, L. Q., Dong, X., Harris, W. G., Bonzongo, J., & Han, F. (2014). Ionic strength reduction and flow interruption enhanced colloid-facilitated Hg transport in contaminated soils. *Journal of Hazardous Materials, 264*, 286-292.

Zhu, Y., Ma, L. Q., Gao, B., Bonzongo, J., Harris, W., & Gu, B. (2012). Transport and interactions of kaolinite and mercury in saturated and media. *Journal of Hazardous Materials, 213-214*, 93-99.

Zillioux, E., Porcella, D., & Benoit, J. (1993). Mercury Cycling and Effects in Freshwater Wetland Ecosystems. *Environmental Technology and Chemistry, 12*, 2245-2264.

Zuyi, T., Taiwei, C., Jinzhou, D., XiongXin, D., & Yingjie, G. (2000). Effect of fulvic acids on sorption of U(VI), Zn, Yb, I and Se(IV) onto oxides of aluminum, iron and silicon. *Applied Geochemistry, 15*, 133-139.

Appendix A: Supporting Information for Chapter 2

The aqueous concentrations of the Chapter 2 control column effluent over time are presented in Figure A.1. Additional effluent concentrations from the varied input column are presented in Figure A.2. The ionic strengths and saturation indices of select minerals calculated by PHREEQC for effluent samples from the control and varied input solution columns are presented in Table A.1 and Table A.2.

In addition to the varied input solution column, two saturated, flow through column experiments were conducted with the riverbank sediment described in Chapter 2. One column received Nano-pure, deionized water as the input solution and the other column received a 3.5 mM Ca (as $CaCl_2$) input solution prepared identically to the Stage 1 input. The effluent concentrations from these two column experiments are presented in Figure A.3 and Figure A.4. The ionic strength and select mineral saturation indices as calculated by PHREEQC for effluent samples from the Nano-pure and 3.5 mM Ca (as $CaCl_2$) are provided in Table A.3 and Table A.4.

Table A.1 - Ionic strength and saturation indices of select minerals of control column effluent samples calculated by PHREEQC.

Sample ID	Pore Volume	Ionic Strength (mol/kgw)	Charge Balance Error (%)	Saturation Indices				
				Calcite	Dolomite	Ferrihydrite	Gypsum	Pyrolusite
MC-1-CTL-2	2.5	0.0101	-3.7	0.37	0.38	1.97	-1.88	-1.31
MC-1-CTL-3	6.2	0.0119	12.0	0.63	0.90	2.74	-2.69	-7.25
MC-1-CTL-9	14.8	0.0081	4.4	0.30	0.16	-1.83	-3.19	-17.37
MC-1-CTL-11	22.1	0.0088	19.6	0.08	-0.29	1.95	-2.95	-10.76
MC-1-CTL-18	42.5	0.0050	7.4	-0.58	-1.46	1.08	-3.28	-13.59
MC-1-CTL-27	81.3	0.0046	6.1	-0.77	-1.73	1.63	-4.40	-1.66
MC-1-CTL-29	106.4	0.0035	9.3	-1.00	-2.15	2.13	-4.04	-6.67
MC-1-CTL-31	130.8	0.0030	6.9	-1.27	-2.71	0.89	-3.09	-8.29

Table A.2 - Ionic strength and saturation indices of select minerals of varied input solution column effluent samples calculated by PHREEQC.

Sample ID	Pore Volume	Ionic Strength (mol/kgw)	Charge Balance Error (%)	Saturation Indices				
				Calcite	Dolomite	Ferrihydrite	Gypsum	Pyrolusite
MC-4-K-2	2.2	0.0153	-22.3	0.14	-0.06	2.12	-1.46	-2.32
MC-4-K-3	6.0	0.0137	-13.3	0.44	0.53	2.34	-1.70	-7.13
MC-4-K-13	29.3	0.0123	-32.1	-0.54	-1.91	1.51	-1.85	-9.23
MC-4-K-18	43.1	0.0457	9.6	0.44	-0.04	1.38	-3.58	-14.74
MC-4-K-24	65.5	0.0453	9.5	0.21	-0.11	3.50	-4.08	-1.87
MC-4-K-28	97.5	0.0460	2.1	-0.01	-0.04	3.32	-3.32	-3.75
MC-4-K-29	107.8	0.0450	2.0	0.52	0.85	1.54	-2.84	-4.98
MC-4-K-32	117.3	0.0496	19.3	-1.41	-2.74	1.80	-3.40	-7.55
MC-4-K-38	134.2	0.0138	15.2	-1.85	-3.55	0.73	-3.97	-6.84
MC-4-K-39	137.5	0.0307	-26.0	-0.75	-1.38	3.39	-2.67	-5.98
MC-4-K-43	148.6	0.0230	-36.8	-0.63	-1.30	4.19	-2.60	-5.96
MC-4-K-45	158.2	0.0517	-15.5	-0.89	-1.84	3.55	-2.64	-6.09
MC-4-K-48	170.8	0.0442	21.0	-0.74	-1.51	2.35	-3.75	-8.09

Table A.3 - Ionic strength and saturation indices for select minerals, calculated by PHREEQC, for effluent derived from column with ultrapure water as input solution.

Sample ID	Pore Volume	Ionic Strength (mol/kgw)	Charge Balance Error (%)	Saturation Indices				
				Calcite	Dolomite	Ferrihydrite	Gypsum	Pyrolusite
MC-2-NP-2	2.3	0.0075	13.0	0.48	0.62	2.50	-2.56	-0.63
MC-2-NP-3	6.2	0.0079	14.2	0.21	0.06	2.99	-3.35	-4.06
MC-2-NP-7	13.4	0.0054	11.0	-0.15	-0.72	-0.99	-3.77	-17.95
MC-2-NP-10	21.2	0.0047	4.8	-0.39	-1.25	2.90	-3.10	-10.01
MC-2-NP-17	44.6	0.0020	-3.0	-1.37	-3.27	2.49	-3.79	-5.54

Table A.4 - Ionic strength and saturation indices of select minerals of column effluent samples from the 3.5 mM Ca (as $CaCl_2$) input solution column calculated by PHREEQC.

Sample ID	Pore Volume	Ionic Strength (mol/kgw)	Charge Balance Error (%)	Saturation Indices				
				Calcite	Dolomite	Ferrihydrite	Gypsum	Pyrolusite
MC-3-CA-2	2.5	0.0140	56.0	0.21	0.08	1.45	-3.03	-3.67
MC-3-CA-4	8.8	0.0206	-1.8	0.41	0.35	1.91	-2.12	-12.10
MC-3-CA-6	11.3	0.0196	-6.4	0.34	0.05	0.44	-2.18	-14.92
MC-3-CA-8	15.0	0.0165	-16.3	-0.09	-1.02	2.31	-2.07	-2.62
MC-3-CA-12	29.8	0.0172	-17.9	-0.29	-1.47	0.83	-2.08	-13.48
MC-3-CA-21	79.5	0.0096	54.9	-0.84	-2.46	1.59	-3.56	-5.79

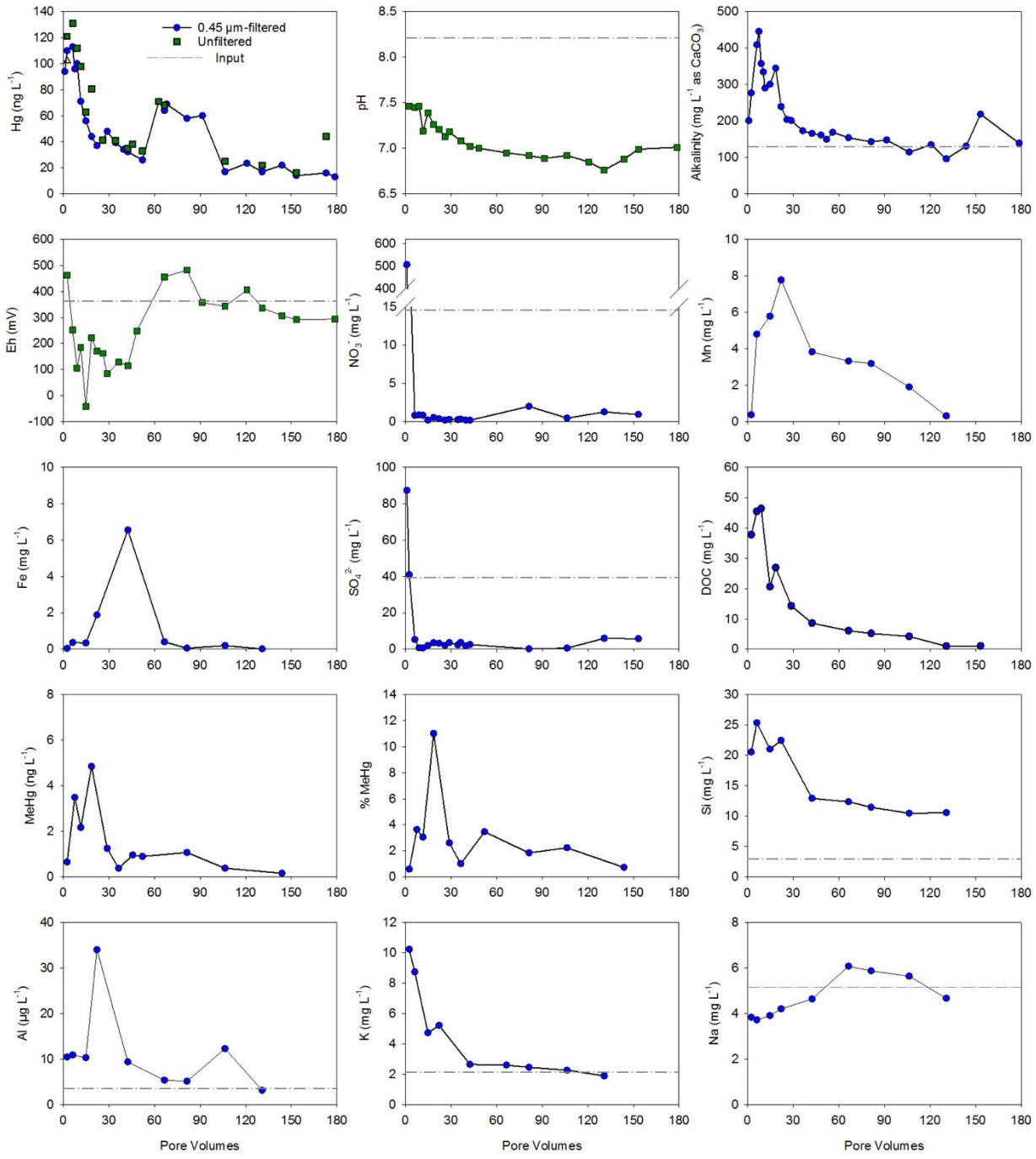

Figure A.1: Aqueous concentrations monitored over time in the control column effluent. The dashed, grey line represents the average input solution (SRW) concentration.

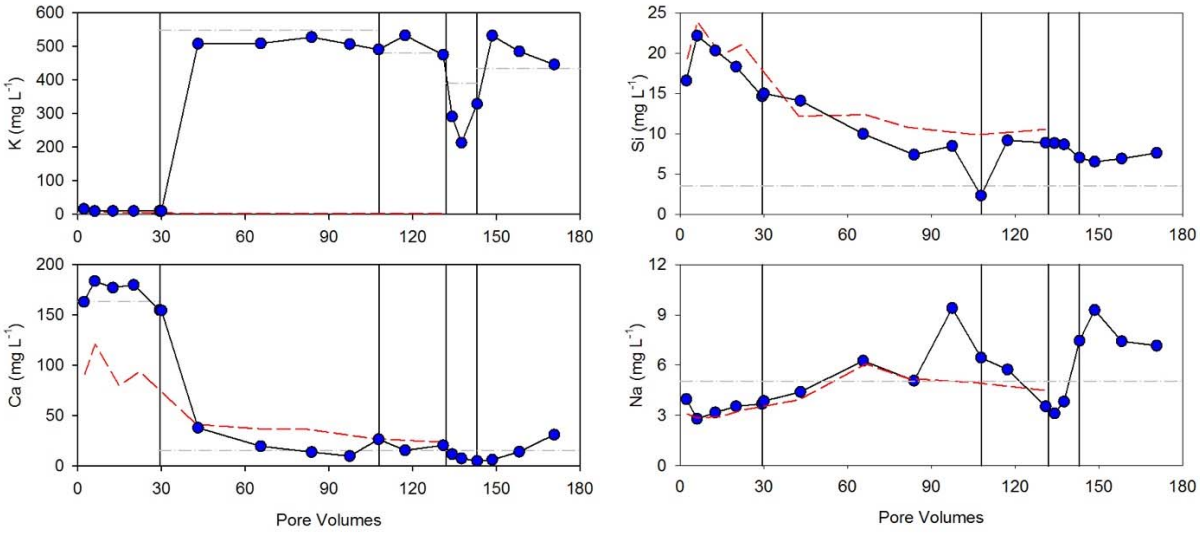

Figure A.2: Additional aqueous concentrations monitored over time in the varied input solution column effluent. Dashed, red lines represent control column effluent concentrations over time. Dashed, grey lines represent the average input solution concentration for each input solution.

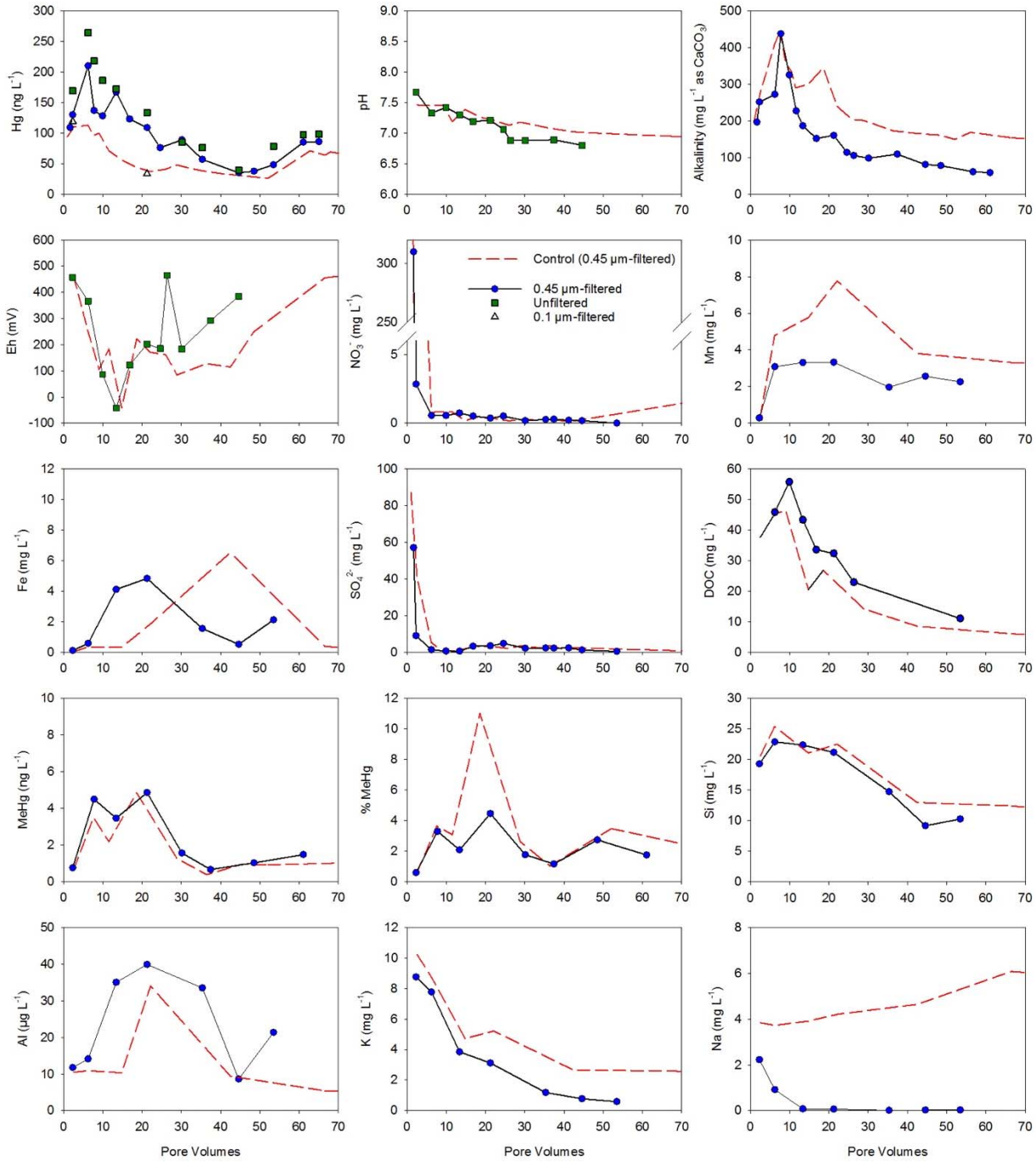

Figure A.3: Aqueous concentrations monitored over time in the nano-pure input solution column effluent. Dashed, red lines represent control column effluent concentrations over time.

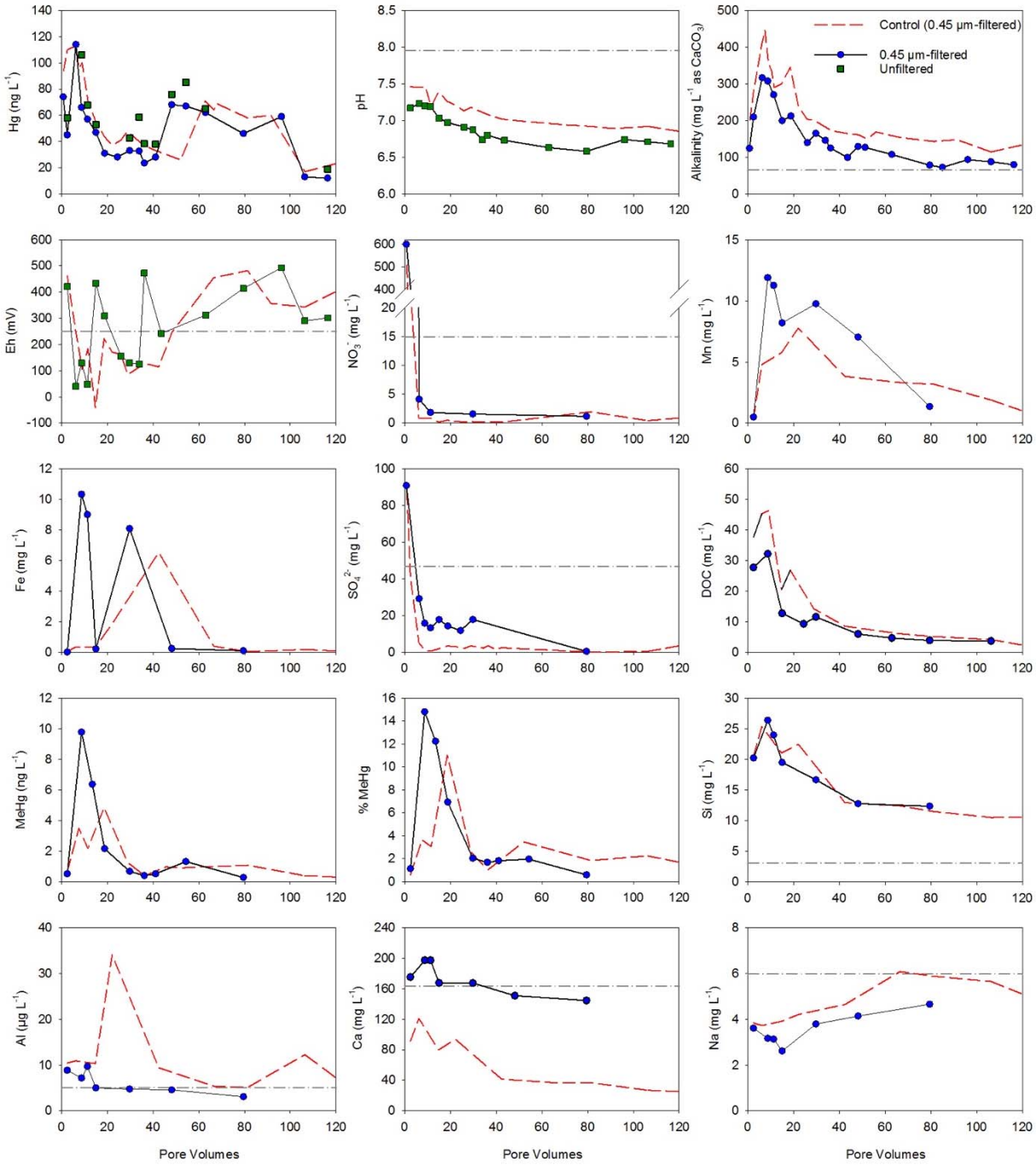

Figure A.4: Aqueous concentrations monitored over time in the $CaCl_2$ input solution column effluent. Dashed, red lines represent control column effluent concentrations over time. Dashed, grey lines represent average input solution concentrations.

Appendix B: Supporting Information for Chapter 3

The ionic strength and saturation indices of select minerals for the aerobic control, anaerobic control and KPS-application columns are provided in Table B.1, Table B.2 and Table B.3, respectively.

Table B.1 - Ionic strengths and saturation indices of effluent samples from the aerobic control column calculated with PHREEQC.

Sample ID	Pore Volume	Ionic Strength (mol/kgw)	Charge Balance Error (%)	Saturation Indices				
				Calcite	Dolomite	Ferrihydrite	Gypsum	Pyrolusite
MC11.8-1-4	9.4	0.0069	34.6	-0.47	-1.49	2.98	-2.43	-0.18
MC11.8-1-5	13.7	0.0057	8.1	-0.40	-0.99	1.63	-2.68	-0.04
MC11.8-1-10	33.3	0.0087	7.5	0.17	0.13	1.50	-4.87	-12.46
MC11.8-1-13	43.6	0.0060	1.1	-0.31	-0.86	3.97	-3.96	-4.60
MC11.8-1-17	59.9	0.0047	7.1	-0.75	-1.72	1.20	-2.46	-11.89
MC11.8-1-19	74.4	0.0037	-0.2	-0.90	-2.03	2.42	-2.80	-5.27

Table B.2 - Ionic strengths and saturation indices of effluent samples from the anaerobic control column calculated with PHREEQC.

Sample ID	Pore Volume	Ionic Strength (mol/kgw)	Charge Balance Error (%)	Saturation Indices				
				Calcite	Dolomite	Ferrihydrite	Gypsum	Pyrolusite
MCGB-2	2.4	0.0034	20.2	-3.64	-4.93	2.50	-5.84	-7.21
MCGB-4	6.3	0.0045	11.9	-2.88	-3.56	3.73	-7.05	-6.89
MCGB-5	10.1	0.0039	-33.6	-3.44	-3.68	-0.02	N/A	-13.47
MCGB-9	20.8	0.0047	-0.2	-2.11	-2.65	1.19	-6.11	-15.44
MCGB-12	45.5	0.0038	-2.0	-2.04	-2.86	0.89	-5.76	-15.50
MCGB-13	56.3	0.0036	-24.2	-2.26	-3.15	1.00	-6.34	-15.30

Table B.3 - Ionic strengths and saturation indices of effluent samples from the KPS-application column calculated with PHREEQC.

Sample ID	Pore Volume	Ionic Strength (mol/kgw)	Charge Balance Error (%)	Saturation Indices				
				Calcite	Dolomite	Ferrihydrite	Gypsum	Pyrolusite
MCKS-2	2.2	0.0038	11.8	-3.36	-4.37	1.31	-5.58	-10.66
MCKS-5	6.2	0.0042	3.7	-3.29	-4.33	2.74	-6.33	-9.21
MCKS-9	18.1	0.0048	0.5	-1.78	-1.54	2.56	-6.49	-13.14
MCKS-12	23.8	0.0052	-2.5	-1.64	-1.31	1.96	-6.39	-14.67
MCKS-15	45.0	0.0037	-15.4	-1.63	-1.77	3.30	-6.63	-11.80
MCKS-16	47.8	0.0033	-9.3	-1.74	-1.96	2.52	-6.35	-13.30
MCKS-18	56.9	0.0048	-13.7	-3.03	-3.37	-0.05	-6.56	-17.11

Appendix C: Quality Assurance and Quality Control for Chapter 2 and 3

Table C.1 - QA/QC for THg analyses from Chapter 2 columns (MC-1-CTL, MC-2-NP, MC-3-CA and MC-4-K).

Sample ID	Date of Sampling	Date of Analysis	THg (ng L^{-1})	Repeat THg (ng L^{-1})	Relative Standard Deviation (%)	Matrix Spike Recovery (%)
MC-1-CTL-5-0.45	11-Aug-14	18-Sep-14	100	109	5.7	
MC-1-CTL-3-THG	05-Aug-14	01-Oct-14	237			93.85
MC-1-CTL-BP1	31-Jul-14	16-Apr-01	266	234	9.07	
MC-1-CTL-TP3	22-Oct-14	21-Jul-15	76	60	16.16	
MC-2-NP-5-0.45	12-Aug-14	19-Sep-14	237	128		90.27
MC-2-NP-7-0.45	19-Aug-14	18-Sep-14	167	179	5.12	
MC-2-NP-10-0.45	03-Sep-14	25-Sep-14	109	110	0.73	
MC-2-NP-17-0.45	21-Oct-14	06-Nov-14	35	38	6.56	
MC-2-NP-19-THG	06-Nov-14	17-Dec-14	79.7	77.8	1.68	
MC-2-NP-21-0.45	20-Nov-14	17-Dec-14	93.9	84.6	7.4	
MCMP1-2-NP	28-Aug-14	16-Apr-15	163	166	1.41	
MC-3-CA-1-0.45	14-Aug-14	18-Sep-14	74.4	73.8	0.56	
MC-3-CA-3-0.45	26-Aug-14	19-Sep-14	214	114		94.2
MC-3-CA-6-THG	08-Sep-14	01-Oct-14	68	67	1.22	
MC-3-CA-14-THG	27-Oct-14	06-Nov-14	38.3	36.7	2.92	
MCTP1-3-CA	18-Aug-14	16-Apr-15	478	471	1.01	
MC-4-K-2-0.45	25-Aug-14	18-Sep-14	54.8	55.8	1.35	
MC-4-K-5-0.45	09-Sep-14	25-Sep-14	74.8	73	1.76	
MC-4-K-5-THG	09-Sep-14	01-Oct-14	394	209		96.74
MC-4-K-3-THG	03-Sep-14	01-Oct-14	183	188	1.82	
MC-4-K-16-THG	03-Nov-14	06-Nov-14	70.7	68.6	2.16	
MC-4-K-18-THG	20-Nov-14	17-Dec-14	188	196	2.85	
MC-4-K-21-0.45	11-Dec-14	17-Dec-14	237	226	3.24	
MCBP2-4-K	30-Oct-14	16-Apr-15	39.3	37.7	3.04	
MC-4-K-TP2	23-Sep-14	21-Jul-15	48.9	47.7	1.72	
MC-4-K-39-0.1	22-Jun-15	15-Jul-15	958	886	5.54	

Table C.2 - QA/QC for THg analyses from Chapter 3 columns [MC11.8-1-1 (aerobic control), MC11.8-CPSA, MCGB (anaerobic control) and MCKS].

Sample ID	Date of Sampling	Date of Analysis	THg (ng L-1)	Repeat THg (ng L-1)	Relative Standard Deviation (%)	Matrix Spike Recovery (%)
MC11.8-1-1-THG	17-Dec-15	14-Jan-15	384	366	3.42	
MC11.8-1-3-0.45	22-Dec-14	14-Jan-15	391			101.57
MC11.8-1-5-0.45	06-Jan-15	14-Jan-15	6106	5929	2.07	
MC11.8-1-6-0.45	11-Jan-15	14-Jan-15	3848	3716	2.46	
MC11.8-1-18-0.45	15-Apr-15	16-Apr-15	273	266	1.75	
MC11.8-1-21-0.45	28-May-15	21-Jul-15	588			103.18
MC11.8-1-25-THG	31-Aug-15	15-Sep-15	1509	1393	5.66	
MC11.8-CPSA-9-0.45	03-Mar-15	10-Mar-15	7789	7545		100.99
MC11.8-CPSA-BP2	06-Mar-15	10-Mar-15	272	266	1.57	
MC11.8-CPSA-10-THG	09-Mar-15	10-Mar-15	15394	15124	1.25	
MC11.8-CPSA-11-THG	17-Mar-15	16-Apr-15	6250	6058	2.21	
MC11.8-CPSA-23-0.45	31-Aug-15	15-Sep-15	478	440	5.84	
MCGB-4-0.45	27-Apr-15	12-May-15	534	544	1.27	
MCGB-10-0.45	08-Jun-15	09-Jun-15	2250	1469		102.05
MCGB-TP2	14-Jul-15	21-Jul-15	10739	11118	2.45	
MCGB-12-0.45	13-Jul-15	15-Jul-15	940	991	3.71	
MCKS-5-0.45	04-May-15	12-May-15	129056	118965	5.75	
MCKS-11-0.45	03-Jun-15	09-Jun-15	12658	11736	5.34	
MCKS-18-0.45	26-Aug-15	15-Sep-15	512	505	0.97	

Table C.3 - THg method detection limits from Hg analyses.

Date	Method Detection Limit (ng L-1)
18-Sep-14	0.19
25-Sep-14	0.25
30-Sep-14	0.14
05-Nov-14	0.19
17-Dec-14	0.08
14-Jan-15	0.09
19-Feb-15	0.31
10-Mar-15	0.14
09-Jun-15	0.32
Average	0.19